Conjugate Mixed Convection with Surface Radiation from a Vertical Channel with Multiple Asymmetrically Mounted Discrete Heat Sources

A Thesis submitted in partial fulfillment of the requirements for the award of the degree of

Doctor of Philosophy

by

S. Sudhakar Babu
(Roll No. 701208)

Under the Supervision of

Prof. C. Gururaja Rao

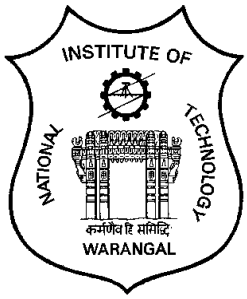

Department of Mechanical Engineering
National Institute of Technology
Warangal [T. S.] 506 004 India

June 2016

Dedicated

to

My Parents

Shri. S. Prakasam

and

Smt. S. Vinayakumari

Thesis Approval for Ph.D.

This Thesis entitled,

"Conjugate Mixed Convection with Surface Radiation from a Vertical Channel with Multiple Asymmetrically Mounted Discrete Heat Sources"

by

Mr. S. Sudhakar Babu

is approved for the degree of

Doctor of Philosophy

Prof. _____

Examiner

Prof. C. Gururaja Rao

Supervisor

Prof. _____

Chairman and **The Head,**

Department of Mechanical Engineering,

National Institute of Technology, Warangal

Date :_____

Certificate

This is to certify that the thesis, entitled, **"Conjugate Mixed Convection with Surface Radiation from a Vertical Channel with Multiple Asymmetrically Mounted Discrete Heat Sources"**, submitted to **National Institute of Technology, Warangal - 506 004**, is the bonafide research work done by **Mr. S. Sudhakar Babu (Roll No. 701208)** under my supervision. The contents of the thesis have not been submitted elsewhere for the award of any degree.

Date:

Place: Warangal

Prof. C. GURURAJA RAO

Research Supervisor

Department of Mechanical Engineering

National Institute of Technology, Warangal

Declaration

This is to certify that the work presented in the thesis entitled, **"Conjugate Mixed Convection with Surface Radiation from a Vertical Channel with Multiple Asymmetrically Mounted Discrete Heat Sources"** is a bonafide work done by me under the supervision of **Prof. C. Gururaja Rao** and was not submitted elsewhere for the award of any degree. I declare that this written submission represents my ideas in my own words and where others' ideas or words have been included, I have adequately cited and referenced the original sources. I also declare that I have adhered to all principles of academic honesty and integrity and have not misrepresented or fabricated or falsified any idea / data / fact / source in my submission. I understand that any violation of the above will be a cause for disciplinary action by the Institute and can also evoke penal action from the sources which have thus not been properly cited or from whom proper permission has not been taken when needed.

Date:

Mr. S. Sudhakar Babu

Registration No. 701208

Acknowledgement

It is indeed a great pleasure to present this thesis, which is the outcome of the research work that would not have been possible without the direct and indirect support of my supervisor, family, colleagues and friends.

I take this opportunity to express my deep sense of sincere thanks and gratitude to my supervisor, **Prof. C. Gururaja Rao**, for his guidance, support and encouragement throughout my research work. It is indeed, a great pleasure and privilege to work with him. The discussions I had with Prof. C. Gururaja Rao have always been fruitful and productive. In spite of his busy schedule, he spared his valuable time, for which I am greatly thankful to him. Apart from the research work, I also learned from him, many other skills such as interpreting, organizing, report writing, presentation, for which I am extremely indebted to him. I consider myself greatly privileged to work under his guidance. I wish to express once more my whole hearted thanks to Prof. C. Gururaja Rao for his invaluable support and guidance without which this thesis would not have been complete.

I wish to place on record my sincere thanks to **Dr. A. V. Narasimha Rao**, Former Professor, Department of Mechanical Engineering, for his encouragement and help throughout my stay here. I also would like to express my sincere gratitude to the **Head**, Department of Mechanical Engineering, all the **members** of **Doctoral Scrutiny Committee** and the **Director**, National Institute of Technology, Warangal, for their Patronage.

Without the whole hearted support and encouragement from my parents and other family members, this work would not have seen the light of the day. Especially, my wife **Indira Priyadarshini** and daughter **Karunya Joyce** were kind enough to tolerate the disturbance caused to them.

I am thankful to my colleagues, friends and fellow research scholars as well for their help and support.

Warangal **S. Sudhakar Babu**

June 2016

Abstract

The present thesis elucidates various key findings of a numerical investigation into the problem of buoyancy-aided conjugate mixed convection with surface radiation from an asymmetrically heated vertical channel. The problem configuration comprises two vertical plates of given height facing each other. The spacing (or width) of the channel could be varied by controlling the aspect ratio that is defined as the ratio of the height to the width of the channel. A total of ten identical discrete heat sources are flush-mounted in the channel walls, with each wall possessing five of them. Asymmetricity is followed while mounting the heat sources along the two walls of the channel. The exterior surfaces of the channel are considered adiabatic resulting in heat dissipation occurring only from the inner surfaces of the two walls. Air, a radiatively transparent medium, is considered to be the cooling agent that is assumed to be of constant thermophysical properties subject to the Boussinesq approximation.

The energy generated in the heat sources embedded in the channel walls gets conducted through them axially before subsequently getting dissipated by combined modes of mixed convection and radiation. Keeping this in mind, the governing equations for temperature distribution along the walls of the channel are obtained employing appropriate energy balance. The calculations related to radiation are performed using the enclosure method, while the view factors therein are computed through the Hottel's crossed-string method. The governing equations for fluid flow and heat transfer concerning the problem are initially transformed from primitive variables to stream function-vorticity formulation. The resulting equations are normalized making use of pertinent non-dimensional parameters. The normalized governing equations thus obtained, in conjunction with the relevant boundary conditions, are later discretized using finite volume method. The algebraic equations thus

obtained are ultimately solved simultaneously using Gauss-Seidel iterative solver. A comprehensive computer code in C++ is written to solve the problem.

The initial results obtained from the computer code are rigorously validated using certain available analytical and experimental results. They are also checked for the mass and energy balance. A detailed grid sensitivity test is performed to arrive at the optimum grid system for the problem. A number of parametric studies are performed bringing out the effects of various independent parameters including aspect ratio, thermal conductivity, surface emissivity and modified Richardson number on various fluid flow and heat transfer results. Efforts are made to explore the exclusive role of surface radiation in the problem. Attempts are also made to demonstrate the role of buoyancy in influencing the various results. Useful correlations for computing the maximum and average non-dimensional channel temperatures and mean friction coefficient are evolved based on a large set of numerical data generated from the computer code written.

Certain comparative studies between the discretely heated channel, considered as the principal problem geometry, and a uniformly heated channel are also performed holding the net rate of heat generation fixed in both the cases.

Table of Contents

List of Tables

List of Figures

Nomenclature

AR	aspect ratio, L/W
A_{r1}	geometric ratio, W/t
A_{r2}	geometric ratio, W/L_h and W/L, respectively, for configuration 1 and configuration 2
$\overline{C}_f$	mean friction coefficient
C_{fx}	local drag coefficient
F_{ik}	view factor from the *i*th element to the *k*th element of an enclosure
g	acceleration due to gravity, 9.81 m/s^2
Gr_w^*	modified Grashof number, $[g \beta \Delta T_{ref} W^3/\nu_f^2]$
J_i	radiosity of a given element *i* of the enclosure, W/m^2
J_i'	non-dimensional radiosity of a given element *i* of the enclosure, $[J_i/(\sigma T_\infty^4)]$
k_f	thermal conductivity of air, W/m K
k_s	thermal conductivity of channel wall as well as heat source, W/m K
L, L_h	heights of channel wall and heat source, respectively, m
M, N	Total number of grids in X and Y directions, respectively
$M_{1, 3, 5, 7, 9}$	Grid number at the top end of the first, second, third, fourth and fifth heat sources, respectively, of the left channel wall
$M_{2, 4, 6, 8}$	Grid number at the bottom end of the second, third, fourth and fifth heat sources, respectively, of the left channel wall
n	total number of elements of the enclosure
I_{RF}	radiation-flow interaction parameter, $[\sigma T_\infty^4/(k_f \Delta T_{ref}/W)]$
$\overline{Nu}_C$	average convection Nusselt number
P	pressure, Pa

Pe_w	Peclet number based on the width of the channel, $[Re_w Pr]$ or $[u_\infty W/\alpha_f]$
Pr_f	Prandtl number of air, $[\nu_f/\alpha_f]$
Q	rate of heat transfer, W
q_v	rate of volumetric heat generation, W/m^3
Re_w	Reynolds number based on the width of the channel, $[u_\infty W/\nu_f]$
Re_L	Reynolds number based on the length of the channel wall, $[u_\infty L/\nu_f]$
Ri_w^*	modified Richardson number based on the width of the channel, $[g\beta\Delta T_{ref} W/u_\infty^2]$ or $[Gr_w^*/Re_w^2]$
t	thickness of channel wall, m
T	local temperature in the computational domain, K or °C
T_∞	free stream temperature of air, K or °C
u, v	vertical and horizontal components of velocity, respectively, m/s
u_∞	free stream velocity of air, m/s
U	non-dimensional vertical velocity of air, $[u/u_\infty]$ or $[\partial\psi/\partial Y]$
V	non-dimensional horizontal velocity of air, $[v/u_\infty]$ or $[-\partial\psi/\partial X]$
W	width or spacing of the channel, m
x, y	vertical and horizontal distances, respectively, m
X, Y	non-dimensional vertical and horizontal distances, x/W and y/W, respectively

Greek symbols

α_f	thermal diffusivity of air, m^2/s
β	isobaric cubic expansivity of air, $[-(1/\rho)(\partial\rho/\partial T)_p]$, K^{-1}
ξ	thermal conductance parameter, $[k_f W/(k_s t)]$
λ	relaxation parameter

δ_c	convergence criterion, $\lvert(\zeta_{new} - \zeta_{old})/\zeta_{new}\rvert$
ε	surface emissivity of the walls of the channel
ζ	dependent parameter (stream function, vorticity or temperature, as the case may be)
θ	non-dimensional temperature, $[(T - T_\infty)/\Delta T_{ref}]$
θ_{val}	temperature difference ratio specifically defined during validation of results, $[(T_R - T_\infty)/(T_L - T_\infty)]$
ν_f	kinematic viscosity of air, m^2/s
ρ, ρ_∞	local and characteristic values of fluid density, respectively, kg/m^3
σ	Stefan-Boltzmann constant, 5.6697×10^{-8} $W/m^2 K^4$
ψ	non-dimensional stream function, $[\psi'/(u_\infty W)]$
ψ'	stream function, m^2/s
ω	non-dimensional vorticity, $[\omega' W/u_\infty]$
ω'	vorticity, s^{-1}

Subscripts

av	average
cond,x,in	conduction heat transfer into an element along the wall
cond,x,out	conduction heat transfer out of an element along the wall
conv	convection heat transfer from an element of the wall
L	left wall
max	maximum
R	right wall
rad	radiation heat transfer from an element of the wall

Miscellaneous symbols

Δx_{hs}	height of the element in the heat source portion of the wall, m
Δx_{nhs}	height of the element in the non-heat source portion of the wall, m
ΔX_{hs}	non-dimensional height of the element in the heat source portion of the wall
ΔX_{nhs}	non-dimensional height of the element in the non-heat source portion of the wall
ΔT_{ref}	modified reference temperature difference, $[q_v L_h t/k_s]$ and $[q_v L t/k_s]$, respectively, for configuration 1 and configuration 2, K or °C

Chapter 1

Introduction

1.1 Background

A fluid flow regime that comprises both inertia forces and buoyancy forces, coupled with viscous forces, wherein the buoyancy either aids or opposes the flow triggered by a mechanical device (fan, blower or pump), is defined as “Combined Free and Forced Convection” or “Mixed Convection”. The relative importance of the inertia and the buoyancy forces helps in dividing mixed convection into three sub-regimes, viz., (i) forced convection dominant regime, (ii) pure mixed convection regime and (iii) free convection dominant regime. The inertia forces are quite larger in comparison to the buoyancy forces in the forced convection dominant regime, while the buoyancy forces override the inertia forces in the free

convection dominant regime. The inertia and buoyancy forces exhibit comparable contributions in the pure mixed convection regime.

The governing parameters concerning free and forced convection phenomena are the well known Grashof number and Reynolds number, respectively. Of these, the Grashof number signifies the ratio of buoyancy forces to viscous forces, while the ratio of inertia to viscous forces represented by the Reynolds number. It then follows that, for mixed convection, the prominent governing parameter would be the ratio of buoyancy to inertia forces that is called as the Richardson number. Mathematically, Richardson number is defined as the ratio of the Grashof number to the square of the Reynolds number. As can be made out, a very large value of Richardson number pertains to flow with free convection dominance, while a smaller value of Richardson number indicates that the flow has forced convection dominance. By the same token, a value of the order of unity for the Richardson number signifies a comparable representation from the mechanisms of free and forced convection that is rightly referred to as pure mixed convection.

A free and forced convection flow has turbulence setting in when once the Rayleigh number (the product of Grashof and Prandtl numbers) and the Reynolds number reach their critical values, which, for the geometry of a vertical plate, are, respectively, equal to 10^9 and 5×10^5. Since the present research work involves laminar mixed convection with other modes of heat transfer coupled to it, one has in it the presence of both free and forced convection phenomena. In view of the above, enough care is taken in not permitting the Rayleigh and Reynolds numbers based on the appropriate characteristic dimension to go beyond the above critical values. This helps in making it sure that the flow considered in the entire thesis work is going to remain laminar.

Interplay between the various modes of heat transfer (conduction, combined free and forced or mixed convection and radiation) finds its importance in a good number of day-to-day and industrial applications. Some of these include: (i) gas cooled nuclear fuel rods, (ii) I.C. engines, (iii) solar collection devices including solar cookers, (iv) gas turbines and (v) electronic gadgets. The fundamental concern of an engineer dealing with thermal control systems catering to a given electronic device is to have a rigorous check on the temperature attained by the device never allowing it to cross a present critical value that usually would be in the range 80-100°C [Incropera (1998)]. This makes it mandatory that any cooling system designed for a given electronic device satisfactorily foregoes the heat that gets generated in the device. Researchers, over the years, have amply demonstrated that any electronic gadget gets its reliability diminished by about 50% even if the maximum gadget temperature increases just by 10°C with reference to the pre-specified critical temperature. This is more than sufficient to underline the necessity of a very efficient thermal control system in electronic applications.

A very commonly encountered geometry in applications concerning cooling of electronic devices is a channel due to its closeness to printed circuit boards mounted with multiple heat sources. During the initial stages of research in the area of electronic cooling, the thermal performance evaluation of a given system was made considering a prescribed isothermal (or isoflux) boundary condition. However, it is quite obvious that the problems of this class have an unknown temperature distribution in the geometry under consideration that has to be obtained as a part of the problem solution itself. A typical multi-mode heat transfer problem would be having internal heat generation (either uniform or discrete) with the heat thus generated getting conducted internally before getting dissipated from the exterior surface of the geometry by convection (free or forced or mixed) and radiation. This is the case with respect to all the situations that have the geometries with a finite non-zero thermal

conductivity and surface emissivity with a radiatively transparent medium like air (or any other gas) serving as cooling agent.

Literature provides quite a large number of analytical, numerical and experimental studies that address free, forced or mixed convection from the classical geometry of a vertical channel. In particular, when it narrows down to interplay of surface radiation with conjugate mixed convection from the above geometry, the number of studies, though available, are relatively few. Fewer still are the studies that cater to a channel that has discrete heating possessing multiple asymmetrically mounted heat sources along its walls taking part in multi-mode heat transfer. Thus, the current research work has been taken up to dwell into the problem of conjugate mixed convection with surface radiation from the geometry of a vertical channel that is flush-mounted with multiple, identical, asymmetrically positioned discrete heat sources in its walls. The present work is essentially fundamental in its nature with a remote application found in electronic boards mounted with discrete heat sources.

An exhaustive numerical investigation into the physics underlying the problem mentioned above forms the core content of the present thesis. Coupled to the above, pertinent correlations that help in calculating the maximum channel temperature, the average channel temperature and the mean friction coefficient would be deduced in conclusion to a very large number of fluid flow and heat transfer studies performed on the problem. Further, a good number of comparative studies between the discretely and uniformly heated channels would also be taken up.

1.2 Organization of the Thesis

The current thesis comprises a total of six chapters inclusive of the present chapter. In what follows, the prominent features of various chapters are enunciated.

Chapter 1 provides a general introduction to the research problem solved in the present thesis. This chapter also describes the broad organization of the thesis spelling out as to what is expected in each of the chapters.

In **Chapter 2**, an exhaustive review of the literature related to the research problem taken up in the present thesis is documented. This is accompanied by the conclusions drawn from the literature review thus made. All the major objectives and the scope of the research work are also included in the same chapter.

Chapter 3 gives, in detail, the general mathematical formulation of the problem connecting heat generation with internal conduction accompanied by mixed convection and radiation. This chapter also lists the various boundary conditions used to tackle the problem along with a detailed account on the solution methodology employed.

Chapter 4 provides an exhaustive coverage of the problem of conjugate mixed convection with surface radiation from a vertical channel possessing a total of ten identical discrete heat sources flush-mounted in it with five per each of its walls. The statement of the problem and the method of solution appear initially in this chapter with the findings of a comprehensive grid sensitivity analysis that help in arriving at the optimum grid system for the problem accompanying them. Subsequently, results of the mass and energy balance checks are provided that are followed by a detailed validation of the results. Then, the variation of (i) the local wall temperature distribution, (ii) the maximum channel temperature,

(iii) the local drag coefficient and (iv) the mean friction coefficient with respect to various pertinent independent parameters is elucidated. Further, the relative contributions of mixed convection and radiation in channel heat dissipation are analyzed qualitatively as well as quantitatively in various regimes of convection and with different surface emissivities of the channel. Also, the exclusive roles exhibited by surface radiation and buoyancy in different fluid flow and heat transfer results are extracted. Attempts are further made to separate out the free and forced convection components of mean friction coefficient not only in different convection regimes but also with various surface emissivities of the channel. In conclusion, appropriate correlations are evolved for (i) maximum non-dimensional channel temperature, (ii) average non-dimensional channel temperature and (iii) mean friction coefficient making use of a very large set of numerical data generated from the computer code written as part of the present thesis.

A qualitative cum quantitative comparison between discretely and uniformly heated channels is attempted in **Chapter 5**. At the outset, the problem of interaction of surface radiation with conjugate mixed convection from a vertical channel with uniform internal heat generation in its walls is tackled. Here too, after narrating the problem statement and the method of solution, an account on the mass and energy balance checks and validation would be provided. Subsequently, comparative studies between discretely and uniformly heated channels are performed and all the prime findings are documented in detail. The results that have been considered for comparison include (i) local wall temperature distribution, (ii) peak channel temperature, (iii) mean friction coefficient and (iv) relative contributions of mixed convection and radiation. A few salient concluding remarks based on the above comparison are also provided.

Chapter 6, which, incidentally, is the final chapter of the thesis, presents all the prominent conclusions of the various studies performed in Chapter 4 and Chapter 5**.** Further, certain concrete suggestions that aid in pursuing the present research work in the area of conjugate mixed convection with radiation involving the geometry of a vertical channel are provided at the fag end of this chapter.

1.3 Closure

The present chapter clearly speaks about the background and the motivation concerning the research problem taken up for investigation in the current thesis. It also documents the various relevant features of all the six chapters of the thesis, which helps in providing an idea to the reader as to what is in store for him in different chapters of the thesis.

Chapter 2

Literature Review

2.1 Introduction

As spelt out in the previous chapter, the research problem being taken up in the current thesis addresses interaction between conjugate mixed convection and surface radiation. Keeping this in mind, a comprehensive review of literature concerning vertical channel geometry has been performed. The literature review is basically split into two components, with the first specifically addressing convection (free, forced or mixed) vis-à-vis channel geometry, while the second catering to multi-mode heat transfer (internal conduction together with either convection alone or both convection and radiation). In what follows, an exhaustive summary of the literature review would be provided.

2.2 Literature Addressing Convection

Elenbaas (1942) takes the credit as the one, who initially came out with the work on channels, reporting the experimental findings of free convection in a vertical symmetrically heated isothermal channel employing air as the cooling medium in his bench mark paper. He also gave a semi-empirical correlation for average Nusselt number based on the width of the channel and inverse of the aspect ratio, which, in turn, was defined as the ratio of the wall height to the channel width. This work of Elenbaas, though related to free convection, is provided in the current literature review addressing mixed convection from a channel owing to the fact that it was Elenbaas, who appears to have initiated the research on channel problems.

Tao (1960) contributed to mixed convection in channels in the first notable work of its kind by providing an analytical solution to mixed convection in a vertical channel assuming the flow to be laminar and fully-developed and further considering a constant wall temperature gradient axially.

A study on combined free and forced convection in a vertical rectangular channel has been performed by Agrawal (1962), where he used variational method and also compared his results with the exact solutions reported in the literature. He, subsequently, extended the same method to study mixed convection in circular ducts.

Approximate analytical solutions for constant-property laminar mixed convection from thermally symmetric as well as asymmetric vertical channels have been presented by Quintiere and Mueller (1973). Free convection has been tackled by them for the geometry of a thermally symmetric channel with uniform wall temperature or with step change in wall temperature and for the geometry of an asymmetric channel with uniform and unequal wall

temperatures. Forced and mixed convection cases are addressed for a thermally symmetric and uniform temperature boundary condition.

Yao (1983) reported an analytical solution for combined convection in the entry region of a heated vertical channel. He considered both constant wall temperature and constant wall heat flux conditions. He indicated that, for the case of constant wall temperature, free convection would be dominant if Gr > Re, and for the case of constant wall heat flux it would happen when Gr^2 > Re.

A few pertinent composite relations for mean Nusselt number for free convection in a vertical channel have been documented by Bar-Cohen and Rohsenow (1984), where they tackled both symmetric and asymmetric constant temperature or constant heat flux boundary conditions. They further arrived at an expression for the optimum spacing of the plates and the corresponding optimum Nusselt number for each of the above conditions.

A numerical solution bringing out the role of buoyancy in influencing the hydrodynamic as well as thermal parameters pertaining to the problem of laminar and vertically upward combined forced and free convection flow of a gaseous medium in a channel has been reported by Aung and Worku (1986a). They solved, making use of the boundary layer approximations, the governing parabolic partial differential equations through an implicit finite difference technique coupled with a marching procedure. Their prime conclusion was that buoyancy dramatically increases the hydrodynamic entrance length, while it diminishes the thermal development distance. Making use of an analytical solution for fully developed flow, they provided criteria for the occurrence of flow reversal.

Aung and Worku (1986b) extended their study to the fully developed mixed convection flow for the case, where the channel walls are maintained at uniform symmetric or

asymmetric temperatures and evolved expressions for dimensionless vertical velocity and bulk temperature distributions across the channel. Even here too, like in their previous work, which is presented above, they based their analysis on the boundary layer approximations and fully developed flow assumption. A buoyancy parameter has been defined as the ratio of Grashof number to Reynolds number by them and they gave results for typical values of this parameter ranging between 0 and 750.

Aung and Worku (1987) came out with a numerical solution to laminar combined free and forced convection in a vertical channel dealing with asymmetric yet uniform surface heat fluxes. They noticed that there would be no reversal of flow for values of buoyancy parameter (defined as above) upto as high as 500 in contrast to the case of asymmetric but uniform wall temperatures.

An analytical solution to the problem of laminar fully-developed mixed convection catering to a vertical channel has been provided by Hamadah and Wirtz (1991). They considered opposing buoyancy and deduced closed-form solutions for velocity and plate heat transfer for three sets of temperature boundary conditions. They also established certain criteria for reversal of flow.

Barletta (1998) reported his studies on mixed convection flow in a vertical channel where he took the viscous dissipation effect into reckoning and focused his work on to fully-developed flow regime. The problem has been solved by him for the case, where the two boundaries were considered to be isothermal, maintained either at equal or at different temperatures. He obtained the velocity and temperature fields as well as Nusselt number using the perturbation series method that employs a perturbation parameter proportional to the Brinkman number.

The experimental heat transfer measurements and analysis pertaining to mixed convection in a vertical square channel have been presented by Dutta et al. (1999). They made use of asymmetric heating condition and selected the water flow directions such that buoyancy either aids or opposes the bulk flow pressure gradient. The heat transfer coefficient distributions were observed to be distinct from those for symmetrically heated channels that were attributed to the formation of buoyancy driven large-scale flow structures.

Barletta and Zanchini (2001) studied, analytically, the fully developed laminar mixed convection of a Newtonian fluid with temperature dependent viscosity in an inclined plane channel with prescribed wall temperatures. They revealed that the changes of viscosity with temperature may yield relevant effects on the dimensionless velocity distribution and on the friction factors even in the case of forced convection, while, for dimensionless pressure drop, it becomes important only when it is coupled with that of buoyancy forces.

Higuera and Ryazantsev (2002) presented an analysis of the laminar natural convection flow due to a localized heat source on the centerline of a long vertical channel or pipe whose walls are kept at a constant temperature. They studied both infinitely long and finitely long channels and found an optimal height of the channel that provides maximum mass flux and minimum temperature for a given heat release rate.

Desrayaud and Fichera (2003) numerically predicted the heat transfer and fluid flow characteristics for laminar natural convection in a vertical channel with a two-dimensional protruding heat-flux module located along one of its walls. They even deduced a composite correlation for the module temperature as a function of all the pertinent parametric variables.

Gunes and Liakopoulos (2003) investigated three-dimensional free convection of a Boussinesq fluid with Prandtl number 0.71 in a vertical channel with spatially periodic, flush-

mounted heat sources making use of spectral element method. They presented the distributions of temperature and velocity and the variations of maximum temperature, maximum velocity and local Nusselt number for the values of Grashof number in the range $0.1 \leq Gr \leq 5\times10^4$. They also provided instantaneous as well as time-averaged solutions for time-dependent flows.

Olsson (2004) considered buoyancy driven flow in vertical channels with the range for Rayleigh number chosen to address from fully developed duct flow to isolated plate boundary layer flow for the boundary conditions of uniform heat flux and uniform wall temperature. He even predicted Nusselt number and flow rate and probed into the influence of Rayleigh number and plate separation on the fluid flow rate.

Bhowmik et al. (2005) performed steady state experiments in order to study convective heat transfer in a vertical rectangular channel containing an array of four in-line square chips flush-mounted on one of the walls simulating discrete heating of the wall making use of water as the cooling medium. They covered a wide range of Reynolds numbers and considered laminar flow under free, mixed and forced convection conditions. They investigated the effects of heat fluxes, flow rates and geometric parameters on various results.

da Silva et al. (2005) used constructal method to determine the optimal distribution and sizes of discrete heat sources in a vertical open channel cooled by natural convection. They considered two classes of geometries, viz., (i) heat sources of fixed size with a fixed heat flux and (ii) a single heat source of variable size with a fixed total heat current. They presented their findings for maximizing the global thermal conductance between the wall and the cold fluid.

Hernandez and Zamora (2005) investigated, numerically, the effects of variable properties and non-uniform heating on laminar air flow induced by natural convection in vertical channels. They employed an elliptic model taking into account the effects of variations in density, viscosity and thermal conductivity and compared the results with those obtained using the Boussinesq approximation and constant thermo physical properties. They compared their numerical results for the critical wall heat flux with analytically derived estimations.

Baskaya et al. (2005) investigated, experimentally, mixed convection heat transfer inside a horizontal rectangular channel equipped with 8×4 flush-mounted discrete heat sources in the lower wall that was subjected to uniform heat flux, while the sidewalls and the upper wall were insulated and adiabatic. They reported, for a fixed aspect ratio, the effects of Reynolds and Grashof numbers on the surface temperature and Nusselt number distributions. They pointed out that the temperatures of heat sources level off and even drop as a result of heat transfer enhancement with increase in the buoyancy affected secondary flow and the onset of instability.

Dogan et al. (2006) reported studies pertaining to mixed convection heat transfer from the configuration as discussed above in Baskaya et al. (2005). However, unlike in the preceding work, here, the effect of change in aspect ratio is studied for various Reynolds and Grashof numbers. They came out with the findings pertaining to the buoyancy affected secondary flow and the onset of instability in the light of change in aspect ratio.

A numerical investigation into laminar free convection involving fluids with far lower Prandtl numbers (liquid metals) for the geometry of a vertical channel having a constant heat flux condition has been contributed by Campo et al. (2006). They presented the velocity and temperature profiles and correlations for dimensionless induced flow rate, maximum

dimensionless wall temperatures, and average Nusselt numbers. The numerical results were compared with the experimental results obtained by them.

Yucel and Guven (2007) numerically investigated the problem of two-dimensional laminar forced convection cooling of heat generating obstacles mounted on adiabatic walls in a parallel-plate channel. They considered the effect of insertion of a porous matrix between the blocks on heat transfer and simulated the temperature and velocity distributions in the problem domain addressing incompressible steady flow.

Yadav and Kant (2007a) presented comparative analysis of numerical and experimental data for an array of heated modules mounted on a simulated printed circuit board (PCB) serving as one of the walls of a vertical channel with the other wall kept insulated. The channel was subjected to buoyancy assisted convection cooling in air considering moderate to high flow velocities and range of heat fluxes resembling those occurring in electronic cooling applications. They studied the effect of array size and substrate thermal conditions on heat transfer characteristics and proposed an empirical relation for Nusselt number within the parametric ranges considered.

In a parallel study, the same authors [Yadav and Kant (2007b)] investigated, numerically and experimentally, the effect of partial and mixed uniform heat flux (UHF) and uniform wall temperature (UWT) heating conditions on a buoyancy assisted convection cooling of a channel configuration described above considering similar ranges for Reynolds number and heat flux. They analyzed the data for various patterns of heat flux and Nusselt number and empirically predicted the Nusselt number under the heating conditions mentioned.

Laminar mixed convection in a vertical channel with a finite section of a linearly varying wall temperature is numerically investigated by Chang (2007). He reported the variations of local velocity, temperature and local as well as average Nusselt numbers to demonstrate the influence of parameters that include Reynolds number, Grashof number and the degree of wall temperature variation. He proposed a correlation to predict Nusselt number and found that it is larger with a linearly increasing wall temperature than that with a linearly decreasing wall temperature.

A study on combined free and forced convection involving the geometry of an oblique channel mounted with three discrete heaters along its bottom wall has been provided by Guimaraes and Menon (2008). They found that the inclination angle has a stronger influence on flow and heat transfer for low Reynolds numbers with the lowest temperature distribution noticed on the modules for the inclination angles of 45° and 90°.

An analysis on combined free and forced convection in a vertical channel that has two finite discrete heat sources provided along one of its walls has been made by Ermolaev and Zhbanov (2009). They employed two-dimensional numerical technique in their work and reported the role played by the distance of separation of the heat sources on both flow and temperature fields.

Aminossadati and Ghasemi (2009) investigated, numerically, mixed convection heat transfer in a two dimensional horizontal channel with an open cavity with a discrete heat source located on one of its walls. They considered three different heating modes, which relate to the location of the heat source on three different walls of the cavity. They performed their studies with a wide range of Richardson numbers and aspect ratios.

Ichimiya and Matsushima (2009) performed a numerical analysis on the effect of inclination angle on mixing flow in a square channel with uniform temperature walls. They solved the three-dimensional governing equations for Re = 100 and Pr = 0.72 and various inclinations (from −90° to 90°). They evaluated the thermal performance using the relationship between Nusselt number ratio and pressure loss ratio with and without buoyancy induced flow as a function of inclination angles.

Roeleveld et al. (2009) studied laminar free convection in an isothermal asymmetrically heated vertical channel and developed empirical correlations for the average Nusselt number for each of the channel walls separately. They obtained a numerical solution for a Prandtl number of 0.71 and for Rayleigh numbers ranging from the conduction regime to the isolated boundary layer regime.

Ramjee and Satyamurty (2010) came out with their study on forced convection between two parallel surfaces at non-identical wall temperatures considering the fluid to be Newtonian with constant thermophysical properties and involved in steady, incompressible and stream-line flow. They presented the plots to obtain the heat transferred from each of the walls, which serve the purpose of mean Nusselt number and further suggested the downstream boundary condition that is applicable for the thermal field.

A numerical investigation into laminar free convection heat transfer in the vertical parallel-plate channel with asymmetric heating has been performed by Terekhov and Ekaid (2011). They obtained numerical solution for a Prandtl number of 0.71 and aspect ratio of 10, while the modified Rayleigh number and heating ratio were varied. They solved the fully elliptic Navier-Stokes and energy equations using finite volume technique with a staggered grid arrangement.

Poskas et al. (2011) made an experimental investigation into the local opposing mixed convection heat transfer in a vertical flat channel with symmetrical heating in laminar-turbulent transition region. They noticed a sharp increase in heat transfer in the region with vortex flow compared to that with turbulent flow.

Parametric studies on mixed convection addressing the geometry of a vertical, isothermal, parallel-plate channel have been made by Sun et al. (2012). They attempted to come out with an optimum spacing that yields maximum heat flux transferred from the above channel that is cooled by combined free and forced convection. They considered air as the cooling agent and made calculations for buoyancy-aided convection assuming a pressure drop at the channel exit instead of opting a constant flow rate.

El-Morshedy et al. (2012) documented their heat transfer results concerning free convection in a vertical channel that resembles the cooling channel of a general material testing reactor in their experimental work. They also developed a correlation for the prediction of the local Nusselt number.

Dritselis et al. (2013) reported the effect of a spaciously periodic thermal boundary condition on laminar combined forced and free convection upward flow taking place in a two-plate vertical channel. They presented the effects of the Grashof and Reynolds numbers, the channel length and the wavelength of the periodic temperature distribution at the colder wall on the flow and thermal characteristics.

Roeleveld et al. (2014) constructed an experimental model to study free convection of air in a vertical channel with antisymmetrical heating, where the hot wall is heated above the ambient temperature by the same amount that the cold wall is cooled below the ambient, giving equal but opposing buoyancy forces inside the channel. They determined the local and

average Nusselt numbers and compared their results with numerical predictions obtained using ANSYS FLUENT. They found that the average convective heat transfer can be approximated using an existing correlation for a sealed tall enclosure available in the literature.

2.3 Literature Addressing Multi-Mode Heat Transfer

Since the present thesis aims at investigating the interplay between all the three modes of heat transfer, viz., conduction, mixed convection and radiation, a broad look into the literature concerning multi-mode heat transfer addressing the geometry of a vertical channel is made here.

Carpenter et al. (1976) appear to be the most significant initial researchers on the above kind of problems. They numerically investigated into the contributory role of radiation in developing laminar natural convection through a vertical channel whose walls have non-symmetric yet uniform heat fluxes. Radiation to the inlet-exit and the cooler opposing entrance walls was found to be significantly altering the non-radiation results by reducing the maximum wall temperature by as much as 50%. They even experimentally verified the numerical results obtained by them.

A vertical channel provided with one constant temperature wall and one insulated wall has been handled by Sparrow et al. (1980) numerically, where they attempted to tackle developing natural convection coupled with radiation. Their main finding was that the heat transfer enhancements of the order of 50 to 70% could be obtained considering the effect of radiation. They further claimed that radiation raises the temperature of the adiabatic wall transforming it into an active convective surface.

A numerical study highlighting the role of plate conduction on natural convection taking place in an asymmetrically heated vertical channel for the configuration of uniform plate temperature is reported, numerically, by Anand et al. (1990). A range of geometric, wall conduction and heat transfer parameters were addressed by them with calculations made for the Grashof number range of $10\text{-}10^6$. They observed a significant impact of wall conduction on heat transfer at large Grashof numbers, low conductivity ratios and high wall thickness to channel width ratios.

A numerical probe into the role of material conductivity in natural convection occurring in an asymmetrically heated vertical channel for uniform heat flux configuration has been documented by Kim et al. (1990). They used an implicit finite difference scheme to solve the governing equations. They observed a maximum increase of 30% in mass flow rate of air for symmetric heating due to wall conduction, while the decrease in the average Nusselt number was found to be by 22%.

A numerical analysis of laminar free convection heat transfer and fluid flow in channels formed between series of vertical parallel plates with embedded line heat sources was reported by Kim et al. (1991). They studied the effect of the repeated temperature boundary condition along the surfaces of the plates that was not known to begin with but had to be obtained as a part of the solution. They also looked into the role of wall conduction on all pertinent results. The salient results that they reported include the mass flow rate, the maximum surface temperature and the average Nusselt number. It was demonstrated that the repeated boundary condition decreases the maximum hot surface temperature while showing an opposite effect on the colder surface. They further concluded that the channels subjected to a repeated boundary condition approach symmetrically heated channels subjected to uniform

wall temperature conditions for the ratio of the solid to fluid thermal conductivity greater than (or equal) to 100.

A series of conducting plates equipped with heat generating blocks and employing air as cooling medium has been tackled for both fluid and heat flow, numerically, by Kim and Anand (1994). They solved the governing equations using finite volume technique and observed that the thermal entry length decreases with increase in substrate conductivity. They characterized the thermal performance of the channel in terms of thermal resistance per unit length of the channel.

A numerical work on laminar forced convection taking place in a parallel-plate array equipped with multiple heaters has been attempted by Kim and Anand (1995). They solved the governing equations by using finite volume technique for a wide range of independent parameters with air as the working medium. They found that the thermal resistance decreases with an increase in substrate conductivity upto a particular value of k_s/k_f, and beyond this value, the thermal resistance did not undergo a further decrease. They further observed that the value of k_s/k_f that does the above is a function of geometric parameters and typically lies between 1 and 10.

Hacohen et al. (1995) studied, both experimentally and numerically, the development of boundary layer and the heat transfer coefficients in different thermally simulated electronic components for both forced and free convection conditions in a channel. They studied the roles of different parameters including the channel geometry, the component array height, the air flow rate and the heat flux on local heat transfer coefficient.

Watson et al. (1996) numerically modeled laminar steady state buoyancy aided mixed convection between a series of vertical parallel plates by including wall conduction. Each

plate was considered to be having a planar (or sheet) heat source on one of the surfaces that manifests itself as a line source in a two-dimensional environment.

Conjugate mixed convection with surface radiation from a vertical channel equipped with a flush-mounted discrete source in each of its walls has been solved through finite volume method by Gururaja Rao et al. (2002). They considered a very wide range of parameters, including aspect ratio, modified Richardson number, surface emissivity and thermal conductivity, and studied the effects that these parameters showed on various fluid flow and heat transfer results. They deduced useful correlations for certain non-dimensional dependent parameters based on a large set of numerical data generated by them.

Cadafalch et al. (2003) carried out numerical computations to obtain a correlation for free convective heat transfer in large air channels bounded by one isothermal plate and one adiabatic plate. They considered surface radiation between plates and different inclination angles and validated their numerical results using their own experimental fluid flow and heat transfer data.

Avelar and Ganzarolli (2004) performed an experimental and numerical analysis on conjugate conduction-convection heat transfer problem in an array of vertical parallel-plates with heated protruding elements attached to one of the walls. They considered uniform and non-uniform heating of the plates and the distance between the plates and the power dissipated per plate were varied. They observed a good agreement between numerical and experimental temperature profiles.

Bahlaoui et al. (2005) studied, numerically, mixed convection coupled with radiation in an inclined channel with fixed aspect ratio that is locally heated from one side. They evaluated convective, radiative and total Nusselt numbers on the cold surface and at the exit

of the channel for different combinations of governing parameters, namely surface emissivity, Reynolds number, inclination of the channel with respect to the horizontal surface and Rayleigh number. They showed that the flow structure gets significantly altered by radiation.

Ko and Anand (2007) simulated, numerically, three-dimensional combined laminar forced convection and radiation heat transfer in a channel. They presented the effects of Reynolds number, conduction-radiation parameters, absorption coefficient and scattering albedo on the Nusselt number and bulk temperature profiles along the channel. It is reported that radiation shows a major impact on temperature field in the range of parameters considered by them.

Madhusudhana Rao and Narasimham (2007) reported a numerical study on conjugate mixed convection from protruding heat generating ribs attached to substrates (printed circuit boards) forming a series of vertical parallel plate channels. They performed parametric studies by varying the heat generation based Grashof number and the fan velocity based Reynolds number with air as the working medium. Correlations were suggested for natural convection induced mass flow rate in mixed convection and the maximum dimensionless temperature. For the parametric values considered, the heat transferred to the working fluid via substrate heat conduction is found to be accounting for 41%-47% of the heat removal from the ribs.

Puangsombut et al. (2007) reported an experimental study of free convection in an inclined rectangular channel at a fixed tilt angle of 15°. They provided uniform constant heat flux to the upper plate, while a radiant barrier was attached to the lower plate. The channel was tested by varying the aspect ratio and the uniform heat flux supplied to the upper plate with an objective to determine the heat transfer coefficient and the induced air flow rate. They developed correlations for the Nusselt and Reynolds numbers as a function of Rayleigh

number and aspect ratios. Heat transfer enhancement due to the radiant barrier was assessed by comparison to a channel equipped with gypsum board.

Barletta et al. (2008) studied the problem of conjugate heat transfer in a parallel-plate channel considering laminar forced convection for the boundary condition that has a temperature distribution on the external side of the channel wall. They determined, both analytically and numerically, the temperature field in the fluid as well as the local and average values of Nusselt number.

Cherif et al. (2009) provided a systematic comparison between experimental and numerical results for turbulent forced convection in a horizontal channel having a cold isothermal lower test plate and an isothermally heated black coated upper plate that provides a controlled radiative heat flux on the lower test plate. They presented the profiles for the heat flux for different Reynolds numbers in the flow direction along the lower plate and also the influence of the presence of an obstacle on the heat flux.

Barhaghi and Davidson (2009) studied mixed convection boundary layer in a vertical channel using large-eddy simulation by applying constant heat flux boundary condition to one of the channel walls while the other wall was kept insulated. The governing equations were solved using two approaches, firstly with the Boussinesq approximation and secondly with temperature dependent fluid properties. They concluded that 11% to 15% heat is transferred to the insulated wall via radiation and also that the Boussinesq approximation is not accurate for very large temperature differences.

Bazdidi-Tehrani and Shahini (2009) dealt with the numerical analysis of combined mixed convection-radiation heat transfer within a vertical channel, taking into account all radiative properties (i.e., emitting, scattering and absorbing). They investigated the influence

of radiation parameters, namely the conduction-radiation parameter and optical thickness, on the occurrence of flow reversal and found that the flow reversal is considerably affected by these parameters.

Barletta et al. (2009) dealt, both analytically and numerically, with the laminar fully developed forced convection in a parallel-plane channel by taking into account the effect of heat conduction in the channel walls. On the external boundary of the channel walls, the heat flux that varies longitudinally with sinusoidal law was prescribed. They evaluated the local and average Nusselt numbers in a longitudinal period.

Premachandran and Balaji (2011) reported the results of their numerical investigation into conjugate mixed convection with radiation from a vertical channel with discrete protruding heat sources mounted on the right wall of the channel. They considered the flow to be laminar and two-dimensional treating it to be developing hydrodynamically as well as thermally.

The contribution of radiation shown on turbulent combined free and forced convection through a horizontal channel has been investigated by Sakurai et al. (2012) employing direct numerical solution technique. It is found that the flow structure and the temperature distribution in the channel change with an increase in the optical thickness of the fluid.

Developing laminar combined free and forced convection flow of a gaseous medium in an asymmetrically heated vertical channel together with wall radiation is handled by Al-Amri and El-Shaarawi (2012). The effect of radiation on temperature distribution, average friction factor and Nusselt number is presented along with the other studies. They also obtained the values of emissivity pertaining to minimum pumping power and the threshold values of emissivity at which one can ignore radiation effects.

Alves and Altemani (2012) worked on a channel comprising parallel-plates and having steady, constant-property and stream-line flow of air through it and came out with their numerical results on coupled conduction-forced convection. They considered an array of two-dimensional heaters protruding from the lower plate (substrate) of the channel. The temperatures of discrete protruding heaters were related to independent power dissipation in each heater with conjugate influence coefficients. They presented the effect of the substrate thermal conductivity, the channel Reynolds number and the height of heaters relative to the height of the channel on the above coefficients.

Amirouche and Bessaih (2012) performed parametric studies on three-dimensional turbulent free convection taking place in a channel. They considered five cubic aluminum heaters resembling electronic components that are equally spaced vertically along the channel. They employed finite volume method to solve the pertinent equations for the above coupled heat transfer problem considering relevant boundary conditions. They studied the influence of Rayleigh number, ratio of air to solid thermal conductivities and other geometric parameters on heat transfer. They concluded that a better cooling is obtained when the Rayleigh number is increased and when the thermal conductivity and the spacing between the vertical walls of the channel are decreased.

An investigation, numerically, has been executed by Madhusudhana (2012) into three-dimensional free convection addressing a vertical channel comprising multiple heat sources on opposite substrate walls. He reported the pertinent fluid and heat flow characteristics considering different Grashof numbers. He examined the effects of spacing between the heated walls, spacing between heaters and substrate conductivity on fluid flow as well as heat transfer. He presented correlations for dimensionless mass flow rate, maximum temperature and average Nusselt number.

The role exhibited by radiation in laminar flow originated in a vertical channel heated asymmetrically has been numerically elucidated by Li et al. (2013) using air as the cooling agent. They accounted for variable property effects and showed that the general effect of surface radiation is to delete the onset of pocket like recirculation at the top part of the channel, to reduce the heated wall temperatures and to increase the facing wall temperatures.

A numerical investigation into mixed convection in air due to the interaction between a buoyancy flow and the flow induced by a moving plate in a vertical channel is carried out by Andreozzi et al. (2013). The effects of the channel spacing, heat flux and moving plate velocity are investigated and results in terms of temperatures of the channel walls and moving plate, air velocity profiles inside the channel, wall stresses along the channel walls and the moving plate and Nusselt numbers are provided.

Bouttout et al. (2014) performed numerical studies on hydrodynamic amplification and thermal instabilities by imposing pulsation during forced convection of air cooling of nine identical heated blocks mounted on a horizontal channel. One salient feature of their studies is that they obtained the band frequencies, where the enhancement factor for all electronic components varies from 25% to 55% compared with steady non-pulsation flow.

2.4 Conclusions from Literature Review

A thorough review of literature on mixed convection and multi-mode heat transfer concerning the geometry of a vertical channel makes it clear that the problem of conjugate mixed convection with surface radiation from a vertical parallel-plate channel with multiple non-identical discrete heat sources mounted asymmetrically along its walls has not been adequately explored. One rarely finds studies aiming at solving the above kind of problems

not resorting to the usually made boundary layer approximations. Also, very few studies are available that have provided correlations for the maximum and average channel temperatures and the mean friction coefficient.

2.5 Objectives and Scope of the Present Work

The preceding sections provided an exhaustive summary of the literature pertaining to the problem considered in the current thesis work. The above exercise made it quite clear that a number of avenues are still open in the studies pertaining to vertical channel configuration. It is quite obvious that any heat generating electronic component working in a gaseous environment (like ambient air) will make it mandatory to consider the interplay between the heat generated, conducted, convected [by free or forced or mixed convection] and radiated. There seem to be very few works that comprehensively address all the aspects of multi-mode heat transfer from the geometry of the vertical parallel-plate channel with identical discrete heat sources flush mounted asymmetrically along its walls. Not many studies tried to evolve the correlations for pertinent dependent parameters as functions of the appropriate independent parameters. In view of the above, the present research work has been taken up to make a comprehensive numerical investigation into conduction-mixed convection-radiation from a discretely and asymmetrically heated vertical channel. The prominent objectives of the work thus taken up include:

1. To solve the fluid flow and heat transfer equations governing the above problem without making use of the boundary layer approximations and the fully developed flow assumption.

2. To write a computer code exclusively for solving the research problem making use of finite volume method.

3. To deduce the correlations for the heat transfer parameters, viz., non-dimensional maximum channel temperature and non-dimensional average channel temperature, which throw light on the degree of cooling needed to be provided for a given working configuration.

4. To generate the correlation for computing the mean friction coefficient along the channel for the above problem that serves as an input in the calculation of the pumping power needed to be expended to induce the fluid flow through the channel.

5. To probe into the effects of various pertinent parameters including modified Richardson number, thermal conductivity, surface emissivity and aspect ratio on all the results concerning the problem. In this context, the prominent results considered include local wall temperature distribution, peak channel temperature, local drag coefficient and mean friction coefficient.

6. To estimate the relative contributions of mixed convection and surface radiation in channel heat dissipation in the entire mixed convection regime. These calculations help in substantiating the role surface radiation exhibits in carrying the mandated heat load on the cooling system.

7. To extract the singular role played by surface radiation in various results of fluid flow and heat transfer pertaining to the problem.

8. To calculate the buoyancy component in heat dissipation from the channel as well as the friction coefficient along the walls of the channel in all the regimes of convection.

This exercise throws light on the significance, if any, of buoyancy in influencing the results related to the problem.

9. To make a comparative study between the configurations possessing a discretely heated channel and the channel that has uniform heating. The prime parameters that would be looked into in the above comparison include local and maximum channel temperatures, mean friction coefficient and contributory roles of convection and radiation in heat dissipation. These comparative studies are to be invariably performed for an identical net rate of heat generation in the channel.

It is to be noted here that the problem taken up in the current thesis and the results presented therein are fundamental in their nature, with their implications perceived in the cooling of electronic equipment and devices.

2.6 Closure

A comprehensive review of the literature concerning the geometry of a vertical channel taking part in (i) mixed convection and (ii) mixed convection with conduction and without or with surface radiation has been documented in the present chapter. In conclusion to the literature review, the factors that prove the appropriateness of consideration of the present research problem are provided. The different principal objectives of the current research work are provided, which helps in knowing as to what can be expected in the thesis. The ensuing chapter (**Chapter 3**) is devoted to the problem definition, its mathematical formulation, boundary conditions and broad solution methodology catering to the problem on hand.

Chapter 3

Mathematical Formulation and Solution Methodology

3.1 Introduction

The present chapter commences with details of problem definition, which would be followed by mathematical formulation addressing both fluid flow and heat transfer. A general treatment of the governing equations would be given and a detailed look at different boundary conditions follows the above. The method of solution employed to tackle the governing equations together with the relevant boundary conditions follows subsequently.

3.2 Mathematical Formulation

The research problem proposed to be dealt with in the current thesis belong to steady, two-dimensional, laminar, mixed (combined free and forced) convection with conduction as well

as surface radiation taken into consideration. The cooling agent considered is air that is assumed to be of constant thermophysical properties subject to the Boussinesq approximation. As mentioned already, the geometry considered in the research problem, which would be exhaustively investigated in **Chapter 4**, is a vertical parallel-plate channel that has ten identical discrete heat sources, with five in each wall, flush-mounted asymmetrically along the walls. Figure 3.1 provides the schematic of the problem geometry taken up, along with the system of coordinates.

As may be noticed from the figure, the heat that is generated in the ten identical discrete heat sources is initially conducted along the walls of the channel before getting dissipated by mixed convection and radiation. Thus, the problem is a classical multi-mode heat transfer problem having heat generation, conduction, convection (free, forced or mixed) and radiation. The wall thickness is fairly small compared to rest of its dimensions resulting in one-dimensional (axial) conduction along the walls of the channel.

The fundamental governing equations for fluid flow and heat transfer concerning the problem are (i) the continuity equation, (ii) the two momentum equations and (iii) the equation of energy. These equations are available in various references [e.g. Bejan (1984)] and they are listed, hereunder, in primitive variables:

$$\frac{\partial u}{\partial x} + \frac{\partial v}{\partial y} = 0 \tag{3.1}$$

$$u\,\frac{\partial u}{\partial x} + v\,\frac{\partial u}{\partial y} = -\frac{1}{\rho}\,\frac{\partial P}{\partial x} + \nu\left(\frac{\partial^2 u}{\partial x^2} + \frac{\partial^2 u}{\partial y^2}\right) + g\left(\frac{\rho_\infty}{\rho} - 1\right) \tag{3.2}$$

$$u\,\frac{\partial v}{\partial x} + v\,\frac{\partial v}{\partial y} = -\frac{1}{\rho}\,\frac{\partial P}{\partial y} + \nu\left(\frac{\partial^2 v}{\partial x^2} + \frac{\partial^2 v}{\partial y^2}\right) \tag{3.3}$$

$$u\frac{\partial T}{\partial x}+v\frac{\partial T}{\partial y}=\alpha\left(\frac{\partial^2 T}{\partial x^2}+\frac{\partial^2 T}{\partial y^2}\right) \tag{3.4}$$

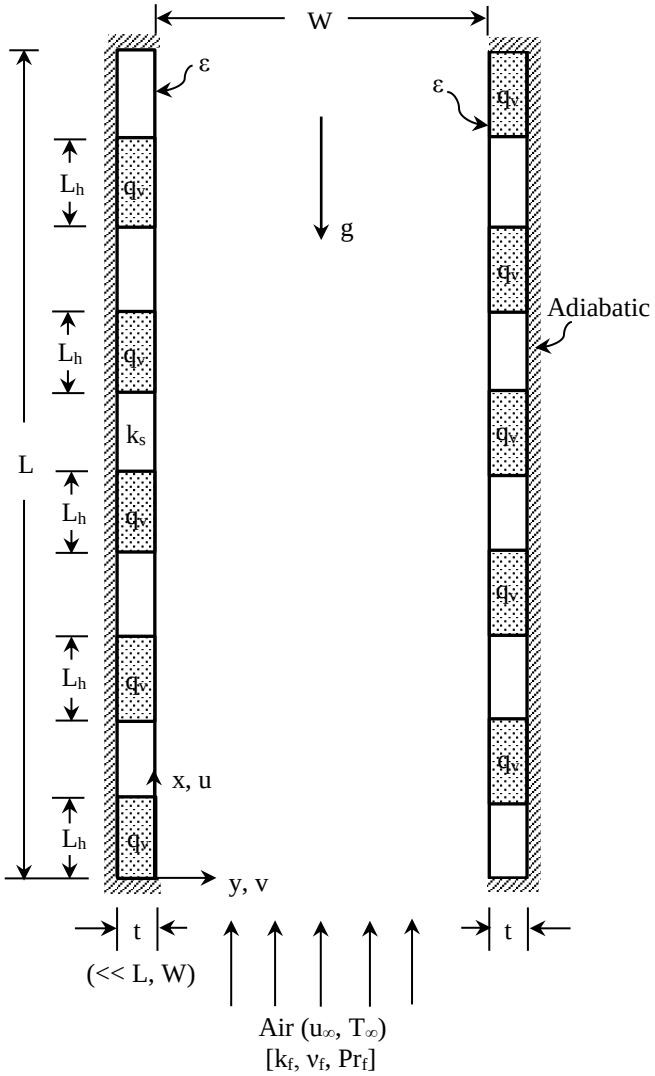

Fig. 3.1 Schematic of the asymmetrically heated vertical channel considered for study along with system of coordinates

In order to impose the Boussinesq approximation, as a first step, the definition of isobaric cubic expansivity (β) of the fluid is considered to be:

$$\beta=-\frac{1}{\rho}\left[\frac{\partial \rho}{\partial T}\right]_P \tag{3.5}$$

The second step involves making an assumption that both temperature and density of the fluid undergo minimal changes in comparison to their corresponding characteristic values, which implies:

$$-\frac{1}{\rho}\frac{(\rho_\infty - \rho)}{(T_\infty - T)} \approx \beta \tag{3.6}$$

The above implies that:

$$(\rho_\infty - \rho)\, g = \rho\, g\, \beta\, (T - T_\infty) \tag{3.7}$$

Upon substituting Eq. (3.7) in Eq. (3.2), the x-momentum equation gets modified into:

$$u\frac{\partial u}{\partial x} + v\frac{\partial u}{\partial y} = -\frac{1}{\rho}\frac{\partial P}{\partial x} + \nu\left(\frac{\partial^2 u}{\partial x^2} + \frac{\partial^2 u}{\partial y^2}\right) + g\,\beta\,(T - T_\infty) \tag{3.8}$$

Now, it is proposed to use the approach that has been suggested and implemented by Gururaja Rao et al. (2000, 2001) and Gururaja Rao (2004). The governing equations in primitive variables provided above are converted into vorticity-stream function (ω- ψ) form. This is done keeping twin objectives in mind. Firstly, it would be possible to eliminate the pressure gradient terms from the Navier Stokes equations and secondly, this would help in bringing down the number of governing equations from four to three. To be able to do this, the basic definitions of stream function (ψ′) and vorticity (ω′) would be considered, which are given by:

$$u = \frac{\partial \psi'}{\partial y} \quad \text{and} \quad v = -\frac{\partial \psi'}{\partial x} \tag{3.9}$$

$$\omega' = \frac{\partial v}{\partial x} - \frac{\partial u}{\partial y} \tag{3.10}$$

Using the above relations for ψ' and ω' and subsequently making relevant mathematical manipulations, the x and y momentum equations combinedly yield the following equation, which is called the vorticity transport equation:

$$u\,\frac{\partial \omega'}{\partial x} + v\,\frac{\partial \omega'}{\partial y} = \nu\left(\frac{\partial^2 \omega'}{\partial x^2} + \frac{\partial^2 \omega'}{\partial y^2}\right) - g\,\beta\,\frac{\partial T}{\partial y} \tag{3.11}$$

Upon substituting the expressions for u and v in the defining relation for ω' above, the following stream function equation would result:

$$\frac{\partial^2 \psi'}{\partial x^2} + \frac{\partial^2 \psi'}{\partial y^2} = -\,\omega' \tag{3.12}$$

The above exercise obviously brings down the number of governing equations concerning the present problem from four to three that are given by Eqs. 3.11, 3.12 and 3.4.

The subsequent step in the mathematical formulation comprises normalization of the above three governing equations making use of the following non-dimensional parameters.

$$X = \frac{x}{W} \quad \text{and} \quad Y = \frac{y}{W} \tag{3.13}$$

$$U = \frac{u}{u_\infty} \quad \text{and} \quad V = \frac{v}{u_\infty} \tag{3.14}$$

$$\psi = \frac{\psi'}{u_\infty\, W} \quad \text{and} \quad \omega = \frac{\omega' W}{u_\infty} \tag{3.15}$$

$$\theta = \frac{(T - T_\infty)}{\Delta T_{ref}} \tag{3.16}$$

Here, ΔT_{ref} is called the modified reference temperature difference and is taken to be equal to $(q_v L_h t)/k_s$, where L_h is the height of each of the discrete heat sources. Substitution of these

non-dimensional parameters in the three governing equations [Eqs. 3.11, 3.12 and 3.4] and subsequent simplification yields the following normalized governing equations:

$$U\frac{\partial\omega}{\partial X}+V\frac{\partial\omega}{\partial Y}=\frac{1}{Re_w}\left(\frac{\partial^2\omega}{\partial X^2}+\frac{\partial^2\omega}{\partial Y^2}\right)-Ri_w^*\frac{\partial\theta}{\partial Y} \tag{3.17}$$

$$\frac{\partial^2\psi}{\partial X^2}+\frac{\partial^2\psi}{\partial Y^2}=-\omega \tag{3.18}$$

$$U\frac{\partial\theta}{\partial X}+V\frac{\partial\theta}{\partial Y}=\frac{1}{Pe_w}\left(\frac{\partial^2\theta}{\partial X^2}+\frac{\partial^2\theta}{\partial Y^2}\right) \tag{3.19}$$

Here, Ri_w^* is called the modified Richardson number, also equally referred to as the modified buoyancy parameter, which is defined as the ratio of modified Grashof number (Gr_w^*) to the square of Reynolds number (Re_w). This modified Richardson number (Ri_w^*) is an important governing parameter indicating the relative dominance of the buoyancy forces in comparison to the inertia forces. It helps in delineating the mixed convection regime into (i) forced convection dominant regime ($Ri_w^* \approx 0$), (ii) pure mixed convection regime ($Ri_w^* \approx 1$) and (iii) free convection dominant regime ($Ri_w^* \approx \infty$).

The above exercise thus culminates with finalization of the governing non-dimensional equations for fluid flow and heat transfer that are now required to be appropriately solved.

3.3 Boundary Conditions

The normalized governing equations concerning the present problem derived as above are elliptic in nature warranting specification of boundary conditions on all the four boundaries. The two channel walls form the solid boundaries, while the entry and exit of the channel are

open (or free) boundaries. It is proposed to use an axially extended computational domain for solving the problem based on certain initial studies performed considering computational domains of different heights. These studies pointed out that an extended computational domain would be very much appropriate in order to capture the physics of fluid flow and heat transfer pertaining to the problem more effectively. This exercise further indicated that it would suffice to use a height of the computational domain equal to two times the channel height (2L) with the width of the domain equal to that of the channel (W) itself. The two dependent parameters, viz., peak channel temperature and mean friction coefficient, became fairly insensitive (within ± 0.24%) beyond a height of 2L with L indicating the height of the channel wall.

It is to be noted that the channel is equipped with a total of ten identical discrete heat sources along its walls. The energy generated in the heat sources gets conducted along the walls and gets subsequently transferred by mixed (free and forced) convection and radiation. Thus, the governing equations for temperature distribution along both the channel walls are to be appropriately deduced. The boundary conditions pertaining to stream function (ψ), vorticity (ω) and temperature (θ) that are employed on all the boundaries of the computational domain for solving the problem are clearly depicted in Fig. 3.2. A detailed discussion on these boundary conditions would be taken up now.

3.3.1 Conditions along the Bottom Boundary

Since the fluid enters the channel from its bottom with uniform velocity u_∞, along the bottom boundary, it follows that $\frac{\partial \psi}{\partial Y} = 1$ or ψ = Y. This indicates that ψ varies linearly along the bottom boundary of the computational domain. Since the flow is irrotational at the entry, the vorticity (ω) along the bottom boundary is taken to be zero here. Further, since the

temperature T_∞ of the fluid entering the channel is uniform, the non-dimensional temperature (θ) here would be zero.

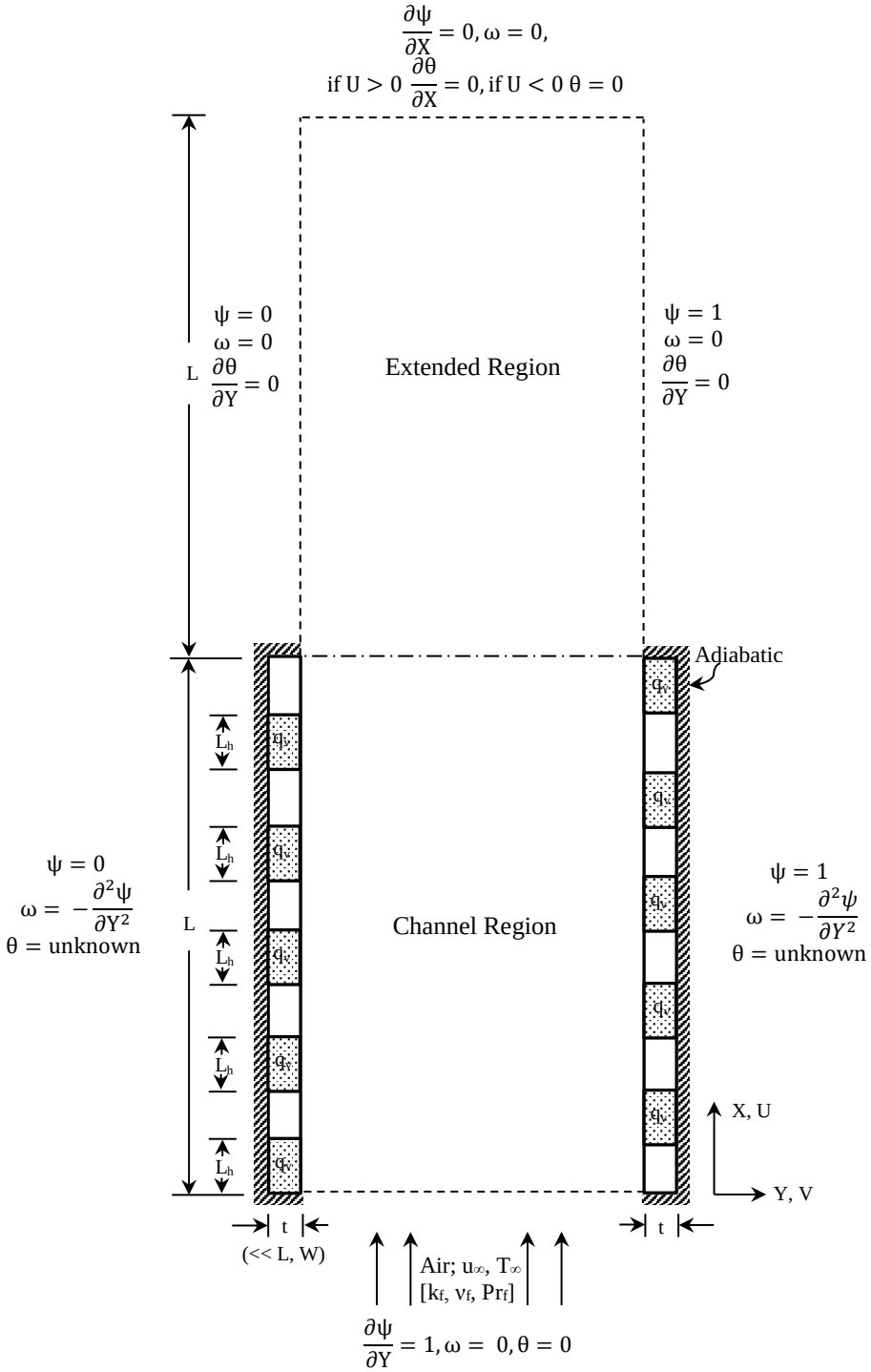

Fig. 3.2 Computational domain used for problem along with the pertinent boundary conditions employed

3.3.2 Conditions along the Left Boundary

Since an axially extended computational domain is employed here, the left boundary has two portions, viz., the first portion that is the channel wall itself and the second one that pertains to the extended length. Thus, the left boundary has a solid boundary accompanied by an open boundary in it. Since the stream function (ψ) is a constant along any solid surface, it is taken to be equal to zero along the channel wall portion. The boundary condition pertaining to vorticity (ω) along the wall is implemented using the approach suggested by Gururaja Rao et al. (2000, 2001). According to this approach, $\omega = -\frac{\partial^2 \psi}{\partial Y^2}$. Since the left wall has heat generation, which is followed by internal conduction and mixed (combined free and forced) convection and radiation at its surface, the temperature (θ) varies along it, which is obtained as a part of the solution to the present problem. The governing equations for temperature distribution along this wall have to be deduced through rigorous energy balance. A separate section (3.3.5) takes up a thorough discussion on the above.

Along the extended portion of the left boundary, the horizontal velocity (V) is assumed to be equal to zero, which means that $\frac{\partial \psi}{\partial X} = 0$. The above, in turn, implies that ψ is a constant along the extended portion of the left boundary. Since ψ is taken to be equal to zero along the left wall portion, the same condition is continued along the extended left boundary as well. As far as vorticity is concerned, the condition of irrotationality is considered to be prevailing over the open extended portion of the left boundary. Therefore, here, one can take ω = 0. As there is no heat transfer across the extended left boundary, owing to the condition of symmetry, the relevant temperature boundary condition in this section turns out to be $\frac{\partial \theta}{\partial Y} = 0$.

3.3.3 Conditions along the Top Boundary

Across the top boundary of the computational domain, $\frac{\partial \psi}{\partial X} = 0$ is used for stream function (ψ), and it looks justified on account of extension of the computational domain by a length equal to the channel height. This implies that the cross or the horizontal velocity (V) is zero along the above boundary. Owing to a similar reason as above, irrotationality condition seems to be valid along this boundary, rendering non-dimensional vorticity (ω) equal to zero. With regard to the boundary condition concerning non-dimensional temperature (θ), when the fluid flow is outward (U > 0), the appropriate condition would be $\frac{\partial \theta}{\partial X} = 0$. However, there could always be a portion of the top boundary that has the fluid getting into, implying U < 0. The condition now becomes $\theta = 0$ under the assumption that the incoming fluid enters at its characteristic temperature (T_∞).

3.3.4 Conditions along the Right Boundary

As with the left boundary, the right boundary also has two portions: (i) channel wall solid boundary and (ii) extended domain open boundary. Along the channel wall portion, the non-dimensional stream function (ψ), which would again be a constant, is taken equal to 1. The non-dimensional vorticity (ω) is calculated using the same wall-vorticity equation as was done with the left wall, viz., $\omega = -\frac{\partial^2 \psi}{\partial Y^2}$. There is heat generation in the right wall too as in the left wall, with the heat again getting dissipated by mixed convection and radiation after its conduction along the wall. Thus, the non-dimensional temperature (θ) varies along the right wall and is obtained as a part of the solution. The governing equations for temperature distribution along the right wall will also be derived as has been done for the left wall making use of energy balance. A detailed discussion on this is taken up in the ensuing section.

As far as the extended portion of the right boundary is concerned, making use of the arguments similar to those used for the extended left boundary, stream function (ψ) is taken to be constant. With $\psi = 1$ used along the right wall portion, the same condition is continued even for the extended right boundary. The boundary conditions regarding vorticity (ω) and temperature (θ) for the extended right boundary are, respectively, $\omega = 0$ and $\frac{\partial \theta}{\partial Y} = 0$, as implemented for the extended left boundary.

3.3.5 Temperature Boundary Conditions along the Channel Walls

To recall from the foregoing section, the nature of variation of local temperature along the two channel walls is obtained making use of energy balance between heat generated, conducted, convected and radiated. It has already been mentioned that the vertical channel taken up here is discretely and asymmetrically heated. Thus, energy balance has been made judiciously on each of the elements concerning the two channel walls. It can be noticed that the left and right walls of the channel together have ten heat source portions and ten non-heat source portions. Further, there are nine interfaces between the heat source and non-heat source portions, other than the top and bottom adiabatic ends, in each of the walls.

Considering a typical interior element of any one of the heat sources in the left wall excluding their ends, one has the various energy interactions as shown in Fig. 3.3. The energy balance on such an element turns out to be:

$$q_v \, t \, \Delta x_{hs} + q_{cond,x,in} = q_{cond,x,out} + q_{conv} + q_{rad} \qquad (3.20)$$

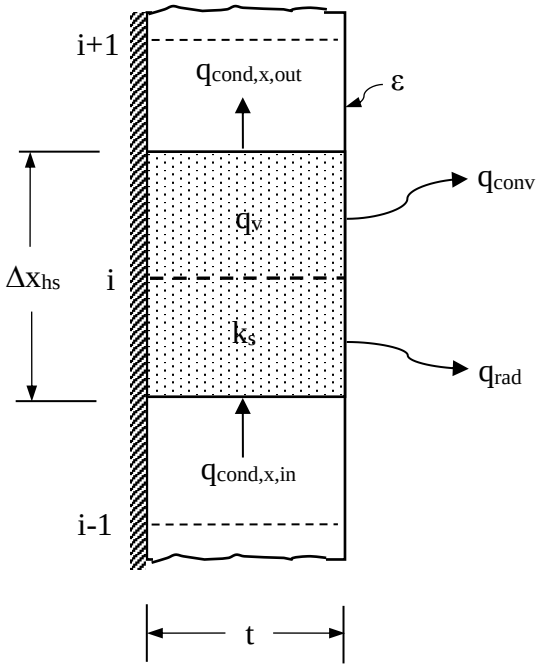

Fig. 3.3 Interior element pertaining to heat source portion of the left channel wall considered for making energy balance

The first term on the right hand side of the above equation is expanded using Taylor's series. Substitution for different terms in the above equation and its subsequent simplification, gives rise to:

$$k_s\, t\, \frac{\partial^2 T}{\partial x^2} + k_f \left(\frac{\partial T}{\partial y}\right)_{y=0} + q_v\, t - \frac{\varepsilon}{1-\varepsilon}\, [\sigma\, T^4 - J_i] = 0 \qquad (3.21)$$

The above equation, after normalization and substitution of relevant parameters, results in:

$$\frac{\partial^2 \theta}{\partial X^2} + \xi \left(\frac{\partial \theta}{\partial Y}\right)_{Y=0} + A_{r1}\, A_{r2} - \frac{\varepsilon}{1-\varepsilon}\, \xi\, I_{RF} \left[\left(\frac{T}{T_\infty}\right)^4 - J_i'\right] = 0 \qquad (3.22)$$

Here, ξ is the thermal conductance parameter that signifies the ratio of the fluid conductance to the solid conductance and is given by $\xi = \frac{k_f\, W}{k_s\, t}$. I_{RF} is the radiation-flow interaction parameter that is defined as the ratio of the black body emissive power to the conduction heat

flux across the fluid layer and is mathematically given by $I_{RF} = \frac{\sigma T_{\infty}^4}{(k_f/W)\,\Delta T_{ref}}$. A_{r1} and A_{r2} are the two non-dimensional geometric parameters, which are defined, respectively, as W/t and W/L_h.

The surface radiation calculations are performed employing the enclosure analysis together with radiosity-irradiation formulation for estimating the radiosities of all the wall elements. J_i' that appears in the last term pertaining to radiation heat transfer in the above equation [Eq. (3.22)], is the non-dimensional radiosity of the i^{th} element. It is defined as the ratio of the radiosity to the black body emissive power and is given by $J_i' = \frac{J_i}{\sigma T_{\infty}^4}$. Here, the general radiosity equation for the i^{th} element of the enclosure is:

$$J_i = \varepsilon \sigma T_i^4 + (1-\varepsilon) \sum_{k=1}^{n} F_{ik} J_k \qquad (3.23)$$

Here, F_{ik} is the view factor from the i^{th} element to the k^{th} element of the enclosure, with n indicating the total number of elements of the enclosure comprised by the four boundaries of the computational domain. The view factors present in the above equations are computed using the crossed-string method of Hottel, the details of which may be seen in various references [e.g., Siegel and Howell (1992)]. The open boundary elements at their respective temperatures are treated to be black having an emissivity equal to unity.

Equation (3.22) provides the temperature distribution along the heat source portions of the left wall of the channel other than the interfaces between the heat source and non-heat source portions and the bottom adiabatic end. The equation that predicts the temperature at the interface between the bottom-most heat source and its immediately adjacent non-heat source portion in the left wall would also be obtained through energy balance as:

$$q_v\, t\, \frac{\Delta x_{hs}}{2} + q_{cond,x,in} = q_{cond,x,out} + q_{conv} + q_{rad} \tag{3.24}$$

Substitution of relevant expressions for different terms in the above equation, non-dimensionalisation and subsequent simplification gives rise to:

$$\frac{\partial^2\theta}{\partial X^2} + \xi\left(\frac{\partial\theta}{\partial Y}\right)_{Y=0} + A_{r1}\, A_{r2}\, \frac{\Delta X_{hs}}{(\Delta X_{hs} + \Delta X_{nhs})} - \frac{\varepsilon}{1-\varepsilon}\, \xi\, I_{RF}\left[\left(\frac{T_i}{T_\infty}\right)^4 - J_i'\right] = 0 \tag{3.25}$$

Similarly, the governing equation for the temperature of the non-heat source portions of the left wall (other than the interfaces and the top adiabatic end) would also arise from energy balance on the pertinent element. It ultimately turns out to be:

$$\frac{\partial^2\theta}{\partial X^2} + \xi\left(\frac{\partial\theta}{\partial Y}\right)_{Y=0} - \frac{\varepsilon}{1-\varepsilon}\, \xi\, I_{RF}\left[\left(\frac{T_i}{T_\infty}\right)^4 - J_i'\right] = 0 \tag{3.26}$$

Further, the governing equations for the temperatures of the bottom and top adiabatic ends of the left wall are obtained separately as:

$$\frac{2}{\Delta X_{hs}}\frac{\partial\theta}{\partial X} + \xi\left(\frac{\partial\theta}{\partial Y}\right)_{Y=0} + A_{r1}\, A_{r2} - \frac{\varepsilon}{1-\varepsilon}\, \xi\, I_{RF}\left[\left(\frac{T_i}{T_\infty}\right)^4 - J_i'\right] = 0 \tag{3.27}$$

$$\frac{2}{\Delta X_{hs}}\frac{\partial\theta}{\partial X} - \xi\left(\frac{\partial\theta}{\partial Y}\right)_{Y=0} + \frac{\varepsilon}{1-\varepsilon}\, \xi\, I_{RF}\left[\left(\frac{T_i}{T_\infty}\right)^4 - J_i'\right] = 0 \tag{3.28}$$

The governing equations catering to the heat source and non-heat source portions of the left wall also address the heat source and non-heat source portions of the right wall with appropriate sign convention employed. The pertinent governing equations for any element in heat source as well as non-heat source portions of the right wall (other than the interfaces between the heat source and non-heat source portions, the bottom adiabatic end and the top adiabatic end) would be obtained, respectively, as:

$$\frac{\partial^2\theta}{\partial X^2} - \xi\left(\frac{\partial\theta}{\partial Y}\right)_{Y=1} + A_{r1}\,A_{r2} - \frac{\varepsilon}{1-\varepsilon}\,\xi\,I_{RF}\left[\left(\frac{T_i}{T_\infty}\right)^4 - J_i'\right] = 0 \tag{3.29}$$

$$\frac{\partial^2\theta}{\partial X^2} - \xi\left(\frac{\partial\theta}{\partial Y}\right)_{Y=1} - \frac{\varepsilon}{1-\varepsilon}\,\xi\,I_{RF}\left[\left(\frac{T_i}{T_\infty}\right)^4 - J_i'\right] = 0 \tag{3.30}$$

Similarly, separate governing equations are required to be deduced for the temperature of the interface elements of heat source and non-heat source portions, the bottom adiabatic end and the top adiabatic end of the right wall, and they, respectively, get evolved as:

$$\frac{\partial^2\theta}{\partial X^2} - \xi\left(\frac{\partial\theta}{\partial Y}\right)_{Y=1} + A_{r1}\,A_{r2}\,\frac{\Delta X_{hs}}{(\Delta X_{hs}+\Delta X_{nhs})} - \frac{\varepsilon}{1-\varepsilon}\,\xi\,I_{RF}\left[\left(\frac{T_i}{T_\infty}\right)^4 - J_i'\right] = 0 \tag{3.31}$$

$$\frac{2}{\Delta X_{hs}}\,\frac{\partial\theta}{\partial X} - \xi\left(\frac{\partial\theta}{\partial Y}\right)_{Y=1} - \frac{\varepsilon}{1-\varepsilon}\,\xi\,I_{RF}\left[\left(\frac{T_i}{T_\infty}\right)^4 - J_i'\right] = 0 \tag{3.32}$$

$$\frac{2}{\Delta X_{hs}}\,\frac{\partial\theta}{\partial X} + \xi\left(\frac{\partial\theta}{\partial Y}\right)_{Y=1} - A_{r1}\,A_{r2} + \frac{\varepsilon}{1-\varepsilon}\,\xi\,I_{RF}\left[\left(\frac{T_i}{T_\infty}\right)^4 - J_i'\right] = 0 \tag{3.33}$$

3.4 Method of Solution Employed

The normalized governing equations for tackling the problem in the present study, as obtained in one of the preceding sections, are non-linear partial differential equations. Solution to these equations is obtained in two stages. In the initial stage of the solution, the governing equations are discretized into finite difference equations making use of the finite-volume method proposed by Gosman et al. (1969). The second stage of the solution comprises solving the set of algebraic equations thus obtained employing the Gauss-Seidel point-by-point iterative technique.

To provide a detailed solution methodology, to begin with, in what follows, the non-dimensional energy equation [Eq. (3.19)] is taken up. The vorticity transport equation [Eq. (3.17)] and the stream function equation [Eq. (3.18)] are also given a similar treatment. Let the final version of the normalized equation of energy be considered as:

$$U\,\frac{\partial\theta}{\partial X}+V\,\frac{\partial\theta}{\partial Y}=\frac{1}{Pe_w}\left(\frac{\partial^2\theta}{\partial X^2}+\frac{\partial^2\theta}{\partial Y^2}\right) \tag{3.34}$$

As is known, the left side terms of the above equation pertain to advection, while the right side terms are the diffusion terms. A finite volume labeled as ne-nw-sw-se is considered with its interfaces mid-way between the neighboring grid points as shown in Fig. 3.4 by dotted lines. An integration of the above equation is performed over the above volume and this result in:

$$\int_{X_s Y_w}^{X_n Y_e}\left(U\,\frac{\partial\theta}{\partial X}+V\,\frac{\partial\theta}{\partial Y}\right)dX\,dY=\frac{1}{Pe_w}\int_{X_s Y_w}^{X_n Y_e}\left(\frac{\partial^2\theta}{\partial X^2}+\frac{\partial^2\theta}{\partial Y^2}\right)dX\,dY \tag{3.35}$$

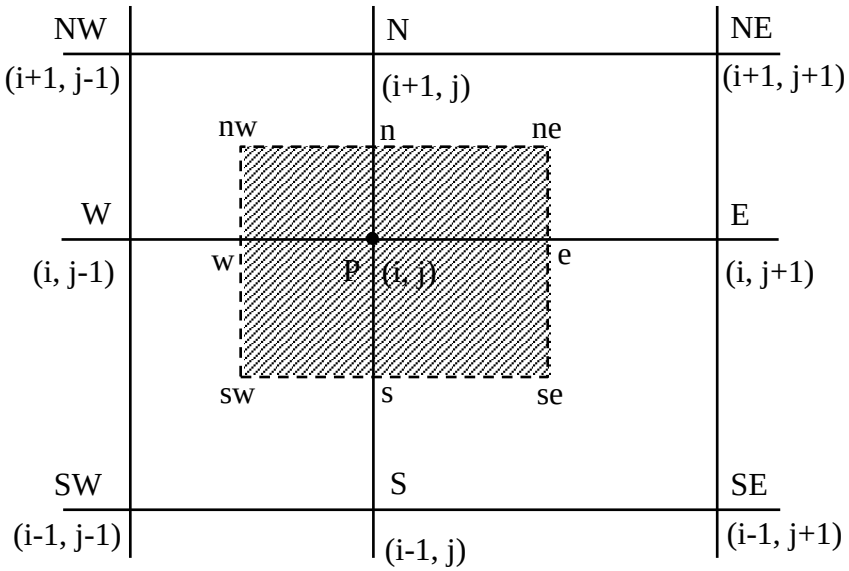

Fig. 3.4 The finite volume considered within the computational domain over which integration is performed

Appropriate simplification of the right hand side portion of the above equation results in:

$$\text{RHS} = \frac{1}{\text{Pe}_w}\left[A_E(\theta_E - \theta_P) + A_W(\theta_W - \theta_P) + A_N(\theta_N - \theta_P) + A_S(\theta_S - \theta_P)\right] \tag{3.36}$$

Here,

$$A_E = \frac{1}{2}\left[\frac{X_N - X_S}{Y_E - Y_P}\right], \qquad A_W = \frac{1}{2}\left[\frac{X_N - X_S}{Y_P - Y_W}\right],$$

$$A_N = \frac{1}{2}\left[\frac{Y_E - Y_W}{X_N - X_P}\right] \quad \text{and} \quad A_S = \frac{1}{2}\left[\frac{Y_E - Y_W}{X_P - X_S}\right]$$

Now, the two advection terms on the left hand side of Eq. (3.35) could be written as:

$$U\frac{\partial\theta}{\partial X} = \frac{\partial(U\theta)}{\partial X} - \theta\frac{\partial U}{\partial X} \quad \text{and} \quad V\frac{\partial\theta}{\partial Y} = \frac{\partial(V\theta)}{\partial Y} - \theta\frac{\partial V}{\partial Y}$$

Substitution of the above on the left hand side of Eq. (3.35) and subsequent simplification gives:

$$\text{LHS} = \iint_{X_s Y_w}^{X_n Y_e} \left\{\frac{\partial(U\theta)}{\partial X} + \frac{\partial(V\theta)}{\partial Y}\right\} dX\, dY \tag{3.37}$$

Now, simplifying the first term of the above equation separately,

$$\iint_{X_s Y_w}^{X_n Y_e} \frac{\partial(U\theta)}{\partial X}\, dX\, dY = \int_{Y_w}^{Y_e} [(U\theta)_n - (U\theta)_s]\, dY \tag{3.38}$$

Further, considering the first term on the right side of the above equation and modifying it as:

$$\int_{Y_w}^{Y_e} (U\theta)_n\, dY = \int_{Y_w}^{Y_e} \left(\frac{\partial\psi}{\partial Y}\right)_n \theta_n\, dY \tag{3.39}$$

By the Green's theorem, defining $\bar{\theta}_n = \dfrac{\int_{Y_w}^{Y_e}\left(\frac{\partial\psi}{\partial Y}\right)_n \theta_n dY}{\int_{Y_w}^{Y_e}\left(\frac{\partial\psi}{\partial Y}\right)_n dY}$, it follows that:

$$\int_{Y_w}^{Y_e}(U\theta)_n\, dY = \int_{Y_w}^{Y_e}\left(\frac{\partial\psi}{\partial Y}\right)_n \theta_n dY = \bar{\theta}_n \int_{Y_w}^{Y_e}\left(\frac{\partial\psi}{\partial Y}\right)_n dY = \bar{\theta}_n\,(\psi_{ne} - \psi_{nw})$$

Adopting a similar treatment, the second term on the right side of Eq. (3.38) turns out to be:

$$\int_{Y_w}^{Y_e}(U\theta)_s\, dY = \bar{\theta}_s\,(\psi_{se} - \psi_{sw})$$

Here, $\bar{\theta}_s$ is defined in a way similar to $\bar{\theta}_n$. Subsequent to this, Eq. (3.38) turns out to be:

$$\iint_{X_s Y_w}^{X_n Y_e} \frac{\partial(U\theta)}{\partial X}\, dX\, dY = \bar{\theta}_n\,(\psi_{ne} - \psi_{nw}) - \bar{\theta}_s\,(\psi_{se} - \psi_{sw})$$

$$= \bar{\theta}_n\,(\psi_{ne} - \psi_{nw}) + \bar{\theta}_s\,(\psi_{sw} - \psi_{se}) \qquad (3.40)$$

In order to write $\bar{\theta}_n$, $\bar{\theta}_s$, $\psi_{ne}, \psi_{nw}, \psi_{sw}$ and ψ_{se} as functions of the values of the concerned variables at the nodes of the discretized grid system considered, the method proposed by Gosman et al. (1969) and also implemented by Gururaja Rao et al. (2000, 2001) has been used. Doing this, Eq. (3.40) turns out to be:

$$\iint_{X_s Y_w}^{X_n Y_e} \frac{\partial(U\theta)}{\partial X}\, dX\, dY$$

$$= \theta_P \frac{\{(\psi_{ne} - \psi_{nw}) + |\psi_{ne} - \psi_{nw}|\}}{2} + \theta_N \frac{\{(\psi_{ne} - \psi_{nw}) - |\psi_{ne} - \psi_{nw}|\}}{2}$$

$$+ \theta_P \frac{\{(\psi_{sw} - \psi_{se}) + |\psi_{sw} - \psi_{se}|\}}{2} + \theta_S \frac{\{(\psi_{sw} - \psi_{se}) - |\psi_{sw} - \psi_{se}|\}}{2} \qquad (3.41)$$

This equation ensures that one of the terms in the curly brackets in the equation will be zero. The term that remains will be the one that indicates the contribution from the node upstream of the appropriate face of the rectangle ne-se-sw-nw. This approach is termed as the second upwind differencing scheme and its further details may be found in Roache (1972). Gosman et al. (1969) further suggested that the value of the stream function at a given corner of the rectangle is the arithmetic mean of the values possessed at its four neighboring nodes. This, for example, means that:

$$\psi_{ne} = \frac{1}{4}[\psi_{NE} + \psi_N + \psi_E + \psi_P] \tag{3.42}$$

Expressions similar to the above are applicable for ψ_{nw}, ψ_{sw} and ψ_{se} too. Adopting the same methodology, the remaining advection term in Eq. (3.37) turns out to be:

$$\int_{X_s Y_w}^{X_n Y_e} \frac{\partial(V\theta)}{\partial Y}\, dX\, dY$$

$$= \theta_P \frac{\{(\psi_{se} - \psi_{ne}) + |\psi_{se} - \psi_{ne}|\}}{2} + \theta_E \frac{\{(\psi_{se} - \psi_{ne}) - |\psi_{se} - \psi_{ne}|\}}{2}$$

$$+ \theta_P \frac{\{(\psi_{nw} - \psi_{sw}) + |\psi_{nw} - \psi_{sw}|\}}{2} + \theta_W \frac{\{(\psi_{nw} - \psi_{sw}) - |\psi_{nw} - \psi_{sw}|\}}{2} \tag{3.43}$$

After the substitution of the two advection terms, as derived above, in Eq. (3.35), one obtains:

$$LHS = B_E(\theta_P - \theta_E) + B_W(\theta_P - \theta_W) + B_N(\theta_P - \theta_N) + B_S(\theta_P - \theta_S) \tag{3.44}$$

Where the coefficients B_E, B_W, B_N and B_S are given as:

$$B_E = \frac{\{(\psi_{ne} - \psi_{se}) + |\psi_{ne} - \psi_{se}|\}}{2} \tag{3.45}$$

$$B_W = \frac{\{(\psi_{sw} - \psi_{nw}) + |\psi_{sw} - \psi_{nw}|\}}{2} \tag{3.46}$$

$$B_N = \frac{\{(\psi_{nw} - \psi_{ne}) + |\psi_{nw} - \psi_{ne}|\}}{2} \tag{3.47}$$

$$B_S = \frac{\{(\psi_{se} - \psi_{sw}) + |\psi_{se} - \psi_{sw}|\}}{2} \tag{3.48}$$

With both the left hand side and the right hand side terms of the integrated form of energy equation now deduced, the non-dimensional temperature (θ_P) at a given point in the computational domain would be:

$$\theta_P = C_{E_{ene}}\,\theta_E + C_{W_{ene}}\,\theta_W + C_{N_{ene}}\,\theta_N + C_{S_{ene}}\,\theta_S \tag{3.49}$$

Here,

$$C_{E_{ene}} = \frac{(A_E + Pe_w\,B_E)}{AB_{ene}}, \qquad C_{W_{ene}} = \frac{(A_W + Pe_w\,B_W)}{AB_{ene}},$$

$$C_{N_{ene}} = \frac{(A_N + Pe_w\,B_N)}{AB_{ene}} \quad \text{and} \quad C_{S_{ene}} = \frac{(A_S + Pe_w\,B_S)}{AB_{ene}}$$

Further, in the above equation,

$$AB_{ene} = (A_E + A_W + A_N + A_S) + Pe_w\,(B_E + B_W + B_N + B_S)$$

Equation (3.49) gives the non-dimensional local temperature at any node in the computational domain. A similar procedure could be made use of in obtaining the pertinent expressions for non-dimensional stream function (ψ_p) as well as non-dimensional vorticity function (ω_p) at the given node. These are obtained considering, respectively, the stream function equation and the vorticity transport equation derived above. Accordingly, the non-dimensional stream function (ψ_p) at a given node turns out to be:

$$\psi_P = C_{E_{st}}\,\psi_E + C_{W_{st}}\,\psi_W + C_{N_{st}}\,\psi_N + C_{S_{st}}\,\psi_S + C_S\,\omega_P \tag{3.50}$$

Here,

$$C_{E_{st}} = \frac{A_E}{A_{st}}, \qquad C_{W_{st}} = \frac{A_W}{A_{st}}, \qquad C_{N_{st}} = \frac{A_N}{A_{st}}, \qquad C_{S_{st}} = \frac{A_S}{A_{st}},$$

$$C_S = \frac{1}{4}\,\frac{(X_N - X_S)(Y_E - Y_W)}{A_{st}} \quad \text{and} \quad A_{st} = A_E + A_W + A_N + A_S$$

The above gives the required expression for local stream function in its non-dimensional form within the computational domain. Similarly, the local non-dimensional vorticity function (ω_p) would be obtained as:

$$\omega_P = C_{E_{ome}}\,\omega_E + C_{W_{ome}}\,\omega_W + C_{N_{ome}}\,\omega_N + C_{S_{ome}}\,\omega_S - C_{ome}\left(\frac{\partial\theta}{\partial Y}\right)_P \tag{3.51}$$

Here,

$$C_{E_{ome}} = \frac{\left(\frac{A_E}{Re_w} + B_E\right)}{AB_{ome}}, \qquad C_{W_{ome}} = \frac{\left(\frac{A_W}{Re_w} + B_W\right)}{AB_{ome}},$$

$$C_{N_{ome}} = \frac{\left(\frac{A_N}{Re_w} + B_N\right)}{AB_{ome}}, \qquad C_{S_{ome}} = \frac{\left(\frac{A_S}{Re_w} + B_S\right)}{AB_{ome}}$$

$$C_{ome} = \frac{1}{4}\,Ri_w^*\,\frac{(X_N - X_S)(Y_E - Y_W)}{AB_{ome}} \quad \text{and}$$

$$AB_{ome} = \frac{1}{Re_w}(A_E + A_W + A_N + A_S) + (B_E + B_W + B_N + B_S)$$

In the above equation, the last term on the right hand side signifies the source term that arises out of buoyancy. Here, the partial derivative $\left(\frac{\partial\theta}{\partial Y}\right)_P$ is deduced using a second degree Lagrangian polynomial as:

$$\left(\frac{\partial\theta}{\partial Y}\right)_P = C_1\,\theta_W + C_2\,\theta_P + C_3\,\theta_E \tag{3.52}$$

Here,

$$C_1 = \frac{(Y_P - Y_E)}{(Y_W - Y_P)(Y_W - Y_E)},\quad C_2 = \frac{(2\,Y_P - Y_E - Y_W)}{(Y_P - Y_E)(Y_P - Y_W)} \quad \text{and} \quad C_3 = \frac{(Y_P - Y_W)}{(Y_E - Y_P)(Y_E - Y_W)}$$

Equation (3.51) gives the normalized vorticity function at any given point within the computational domain.

The above discretized equations, along with the relevant boundary conditions, are solved making use of the Gauss-Seidel method. As far as relaxation employed on dependent parameters is concern, it is observed that under relaxation would be warranted on both vorticity (ω) and stream function (ψ). Comprehensive initial experiments performed on the computer code prepared to solve the problem indicated that 0.3 could be an appropriate relaxation parameter for ω and ψ. Full relaxation (λ = 1) has been found to be adequate for non-dimensional temperature (θ). Convergence test is performed at the end of each of the iterations in the Gauss-Seidel solver and for this purpose a convergence criterion (δ_c) has been defined as:

$$\delta_c = \left|\frac{(\zeta_{new} - \zeta_{old})}{\zeta_{new}}\right| \tag{3.53}$$

Here, ζ is any dependent variable (ψ, ω or θ) that is subjected to the convergence test, while the subscripts "new" and "old" stand for the values of ζ obtained in two successive iterations.

Again, certain initial numerical experiments hinted that the appropriate convergence criteria (δ_c) on stream function, vorticity and temperature are, respectively, equal to 1×10^{-4}, 5×10^{-4} and 1×10^{-4}.

Lagrangian three-point formula is used for evaluating all the derivatives present in the boundary conditions. A similar procedure is used wherever it is required to calculate the derivatives in the study. The integrations needed in all the calculations are performed using an extended Simpson's 1/3 rule for non-uniform step sizes.

3.5 Closure

The definition of the research problem taken up along with the full-fledged mathematical formulation has been provided at the beginning of the current chapter. This is accompanied by the different boundary conditions that are made use of while solving the elliptic partial differential equations. Special attention has been focused on the derivation of the appropriate governing equations for temperature distribution along each of the channel walls taking into account the interplay between the multiple modes of heat transfer therein. Later, a detailed account on the method of solution employed has been provided. The ensuing chapter (**Chapter 4**) dwells into the numerical investigation carried out on the research problem, viz., conjugate mixed convection with surface radiation from a vertical channel flush-mounted with multiple asymmetrically-spaced identical discrete heat sources along its walls.

Chapter 4

Vertical Channel with Multiple Asymmetrically Mounted Discrete Heat Sources

4.1 Introduction

A detailed literature review pertaining to the geometry of a two-dimensional vertical parallel-plate channel involved in either convection alone or conjugate convection without or with surface radiation has been provided in **Chapter 2**. A comprehensive look into different reported works revealed that not many studies probing into interaction of surface radiation with conjugate mixed convection from an asymmetrically and discretely heated vertical channel are available in the literature. Further, there are hardly any studies that provide correlations that aid in calculation of the heat transfer and fluid flow parameters like

maximum and average channel temperatures and mean friction coefficient for problems of this class.

Keeping the above factors in mind, the present chapter (**Chapter 4**) tackles, quite elaborately, the problem of conjugate mixed convection with surface radiation from a vertical channel that has both of its walls flush-mounted with asymmetrically-spaced multiple identical discrete heat sources. As already mentioned, the problem would be solved, numerically, employing finite volume method. An explicit computer code would be prepared for the job. After a thorough validation of results obtained from the code, a large number of parametric studies elucidating the effects of all the governing independent parameters on various fluid flow and heat transfer results have been performed. Subsequently, useful correlations that aid in calculation of the maximum and the average non-dimensional channel temperatures and the mean friction coefficient are evolved making use of a large set of numerical data obtained from the computer code covering very broad ranges of different independent parameters.

4.2 Problem Statement and Solution Methodology

Figure 1 shows a vertical parallel-plate channel, along with the system of coordinates, equipped with a total of ten discrete heat sources in its walls. The channel is of height L with its walls sufficiently thin (thickness t << L), while the spacing or width (W) varies based on the aspect ratio (AR). For a given height L, an aspect ratio is defined as L/W such that a smaller AR makes the walls of the channel wider apart with a larger AR rendering the channel narrower. There are five heat sources in each wall flush-mounted asymmetrically as shown. It may be noted that the heat sources are of identical size ($L_h \times t$) and have a volumetric heat generation q_v. The thermal conductivity of the wall material is taken to be k_s, while the

surface emissivity is assumed to be ε. Air, moving upward against the gravity and assumed to be a radiatively transparent medium, is the cooling agent that enters the channel from its bottom end at characteristic velocity u_∞ and temperature T_∞. It is assumed to be of constant thermophysical properties subject to the Boussinesq approximation. As can be seen from the figure, the top, left and bottom surfaces of the left wall and the top, right and bottom surfaces of the right wall are adiabatic implying that the heat generated in the ten heat sources possessed by the walls gets exchanged between the interior surfaces of the two walls via the intervening medium (air). Since the walls of the channel are sufficiently thin compared to other dimensions, there are no cross temperature gradients in them.

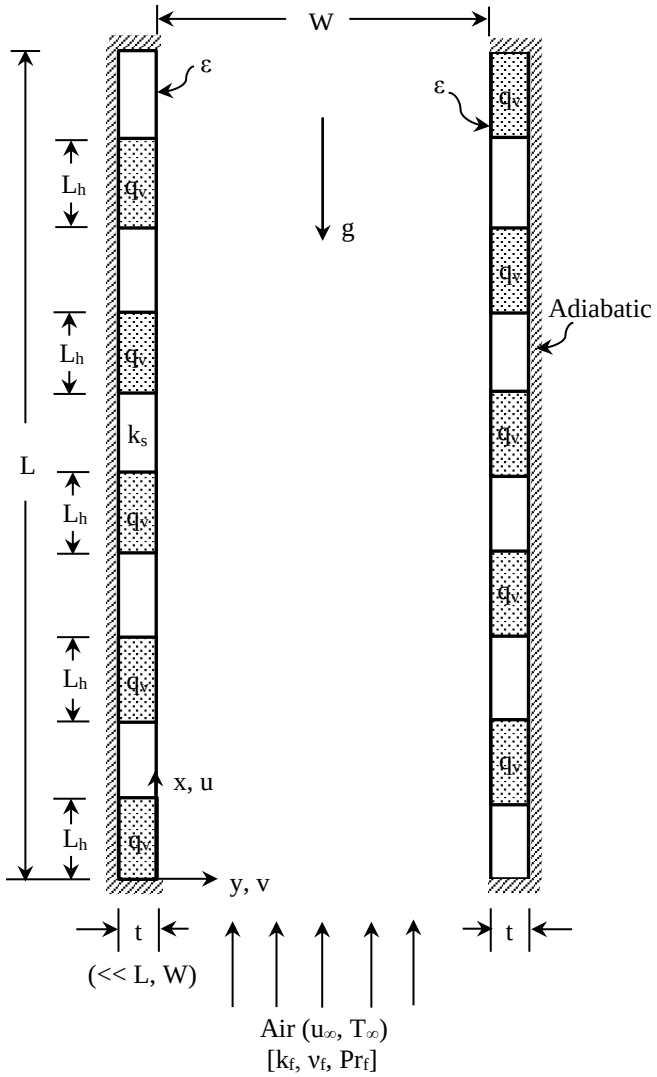

Fig. 4.1 Vertical channel with multiple identical discrete heat sources in its walls considered for study along with system of coordinates

The fundamental governing equations for fluid flow and heat transfer concerning the research problem, their conversion into vorticity-stream function (ω- ψ) form together with their non-dimensionalisation and all the pertinent boundary conditions are discussed elaborately in **Chapter 3**. However, for completeness, the final set of normalized governing equations is provided again hereunder:

$$U\frac{\partial\omega}{\partial X}+V\frac{\partial\omega}{\partial Y}=\frac{1}{Re_w}\left(\frac{\partial^2\omega}{\partial X^2}+\frac{\partial^2\omega}{\partial Y^2}\right)-Ri_w^*\frac{\partial\theta}{\partial Y} \tag{4.1}$$

$$\frac{\partial^2\psi}{\partial X^2}+\frac{\partial^2\psi}{\partial Y^2}=-\omega \tag{4.2}$$

$$U\frac{\partial\theta}{\partial X}+V\frac{\partial\theta}{\partial Y}=\frac{1}{Pe_w}\left(\frac{\partial^2\theta}{\partial X^2}+\frac{\partial^2\theta}{\partial Y^2}\right) \tag{4.3}$$

It has already been stated that Ri_w^* in Eq. (4.1) is the modified Richardson number that is based on a modified reference temperature difference, which, in turn, is given by $\Delta T_{ref} = (q_v L_h t)/k_s$, where L_h is the height of each of the heat sources. Indeed, Ri_w^* is the principal governing parameter of the present study that helps in delineation of the mixed convection regime into (i) forced convection dominant regime, (ii) pure mixed convection regime and (iii) free convection dominant regime.

An extended computational domain is used in order to capture the fluid flow and heat transfer more effectively. The complete grid structure employed for the present problem together with the relevant boundary conditions is shown in Fig. 4.2. The figure further indicates that a height of 2L and a width of W have been considered for the computational domain on the basis of certain preliminary studies. The above height is decided for the computational domain on the basis of certain initial studies made considering different possible heights. The local temperature distribution along the walls of the channel depends on

parameters that include the rate of volumetric heat generation (q_v), the thermal conductivity of the material of the channel walls (k_s), the surface emissivity of the channel walls (ε), the regime of flow and the thermophysical properties of the fluid. In view of this, enough attention has been paid on discretization of the computational domain. On account of the fact that both the gradients of velocity and temperature are quite large nearer to the channel walls, cosine grids that look finer nearer to the wall surfaces getting coarser as one moves towards the central plane have been selected in the transverse (y) direction. As far as the velocity (x) direction goes uniform grids with varying fineness have been employed for heat source and non-heat source sections of the channel wall and the extended domain. Since the temperature variation along the wall will be significant along the heat source and non-heat source portions, finer grids are used. As far as the extended domain is concerned, coarser grids would be adequate and the same is done here.

A detailed grid sensitivity analysis is performed in order to arrive at the optimum number of grids for the above discretization. The results of this analysis would be presented subsequently. Even for calculating the view factors and radiosities as part of radiation computations, the same non-equispaced grid system as used for convection computations is maintained in order to provide grid compatibility.

The broad solution methodology adopted for the problem has already been presented in **Chapter 3**. A computer code in C++ is exclusively written to solve the problem. The solution thus obtained provides the local values of non-dimensional stream function (ψ), vorticity (ω) and temperature (θ) pertaining to the entire computational domain including the channel walls. The peak non-dimensional temperature (θ_{max}) is extracted from the local values of wall temperature and even the average non-dimensional temperature (θ_{av}) is calculated. Further, the net rates of heat dissipation by convection (free, forced and mixed) and radiation

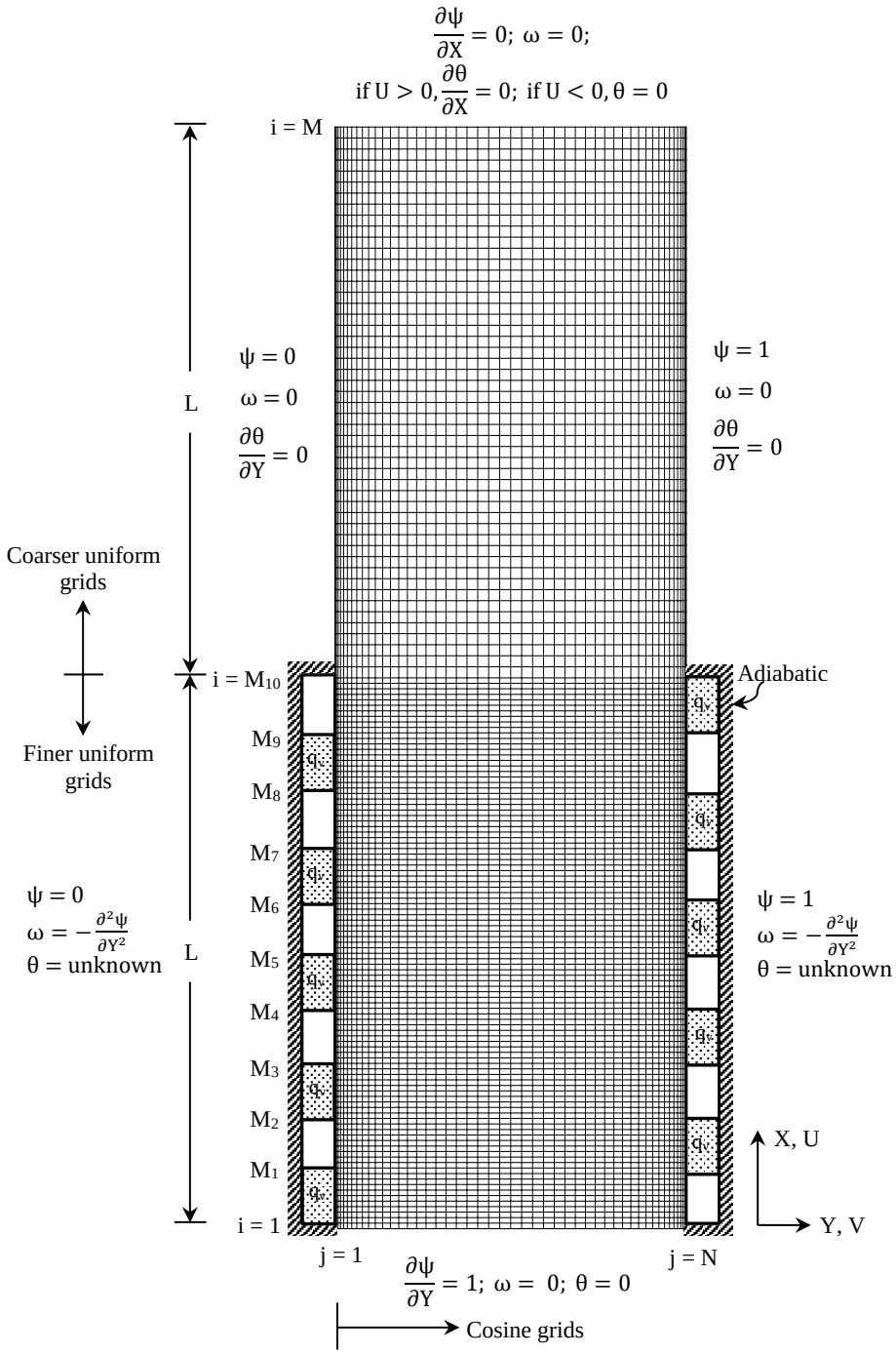

Fig. 4.2 Discretized extended computational domain used along with various boundary conditions employed

are obtained upon integrating the corresponding local values along the walls of the channel. Subsequently, the local drag coefficient (C_{fx}) and the mean friction coefficient ($\overline{C}_f$) too are calculated.

4.3 Parametric Range Considered

Air ($Pr_f = 0.71$) has been used as the cooling medium for all the computations considering it to be non-participating radiatively. Further, the cooling medium is considered to be Boussinesq. The channel height (L) is fixed at 20 cm and the wall thickness (t) is chosen to be 1.5 mm. All the ten discrete heat sources are identical and are of height (L_h) equal to 2 cm. For the fixed height (L) of the channel, a varying aspect ratio (AR = L/W) tends to vary the width or spacing (W) of the channel. The appropriate range for AR is considered to be 4 to 20 taking into account studies of the present kind performed by Peterson and Ortega (1990). The range $0.05 \leq \varepsilon \leq 0.85$ is considered to be apt for surface emissivity (ε) keeping in mind the limiting cases of a good reflector and a good emitter. As far as wall thermal conductivity (k_s) is concerned the range $0.25 \leq k_s \leq 1$ W/m K seems to be appropriate keeping in mind the fact that electronic cooling applications typically employ materials with thermal conductivity of the order of unity [Peterson and Ortega (1990)]. The modified Richardson number (Ri_w^*) is varied between 0.01 and 250. Here, the lower and upper limits, respectively, stand for the asymptotic values of forced and free convection. These limiting values for Ri_w^* have been frozen through some preliminary tests made with a set of values for the same. The maximum wall temperature becomes greater than 150^{o}C upon opting $Ri_w^* > 250$, while it drops down to less than 30^{o}C upon opting $Ri_w^* < 0.01$. Majority of applications concerning cooling of electronic devices have the device working temperature range between 30-120^{o}C, the above decision for Ri_w^* seems to be appropriate. With regard to Reynolds number (Re_w), the range

considered is $40 \leq Re_w \leq 22650$. This range has been arrived at based on the range for Ri_w^* that has been fixed as above.

4.4 Results and Discussion

4.4.1 Grid Convergence Test

The grid system employed for discretizing the computational domain has been already explained in section 4.2. Prior to performing different parametric studies pertaining to the present problem, the optimum grid system to be employed for discretizing the computational domain has to be finalized. In view of the above, a detailed grid convergence test is performed for a standard input of $q_v = 2\times10^5$ W/m^3, $k_s = 0.25$ W/m K, AR = 12 and $\varepsilon = 0.45$. Out of the three typical values of Ri_w^*, viz., 250, 1 and 0.01, the value $Ri_w^* = 1$ that pertains to pure mixed convection has been considered initially. The studies conducted in three phases and the results are enumerated in Tables 4.1, 4.2 and 4.3. In the first phase of the grid convergence test (Table 4.1), the number of grids across the channel (N) is varied holding the total number of grids (M) in the axial direction fixed at 161 with 6 grids employed per cm in heat source as well as non-heat source portions of each of the channel walls. The table reveals that θ_{max} changes by 0.5086% as N is increased from 21 to 41, while it changes by a further 0.5374% as N subsequently increases to 61. Upon further increasing N to 81, the change in θ_{max} is not that appreciable as earlier and is noticed to be by 0.5484%. The same trend continues with further increase in N. Owing to the above, N = 81 is frozen to be optimum. Keeping N fixed at 81, the second phase of the study is carried out holding the number of grids along the extended length in the axial direction (M–M_{10}) randomly fixed at 41. Here, the number of grids per cm length of heat source and non-heat source portions of the channel walls is varied that results in a variation in M_{10} as well. Table 4.2 provides results of this particular phase of

grid study. It can be seen that clustering of grids per cm of each channel wall from 6 to 7 changes θ_{max} by 0.0099%. A further increase in the above number to 8 from 7 changes θ_{max} by 0.0035%. Not a very appreciable change in θ_{max} is observed upon subsequently increasing the number of grids per cm of the wall. In view of the above, seven grids turn out to be adequate per cm of channel wall. The third phase of grid study is performed with frozen values of N = 81 and M_{10} = 141 (7 grids per cm of each wall). Here, the number of grids along the extended length ($M–M_{10}$) is varied. Table 4.3, listing the results of this particular phase of study, indicates that θ_{max} changes by 0.5519% as ($M–M_{10}$) is increased to 40 from 20. Upon increasing ($M–M_{10}$) to 60, θ_{max} undergoes a far decreased change, i.e., by 0.1982%. Subsequent increase in ($M–M_{10}$) to 80 brings only a 0.1092% change in θ_{max}. Further attempts of increasing ($M–M_{10}$) are not found to bring notable changes in θ_{max}. These observations hint at ($M–M_{10}$) = 80 as the optimum. The above three phases of grid study are extended to the upper and lower limits of Ri_w^* (250 and 0.01, respectively) as well. Similar trends as noticed with Ri_w^* = 1 (pure mixed convection) are noticed even here. Here, as an example, the results pertaining to studies made for the other two limiting values of Ri_w^*, viz., 250 and 0.01, with other input parameters fixed as above, are provided in Tables 4.4 to 4.9. In view of the above, all the ensuing parametric studies are conducted employing M×N = 221×81 and ($M–M_{10}$) = 80 with 7 grids used per cm of heat source and non-heat source portions of the channel walls.

Table 4.1 First stage of grid independence test for $Ri_w^* = 1$

[To fix number of grids across the channel (N)]

[$q_v = 2\times10^5$ W/m^3, $k_s = 0.25$ W/m K, $\varepsilon = 0.45$, AR = 12, M = 161, No. of grids per cm in heat source and non-heat source portions of each wall = 6 and $(M–M_{10}) = 40$]

Total no. of grids along y direction, N	θ_{max}	Percentage change in θ_{max} (abs.)	Percentage discrepancy in energy balance
21	2.0036	-	0.3922
41	2.0148	0.56	0.5086
61	2.0170	0.11	0.5374
81	2.0181	0.05	0.5484
101	2.0186	0.025	0.5536

Table 4.2 Second stage of grid independence test for $Ri_w^* = 1$

[To fix number of grids in the heat source and non-heat source portions of the channel walls]

[$q_v = 2\times10^5$ W/m^3, $k_s = 0.25$ W/m K, $\varepsilon = 0.45$, AR = 12, N = 81 and $(M–M_{10}) = 40$]

No. of grids/cm in heat source and non-heat source portions	θ_{max}	Percentage change in θ_{max} (abs.)	Percentage discrepancy in energy balance
5	2.0179	-	0.6391
6	2.0181	0.0099	0.5484
7	2.0183	0.0099	0.4808
8	2.01837	0.0035	0.4276
9	2.01846	0.0045	0.3848
10	2.01851	0.0025	0.3492
11	2.01856	0.0025	0.3192
12	2.01859	0.0015	0.2933

Table 4.3 Third stage of grid independence test for $Ri_w^* = 1$

[To fix number of grids in the extended domain along x-direction]

[$q_v = 2\times10^5$ W/m^3, $k_s = 0.25$ W/m K, $\varepsilon = 0.45$, AR = 12, $M_1 = 15$, $M_2 = 29$, $M_3 = 43$, $M_4 = 57$, $M_5 = 71$, $M_6 = 85$, $M_7 = 99$, $M_8 = 113$, $M_9 = 127$, $M_{10} = 141$ and N = 81]

No. of grids in extended domain along x-direction, ($M–M_{10}$)	θ_{max}	Percentage change in θ_{max} (abs.)	Percentage discrepancy in energy balance
20	2.0295	-	0.4815
40	2.0183	0.5519	0.4808
60	2.0143	0.1982	0.4807
80	2.0121	0.1092	0.4808
100	2.0106	0.0745	0.4810

Table 4.4 First stage of grid independence test for $Ri_w^* = 250$

[To fix grids across the channel (N)]

[$q_v = 2\times10^5$ W/m^3, $k_s = 0.25$ W/m K, $\varepsilon = 0.45$, AR = 12, M = 161, No. of grids per cm in heat source and non-heat source portions of each wall = 6 and ($M–M_{10}$) = 40]

Total no. of grids along y direction, N	θ_{max}	Percentage change in θ_{max} (abs.)	Percentage discrepancy in energy balance
21	7.5346	-	0.1674
41	7.4887	0.610	0.0428
61	7.4317	0.760	0.5654
81	7.4298	0.026	0.6204
101	7.4635	0.450	0.6852

Table 4.5 Second stage of grid independence test for $Ri_w^* = 250$

[To fix number of grids in the heat source and non-heat source portions]

[$q_v = 2\times10^5$ W/m^3, $k_s = 0.25$ W/m K, $\varepsilon = 0.45$, AR = 12, N = 81 and $(M–M_{10}) = 40$]

No. of grids/cm in heat source and non-heat source portions	θ_{max}	Percentage change in θ_{max} (abs.)	Percentage discrepancy in energy balance
5	7.3830	-	0.6298
6	7.4298	0.6339	0.6204
7	7.4259	0.0525	0.2769
8	7.4779	0.7003	0.1140
9	7.4771	0.0107	0.1537
10	7.5039	0.3584	0.2502
11	7.5162	0.1639	0.2808
12	7.5311	0.1982	0.2964

Table 4.6 Third stage of grid independence test for $Ri_w^* = 250$

[To fix number of grids in the extended domain along x-direction]

[$q_v = 2\times10^5$ W/m^3, $k_s = 0.25$ W/m K, $\varepsilon = 0.45$, AR = 12, $M_1 = 15$, $M_2 = 29$, $M_3 = 43$, $M_4 = 57$,

$M_5 = 71$, $M_6 = 85$, $M_7 = 99$, $M_8 = 113$, $M_9 = 127$, $M_{10} = 141$ and N = 81]

No. of grids in extended domain along x-direction, $(M–M_{10})$	θ_{max}	Percentage change in θ_{max} (abs.)	Percentage discrepancy in energy balance
20	7.4850	-	0.1025
40	7.4259	0.7896	0.2769
60	7.4333	0.0997	0.3820
80	7.4288	0.0605	0.1902
100	7.6329	2.7474	0.5165

Table 4.7 First stage of grid independence test for $Ri_w^* = 0.01$

[To fix grids across the channel (N)]

[$q_v = 2\times10^5$ W/m^3, $k_s = 0.25$ W/m K, $\varepsilon = 0.45$, AR = 12, M = 161, No. of grids per cm in heat source and non-heat source portions of each wall = 6 and $(M–M_{10}) = 40$]

Total no. of grids along y direction, N	θ_{max}	Percentage change in θ_{max} (abs.)	Percentage discrepancy in energy balance
21	0.9147	-	0.3259
41	0.9371	2.45	0.4032
61	0.9415	0.47	0.4320
81	0.9429	0.15	0.4390
101	0.9424	0.053	0.4223

Table 4.8 Second stage of grid independence test for $Ri_w^* = 0.01$

[To fix number of grids in the heat source and non-heat source portions]

[$q_v = 2\times10^5$ W/m^3, $k_s = 0.25$ W/m K, $\varepsilon = 0.45$, AR = 12, N = 81 and $(M–M_{10}) = 40$]

No. of grids/cm in heat source and non-heat source portions	θ_{max}	Percentage change in θ_{max} (abs.)	Percentage discrepancy in energy balance
5	0.9417	-	0.5138
6	0.9429	0.1274	0.4390
7	0.9437	0.0848	0.3841
8	0.9443	0.0636	0.3415
9	0.9448	0.0529	0.3074
10	0.9452	0.0423	0.2792
11	0.9455	0.0317	0.2553
12	0.9457	0.0212	0.2349

Table 4.9 Third stage of grid independence test for $Ri_w^* = 0.01$

[To fix number of grids in the extended domain along x-direction]

[$q_v = 2\times10^5$ W/m^3, $k_s = 0.25$ W/m K, $\varepsilon = 0.45$, AR = 12, $M_1 = 15$, $M_2 = 29$, $M_3 = 43$, $M_4 = 57$, $M_5 = 71$, $M_6 = 85$, $M_7 = 99$, $M_8 = 113$, $M_9 = 127$, $M_{10} = 141$ and N = 81]

No. of grids in extended domain along x-direction, (M–M_{10})	θ_{max}	Percentage change in θ_{max} (abs.)	Percentage discrepancy in energy balance
20	0.9460	-	0.3833
40	0.9437	0.2431	0.3841
60	0.9430	0.0742	0.3842
80	0.9425	0.0530	0.3843
100	0.9423	0.0212	0.3843

4.4.2 Check for Mass and Energy Balance

The correctness of the results of the present problem as obtained from the computer code written for the purpose is tested through mass and energy balance checks in the entire mixed convection range ($0.01 \leq Ri_w^* \leq 250$). The check for mass conservation is performed by comparing the net rate of mass in-flow with that of the mass-out flow. The energy conservation check is made by calculating the net heat dissipation rates by mixed convection and radiation through numerical integration of their corresponding local values over the entire lengths of the left and the right walls of the channel. The rate of heat dissipation cumulatively taking place by the combined modes of mixed convection and radiation is subsequently obtained. The above is compared with the total rate of heat generation in the two walls of the channel calculated as $10\times q_v\times L_h\times t$. As an example, for a standard input comprising $q_v = 2\times10^5$ W/m^3, $k_s = 0.25$ W/m K, $\varepsilon = 0.45$ and AR = 12, the results have been obtained pertaining to five typical values of Ri_w^*, viz., 0.01, 0.1, 1, 25 and 250. Both the mass and energy balance checks turned out to be satisfactory within, respectively, ± 0.15% and ± 0.60%. Similar trends

of the above kind are noticed even while operating with various other values of independent parameters.

4.4.3 Validation of Results

As has already been mentioned, the present problem has been solved making use of a computer code explicitly written. The fluid flow and heat transfer results obtained from the above code are validated with certain available analytical, experimental and numerical results. To begin with, the velocity and temperature distributions are compared with those of Aung and Worku (1986a and 1986b). As far as the other fluid flow results are concerned, the calculation of the mean friction coefficient ($\overline{C}_f$) is checked with the analytical solution of Blasius (1908). The correctness of the heat transfer results is verified with the works of Elenbaas (1942) and Bar-Cohen and Rohsenow (1984). In order to do the above, results are obtained from the code for the appropriate limiting cases as suggested in the work, in respect of which the comparison is sought. A summary of the results of a thorough validation thus carried out is provided in the present section.

4.4.3.1 Validation for local velocity and temperature distributions

Aung and Worku (1986a and 1986b) have provided equations for non-dimensional vertical velocity (U) and non-dimensional temperature (θ) for mixed convection in a vertical channel with symmetric and asymmetric wall temperatures. Their work made use of the boundary layer approximations and further assumed the flow to be fully-developed to solve the pertinent fluid flow and energy equations. In comparison, the present work has not made these simplifying assumptions.

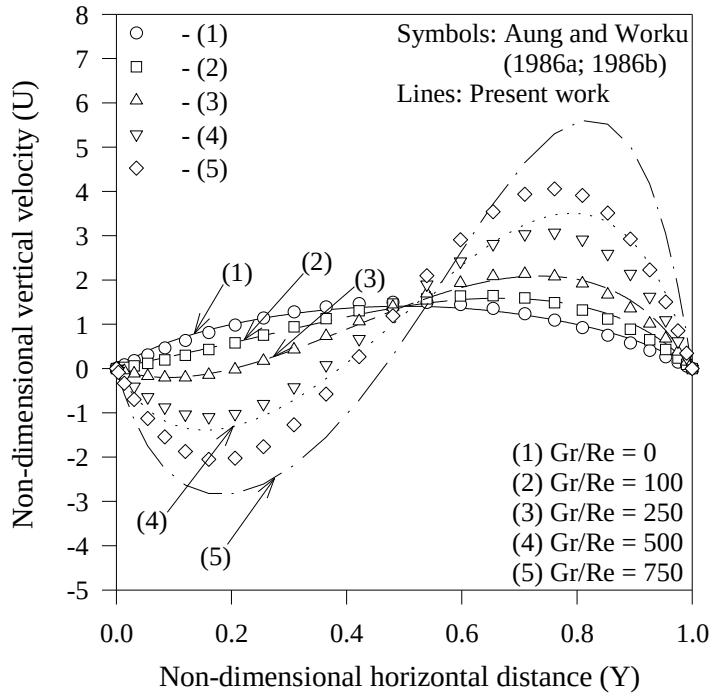

(a) Validation for vertical velocity

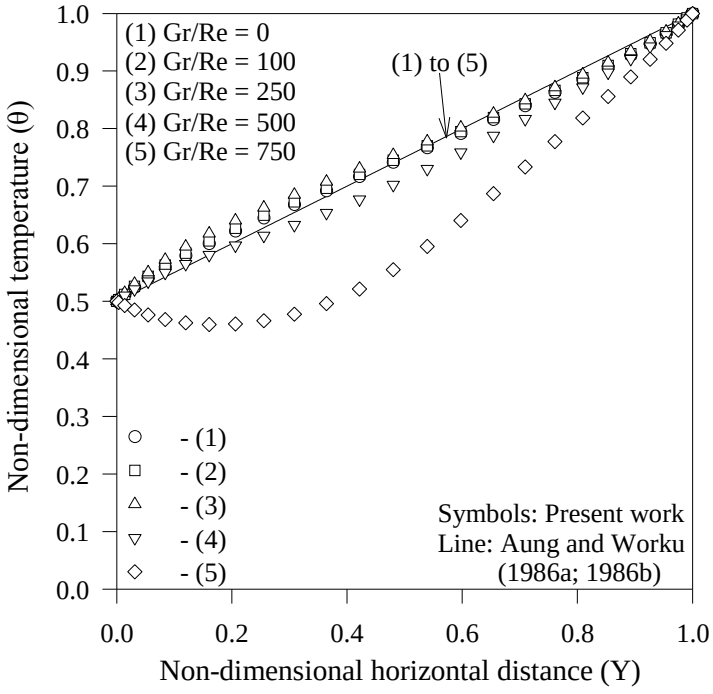

(b) Validation for temperature

Air (Pr_f = 0.71), AR = 8, θ_{val} = 0.5

Fig. 4.3 Comparison of the velocity and temperature profiles at the channel exit obtained in the present study with available results

Nevertheless, the velocity and temperature profiles of the present study are compared with those of Aung and Worku. It is to be noted that Aung and Worku considered the right wall to be hot with the left wall being cold in contrast to the present study that has channel with asymmetric heat generation in both the walls. Further, they have considered Gr_w/Re_w as the prominent mixed convection parameter, while the present work makes use of Gr_w^*/Re_w^2. Keeping the above factors in mind, the solution to the present problem too is obtained making appropriate modification in the computer code. Figure 4.3 shows a comparison of the present profiles of U and θ at the exit of the channel with those of Aung and Worku (1986a and 1986b). It has been noticed that the velocity and temperature profiles at the channel exit from the present work concerning Gr_w/Re_w = 0, 100 and 250 almost merge with those of Aung and Worku with disparities getting revealed towards larger values of Gr_w/Re_w (500 and 750). The above mismatch may be attributed to the employment of the boundary layer approximations coupled with fully-developed flow assumption by Aung and Worku.

4.4.3.2 Validation for mean friction coefficient calculation

Figure 4.4 shows (a) the non-dimensional vertical velocity and (b) the non-dimensional temperature profiles at the exit of the channel. A few preliminary studies have been conducted for certain representative cases for different values of aspect ratio (AR) in the asymptotic forced convection limit ($Ri_w^* = 0.01$). These studies revealed that the fluid flow through the channel is far from fully-developed for lower values of AR. Even for the upper limit of AR (i.e., 20), the velocity and temperature profiles have not been observed to merge with the fully developed velocity and temperature profiles of plane-Poiseuille flow. The inference from the above observations is that the lowest aspect ratio (i.e., 4) employed here may as well be treated as the flat plate limit, which means that the two channel walls here are almost isolated from each other.

Thus, the fluid flow results are validated with a comparison of the mean friction coefficient calculations of the present work with the exact flat plate solution of Blasius (1908) in the asymptotic forced convection limit ($Ri_w^* = 0.01$). For doing this, a set of 15 data is generated for $Ri_w^* = 0.01$ and AR = 4. The $\overline{C}_f$ of the present work is observed to be in a decent agreement with the corresponding value of Blasius subjected to a maximum deviation of ±7.8%. Pursuing the above, a correlation for $\overline{C}_f$ is evolved using the above data that turned out to be: $\overline{C}_f = 5.5714\ Re_L^{-0.6392}$ that has a correlation coefficient of 0.999 with an error band ±0.89%. The above correlation is later modified, adjusting the exponent of Re_L to –0.5, as: $\overline{C}_f = 1.382\ Re_L^{-0.5}$.

This results in ±4.1% difference between the present correlation and the one given by Blasius (1908). Remembering that $Ri_w^* = 0.01$ is only an asymptotic forced convection limit for the present problem configuration with the solution of Blasius accounting for flow past an isothermal flat plate, this indeed is a very satisfactory match serving as validation to the fluid flow calculation of the present study.

4.4.3.3 Validation for heat transfer results

The heat transfer results of the present problem are validated through comparison with the studies of Elenbaas (1942) and Bar-Cohen and Rohsenow (1984). To be able to do this, the complexity in the present problem is brought down to a special simple case that has the two walls of the channel not possessing any heat sources but instead remaining isothermal. A set of 18 data is generated catering to the whole range of aspect ratios ($4 \leq AR \leq 20$) for $Ri_w^* = 500$, which is much larger than the asymptotic free convection limit chosen in the present study ($Ri_w^* = 250$). The average convection Nusselt number ($\overline{Nu}_C$) thus obtained is checked with the semi-empirical correlation of Elenbaas (1942) and the analytical solution of Bar-

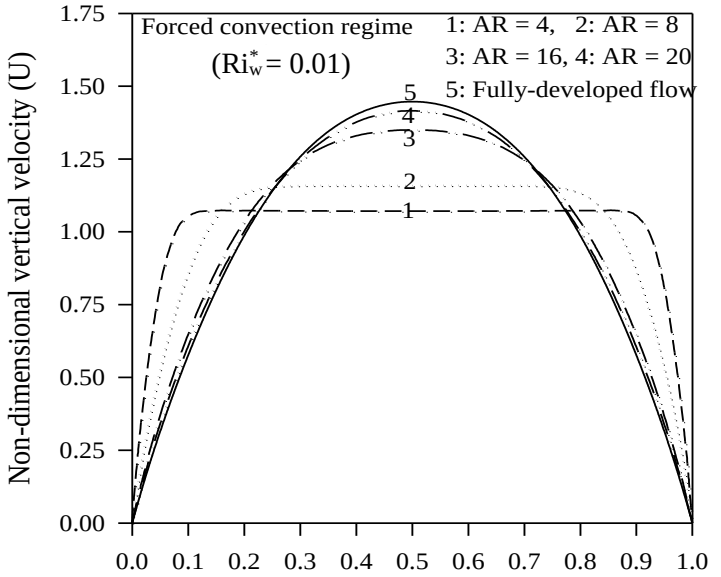

(a) Non-dimensional vertical velocity

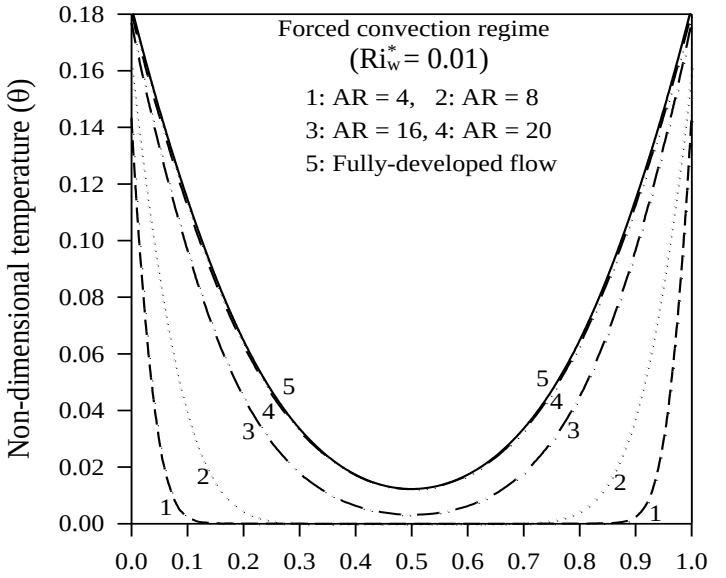

(b) Non-dimensional temperature

[$q_V = 5x10^5$ W/m^3, $k_s = 0.5$ W/m K and $\varepsilon = 0.45$]

Fig. 4.4 Non-dimensional vertical velocity and temperature profiles at the channel exit for different aspect ratios in the forced convection dominant regime

Cohen and Rohsenow (1984). It is to be noted that the above two reported works pertain to free convection in air in a vertical channel with symmetric isothermal walls. A reasonably

acceptable agreement is noticed between the present and the reported works with peak deviations limited to ±9.7% and ±8.6%, respectively.

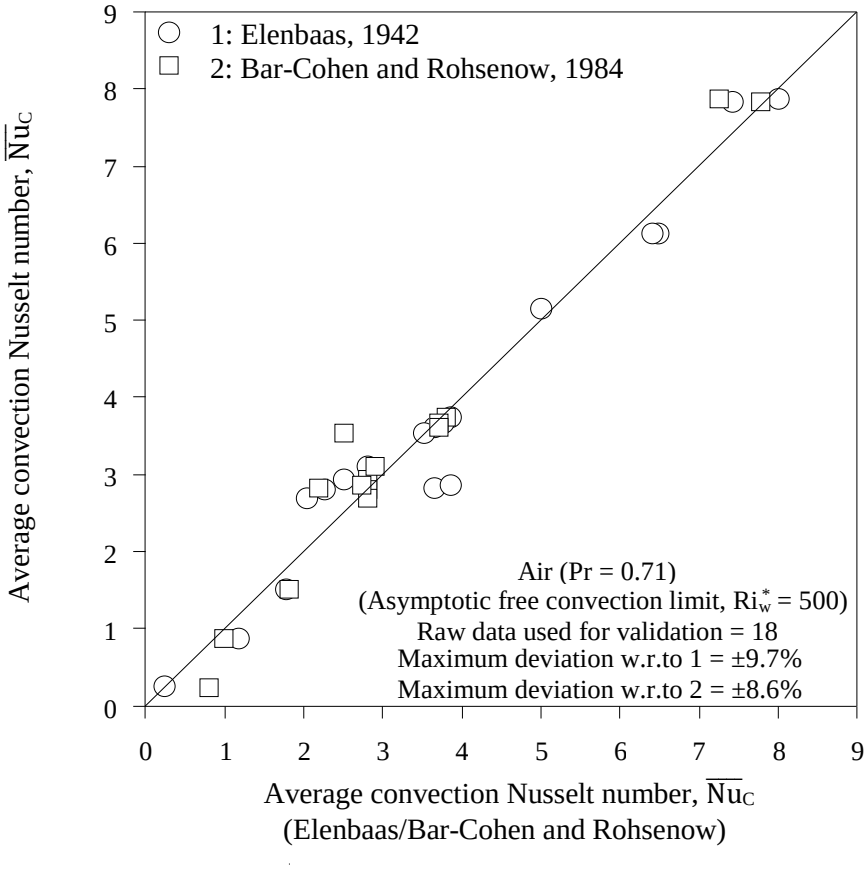

Fig. 4.5 Validation for average convection Nusselt number with the available results in the asymptotic free convection limit

4.4.4 Variation of Non-dimensional Local Wall Temperature with Other Parameters

The present section throws light on the studies performed to understand the nature of variation of the local non-dimensional temperature along the two channel walls with respect to relevant independent parameters.

4.4.4.1 Variation with aspect ratio of the channel

In order to establish the effect of aspect ratio (AR) on the local temperature distribution in both the channel walls, a study is performed using a fixed input of k_s = 0.25 W/m K, q_v = 2×10^5 W/m^3, Ri_w^* = 1 and ε = 0.45. It can be noticed from Fig. 4.6 (a) that, for a given AR, the local temperature of the left wall [$\theta_L(X)$] increases very sharply from the channel entry, reaches a local maximum somewhere near the end of the bottommost heat source. It subsequently decreases in the immediately succeeding non-heat source portion. After reaching a local minimum, it shoots up again as one moves through the second heat source exhibiting a similar behavior as noticed in the first heat source portion. The trend continues in the rest of the wall and one can see five local maxima and five local minima in the temperature profile. This nature of variation, understandably, is on account of the discreteness in heat generation in the wall with heat source and non-heat source portions present alternately. The largest of the five local peaks, which, incidentally, is the maximum left wall temperature of the channel, occurs in the fifth heat source from the bottom end of the left wall. The figure further shows that the local temperature increases with increasing AR from 4 to 20 (i.e., the channel progressively getting narrower). The above is attributed to an enhanced radiation exchange owing to reduced spacing between the channel walls. In the present case, the maximum non-dimensional left wall temperature of the channel is seen to rise by 92.49% as aspect ratio increases from 4 to 20. Figure 4.6 (b) concerning the right wall hints at a similar nature of variation of local temperature [$\theta_R(X)$] along it as that observed along the left wall with the waviness in the profile getting shifted in tune with the changed positions of the heat sources in it. Here too, an increasing AR, expectedly, tends to increase the local temperature. In the specific case considered here, there is a 103.89% increase in $\theta_R(X)$ at the channel exit with AR increasing from 4 to 20. The above findings prohibit the designer from

unduly packing the channel walls closer, for a given height, since it leads to an unwanted increase in the peak channel temperature.

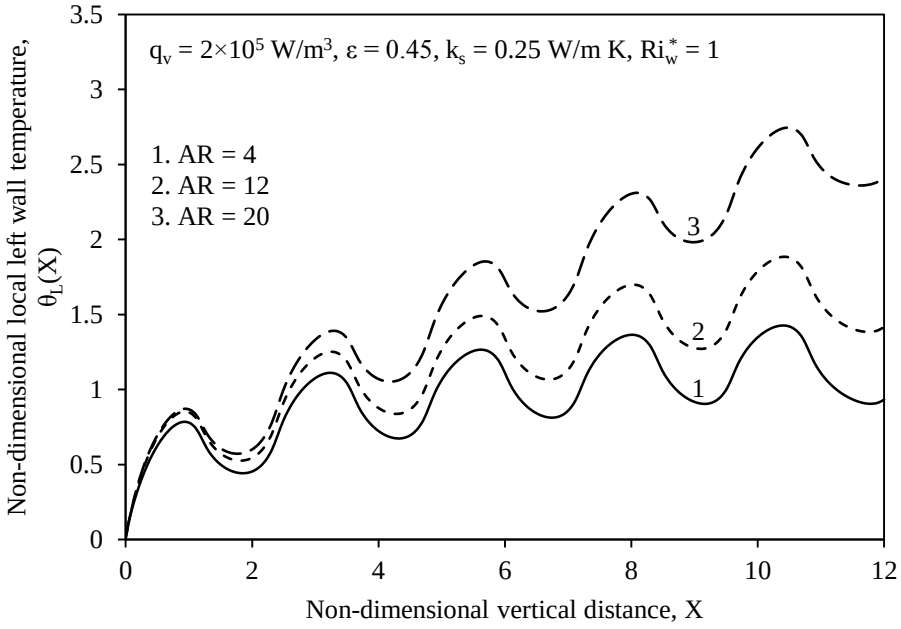

(a)

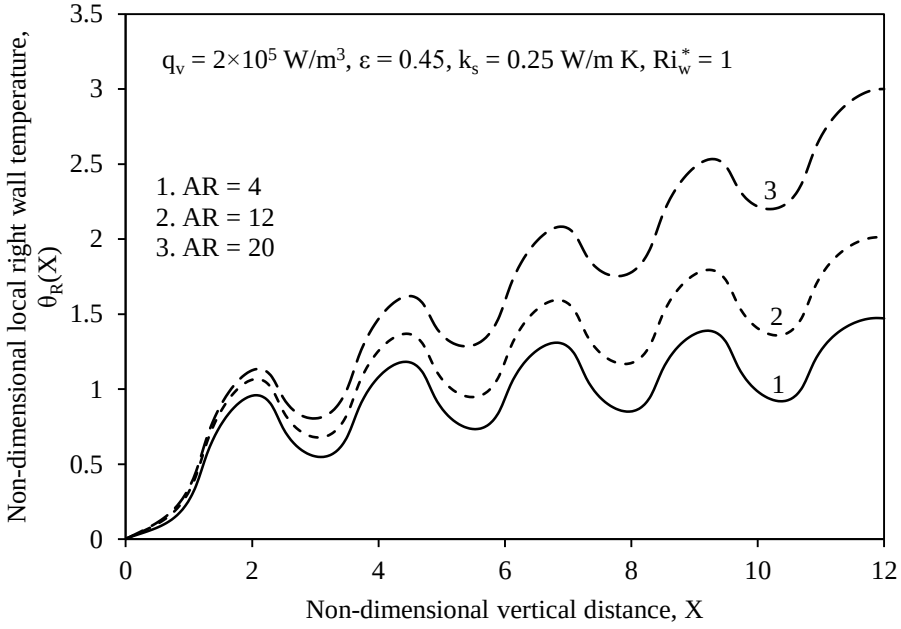

(b)

Fig. 4.6 Local non-dimensional temperature profiles for (a) left wall (b) right wall for different aspect ratios of the channel

4.4.4.2 Variation in different regimes of mixed convection

The local temperature profiles along the left and right walls of the channel are plotted in various regimes of mixed convection (Ri_w^* = 250, 25, 1, 0.1 and 0.01) and are shown in Figs. 4.7 (a) and (b). Here, it is recalled that Ri_w^* = 0.01 and 250 pertain to the asymptotic limits of forced and free convection, while Ri_w^* = 1 caters to pure mixed convection. It is observed from Fig. 4.7 (a) that the local left wall temperature [$\theta_L(X)$], for a given value Ri_w^*, follows the trend similar to that already discussed with regard to Fig. 4.6 (a). The peak left wall temperature is observed near the top end of the fifth heat source for all the values of Ri_w^* other than Ri_w^* = 250, for which it indeed occurs somewhere nearer to the centre of the fourth heat source itself. The figure further reveals that, for an identical set of independent parameters given, the local temperature decreases with decreasing Ri_w^* owing to enhanced convective heat dissipation from the wall due to increased impressed velocity (u_∞). A minor deviation in this regard is noticed only in the local temperature profile concerning Ri_w^* = 250 near the channel exit. This effect of Ri_w^* on the local temperature is more pronounced between Ri_w^* = 250 and Ri_w^* = 1 and gets diminished towards smaller values of Ri_w^*. In the present example, the maximum left wall temperature is seen to decrease by 74.65% as Ri_w^* decreases from 250 to 1 as against the 52.56% drop noticed upon decreasing Ri_w^* further to 0.01. Figure 4.7 (b) throws light on a similar behavior exhibited by the local right wall temperature too. In the case considered here, the maximum non-dimensional right wall temperature drops by 72.46% between Ri_w^* = 250 and Ri_w^* = 1, while it comes down by a further 53.16% due to a subsequent decrease in Ri_w^* to 0.01.

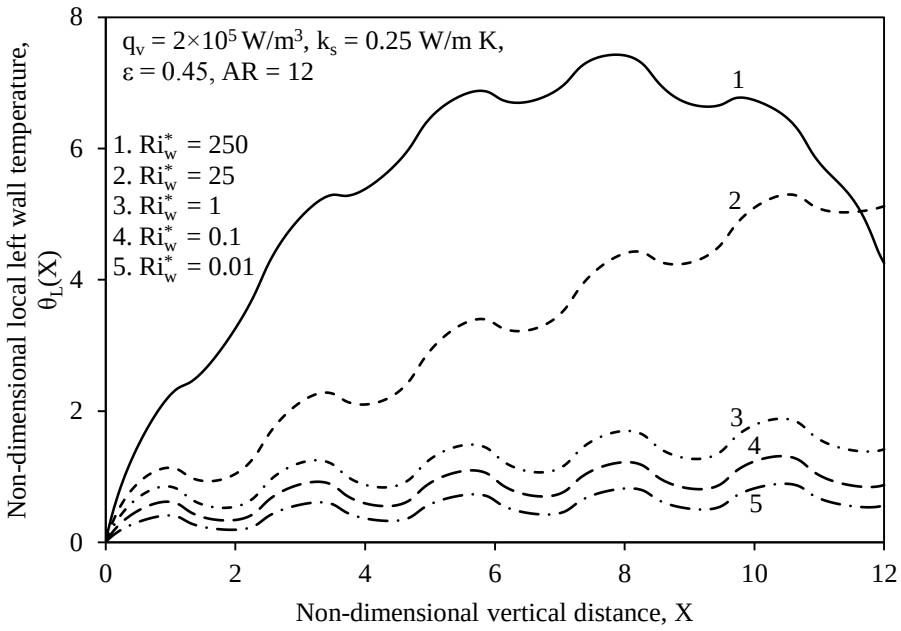

(a)

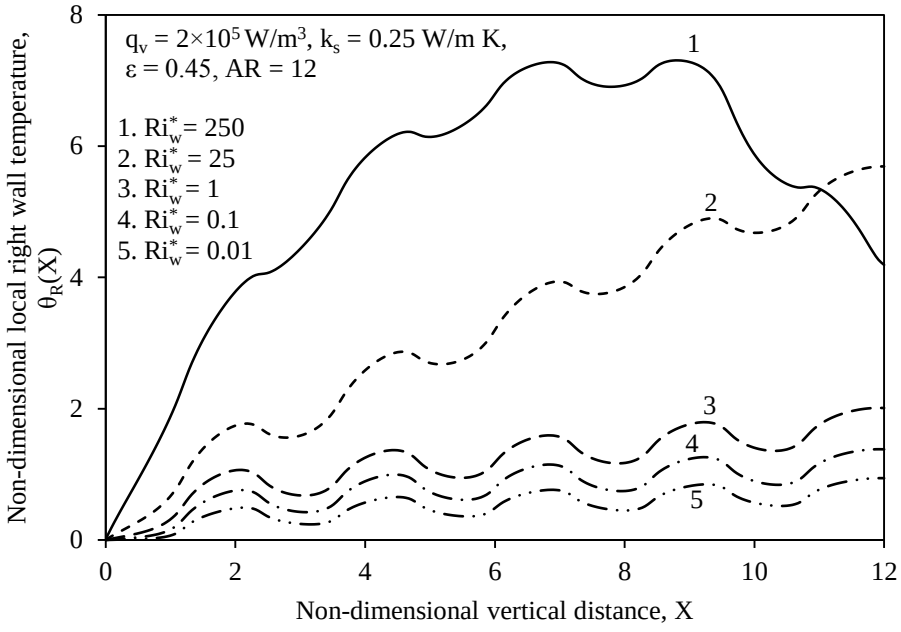

(b)

Fig. 4.7 Local non-dimensional temperature profiles for (a) left wall and (b) right wall in different regimes of mixed convection

4.4.4.3 Variation with surface emissivity of the channel

The nature of variation exhibited by the local non-dimensional temperature along the two channel walls for three typical values of surface emissivity (ε = 0.05, 0.45 and 0.85) is depicted in Fig. 4.8. The study is performed for fixed values of input comprising $q_v = 2\times10^5$ W/m^3, k_s = 0.25 W/m K, Ri_w^* = 250 and AR = 12. The general nature of the local wall temperature profiles is similar to that seen in the preceding results. Further, with emissivity (ε) increasing from 0.05 to 0.85, both the left and right wall temperatures are observed to rise slightly to begin with. After a certain height from the channel entry, however, these temperatures are seen to decrease with increasing ε. This drop in the temperatures that the walls experience is much larger than the rise in the temperatures exhibited by them in their initial portions. This may be attributed to the asymmetric positioning of the discrete heat sources in the walls with the left wall having its first heat source at the channel entry and the right wall possessing its last heat source at the channel exit. In the present example, the first local peak temperature in the left wall that occurs nearer to channel entry is getting increased by 21.58%, while the last local peak temperature in the same wall occurring at the fag end of the channel is decreasing by 21.78%, with ε increasing to 0.85 from 0.05. By the same token, the above exercise brings a 26.17% increase and a 22.83% decrease in the temperatures of the right wall at its corresponding locations.

4.4.4.4 Variation with thermal conductivity of the channel material

In order to probe into the effect of thermal conductivity (k_s) of the channel wall material on the local left and right wall temperature distribution, a study is performed by considering four different values of k_s, viz., 0.25, 0.5, 0.75 and 1 W/m K. The results are shown in Figs. 4.9 (a) and 4.9 (b), which correspond, respectively, to the left and right wall temperature profiles. The study, as can be seen, pertains to pure mixed convection regime (Ri_w^* = 1), with the rest of

the input, viz., AR = 12, $\varepsilon = 0.45$ and $q_v = 5\times10^5$ W/m^3, held fixed. Figure 4.9 (a) shows that, for a given k_s, the general nature of variation of temperature along the left wall of the channel is expectedly similar to that noticed in Fig. 4.6 (a). However, as the thermal conductivity increases, though there is an expected drop in temperature in the heat source portions of the left wall, the trend is completely reversed in the non-heat source portions of it. This is attributed to the fact that the non-heat source potions of the wall are passive merely percolating the heat generated in the heat sources in it. For example, the maximum non-dimensional left wall temperature reduces by 4.06% as k_s increases from 0.25 to 0.5 W/m K and further by 5.23% with a subsequent increase in k_s to 1 W/m K.

With regard to the right wall of the channel, Fig. 4.9 (b) reveals that the broad nature of variation of local temperature is the same as that noticed in Fig. 4.6 (b). Further, here also, like for the left wall, the local temperature decreases as k_s increases with other parameters held constant. In the present case, the maximum non-dimensional temperature of the right wall is reducing by 4.79% as k_s increases from 0.25 to 1 W/m K.

4.4.4.5 Exclusive effect of surface radiation on local temperature distribution

In order to extract the exclusive role surface radiation plays in the distribution of temperature along the left and right walls of the channel, two limiting cases are considered. One of them pertains to $\varepsilon = 0$ (no radiation), while the other addresses $\varepsilon = 0.99$ (maximum possible radiation), with the rest of the input, viz., $q_v = 2\times10^5$ W/m^3, $k_s = 0.25$ W/m K, AR = 12 and $Ri_w^* = 250$, remaining fixed. Figures 4.10 (a) and (b) bring out the findings of this study. There is a remarkable drop in the local non-dimensional temperature along the left and right walls upon replacing a non-radiating surface with the one having maximum possible emissivity. An exception to this is noticed in the initial portions of the two channel walls owing to reasons

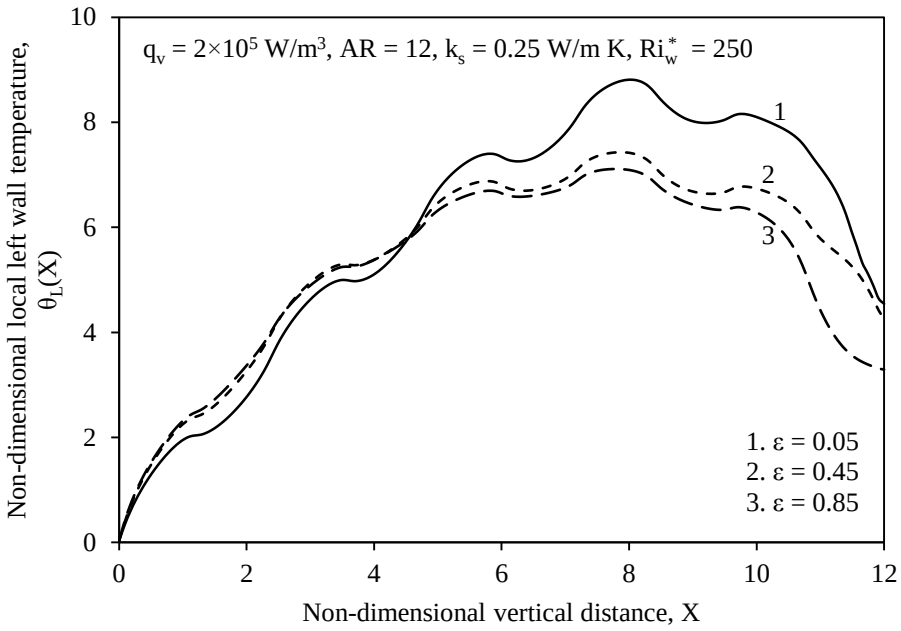

(a)

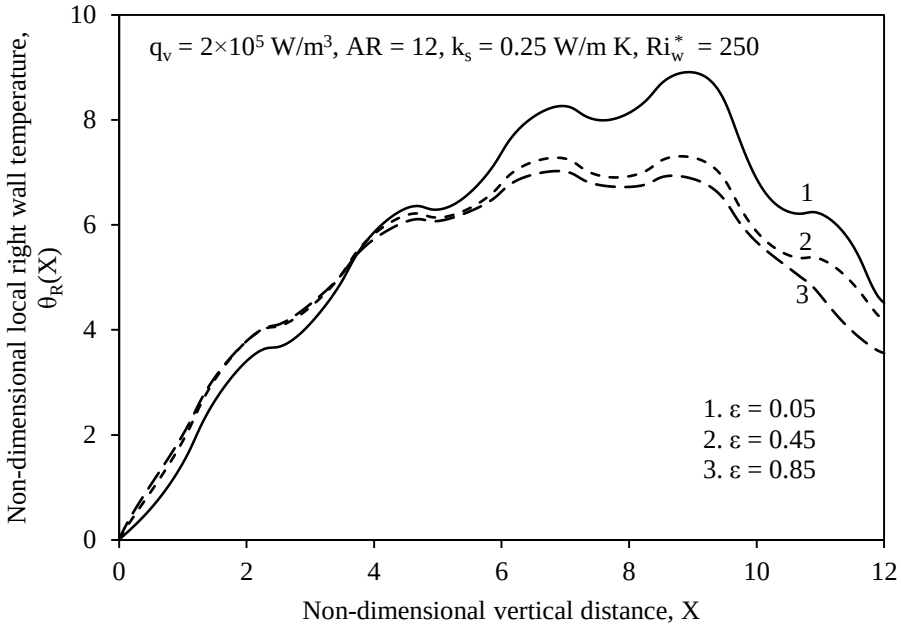

(b)

Fig. 4.8 Local non-dimensional temperature profiles for (a) left wall and (b) right wall for different surface emissivities

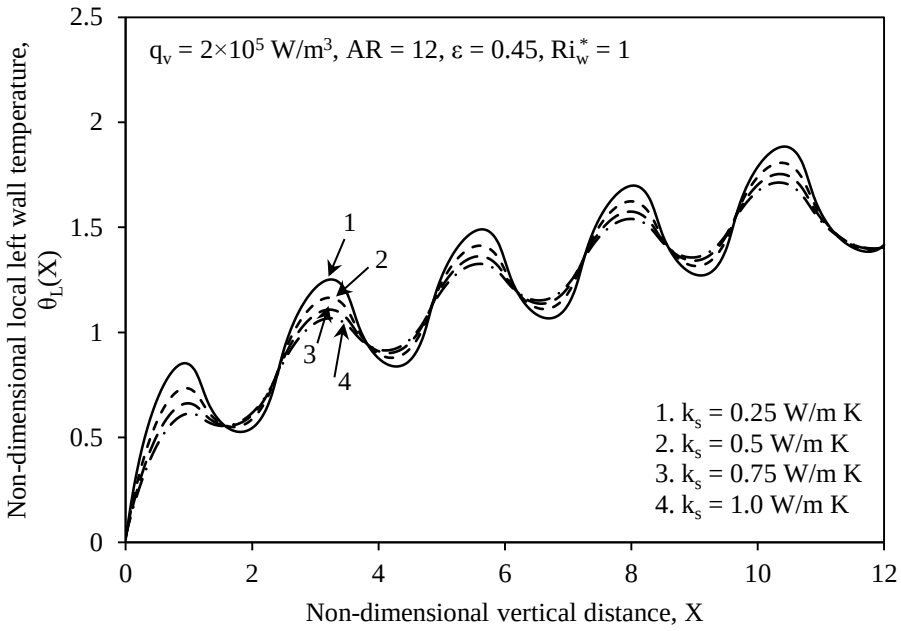

(a)

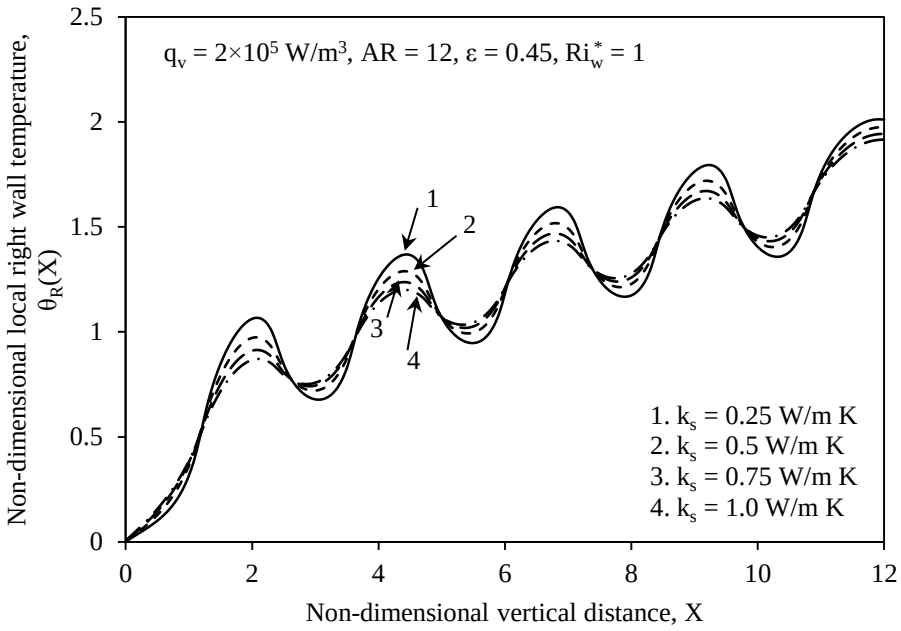

(b)

Fig. 4.9 Local non-dimensional temperature profiles for (a) left wall and (b) right wall for different thermal conductivities of the wall material

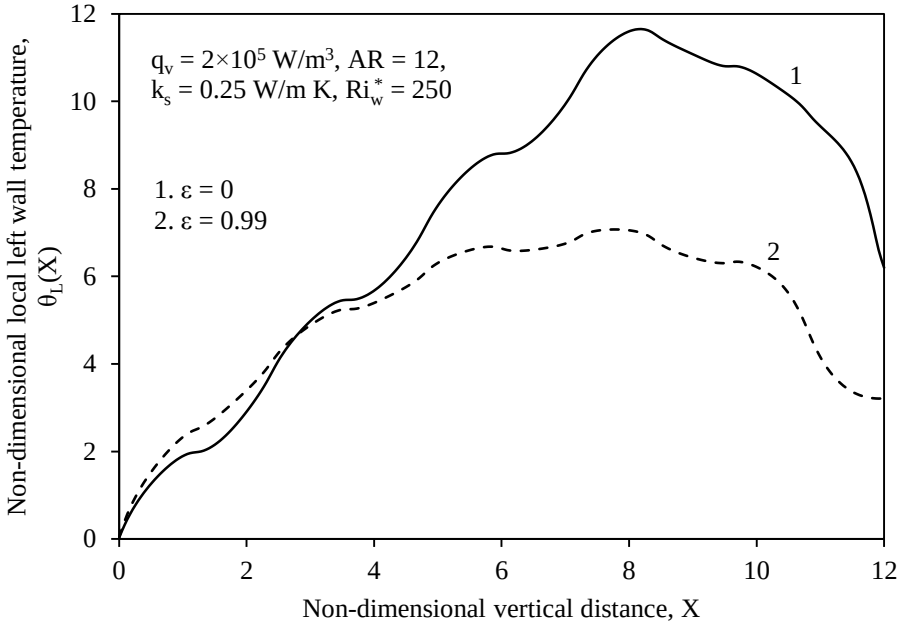

(a)

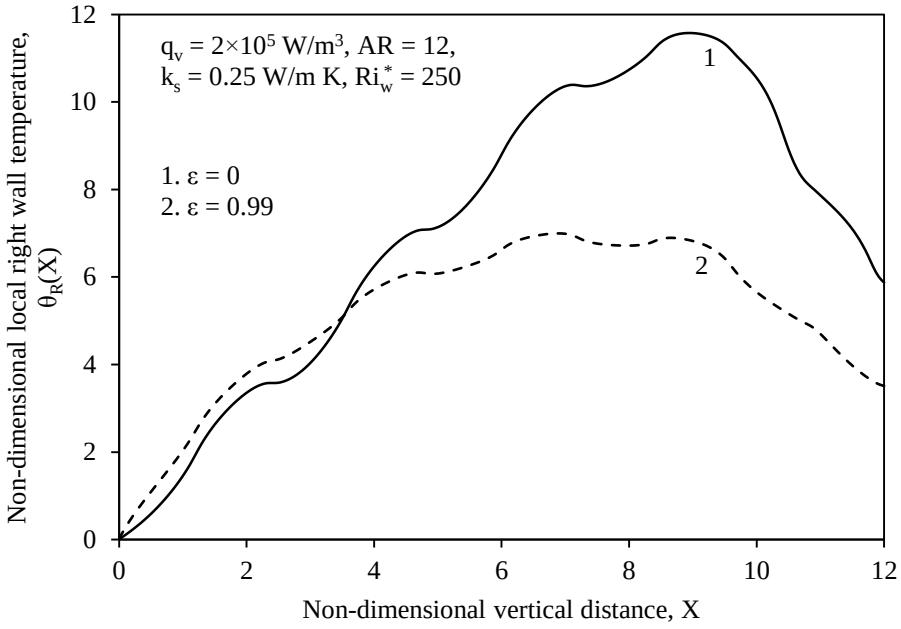

(b)

Fig. 4.10 Extraction of singular role of radiation in non-dimensional local (a) left wall and (b) right wall temperature distributions

spelt out already. In the present example, the maximum left wall temperature comes down by 39.29% with the maximum right wall temperature coming down by 39.56% when radiation (with $\varepsilon = 0.99$) is considered as against the situation without radiation ($\varepsilon = 0$). Thus, it is strongly recommended to take radiation into reckoning while tackling the present kind of problems.

4.4.5 Variation of Maximum Temperature of the Channel with Other Parameters

The results that throw light on the effect of all relevant independent parameters on the maximum channel temperature are discussed in the present section.

4.4.5.1 Variation with surface emissivity in different regimes of mixed convection

Figure 4.11 demonstrates the effect of surface emissivity (ε) in controlling the maximum non-dimensional temperature of the channel (θ_{max}) in various regimes of mixed convection. Five different values of ε and Ri_w^* are chosen as shown in the figure that also gives the remaining input parameters held fixed in the study. Here, $Ri_w^* = 250$ represents the asymptotic free convection limit, while $Ri_w^* = 0.01$ indicates the asymptotic forced convection limit. It is observed that θ_{max} decreases with increasing ε in all the regimes of mixed convection, with the degree of decrease getting more pronounced in the free convection dominant regime when compared to the forced convection dominant regime. This is due to an enhanced convection activity in the forced convection dominant regime that overrides dissipation by radiation. For example, in the study performed here, θ_{max} comes down by 20.19% and 7.38%, respectively, for $Ri_w^* = 250$ and 0.01, with ε increasing from 0.05 to 0.85.

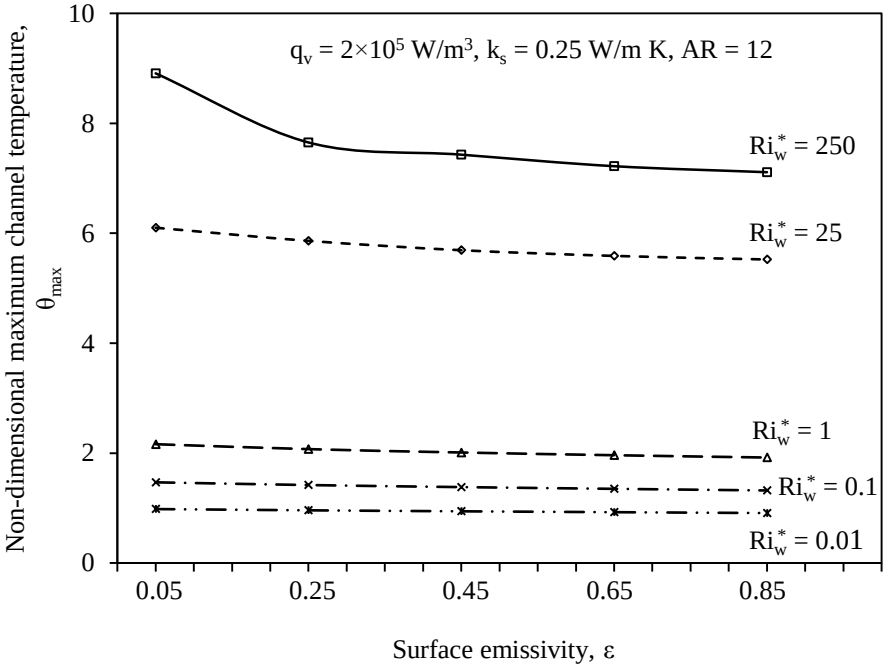

Fig. 4.11 Variation of non-dimensional maximum temperature of the channel with surface emissivity in different regimes of mixed convection

The figure further reveals that, for a given surface coating (ε), the peak channel temperature diminishes with decreasing Ri_w^*. This is due to the transit of flow regime from free convection dominance to forced convection dominance leading to enhanced convective heat dissipation that brings down θ_{max}. In particular, one can notice a far larger decrement in θ_{max} between $Ri_w^* = 250$ and $Ri_w^* = 1$ than that between $Ri_w^* = 1$ and $Ri_w^* = 0.01$. Quantifying the above observation, for a moderately emitting surface ($\varepsilon = 0.45$), θ_{max} is seen to coming down by 72.91% owing to a change in Ri_w^* from 250 to 1, while a similar attempt of decreasing Ri_w^* further down to 0.01 from 1 is bringing only a 53.16% drop in θ_{max}. These findings provide the designer the needed choice in controlling the peak temperature attained by the channel either by appropriately selecting the surface coating in a given operating regime or by regulating the induced velocity of flow for a given surface coating.

4.4.5.2 Variation with surface emissivity for materials of different thermal conductivities

The interplay between material property (k_s) and surface property (ε) in deciding the peak channel temperature in pure mixed convection regime ($Ri_w^* = 1.0$) is narrated in Fig. 4.12. Five values of ε, viz., 0.05, 0.25, 0.45, 0.65 and 0.85, and three different values of k_s, namely 0.25, 0.5 and 1 W/m K, are used for carrying out the study. The rest of the input parameters, viz., AR, q_v, and Ri_w^*, are held constant during the study as shown in the figure. For a given k_s, θ_{max} is decreasing with increasing ε, due to an understandable rise in the rate of radiative heat dissipation from the channel wall. The nature of decrease in θ_{max} is broadly similar for all the values of k_s. In the present example, for k_s = 0.25 W/m K, θ_{max} is seen to decrease by 11.21%

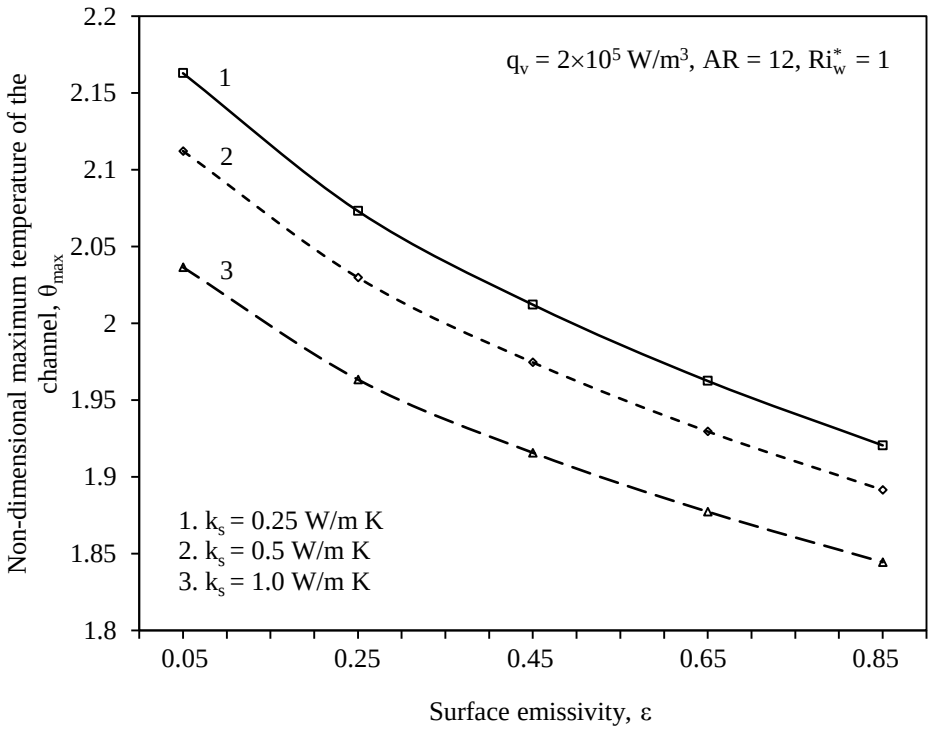

Fig. 4.12 Variation of non-dimensional maximum channel temperature with surface emissivity for different thermal conductivities of wall material

as ε increases to 0.85 from 0.05, while it drops by 9.43% for k_s = 1 W/m K between the same limits of ε. The figure further shows that, for a given ε, θ_{max} decreases with increasing k_s due to an enhanced rate of percolation of heat through the wall. Quantifying this observation for ε

= 0.05 and 0.85, θ_{max} is dropping down by 5.84% and 3.96%, respectively, as the thermal conductivity of the channel material is increased from 0.25 to 1 W/m K.

4.4.5.3 Variation with modified Richardson number for different thermal conductivities

Figure 4.13 shows the variation the peak channel temperature (θ_{max}) undergoes with modified Richardson number ($0.01 \leq Ri_w^* \leq 250$) for three different materials chosen (k_s = 0.25, 0.5 and 1 W/m K). The results are obtained for a constant input of AR = 12, ε = 0.45 and $q_v = 5\times10^5$ W/m^3. The figure reveals that θ_{max} is coming down with decreasing Ri_w^*, for a given k_s, on account of transit of flow from free to forced convection. The above effect is more revealing in the free convection dominant regime than in the forced convection dominant regime.

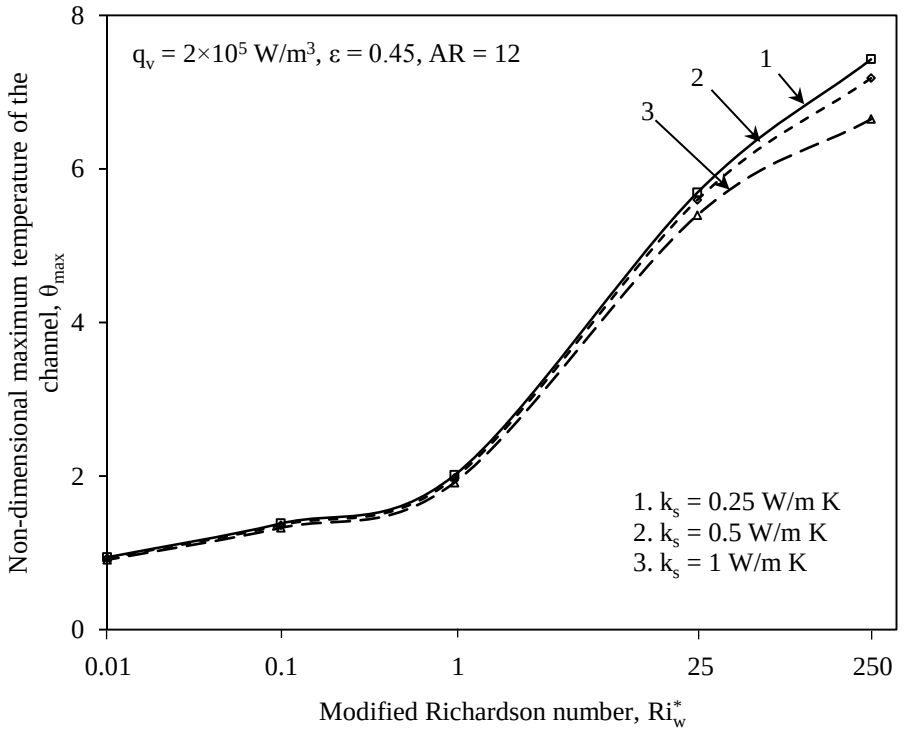

Fig. 4.13 Variation of non-dimensional maximum channel temperature with modified Richardson number for different wall materials

In the present case, for k_s = 0.25 W/m K, θ_{max} is dropping down by 23.39% as Ri_w^* comes down from 250 to 25, while it experiences a further drop of 64.65% with Ri_w^* getting

subsequently reduced to 1. It is further noticed that θ_{max} is decreasing with increasing k_s in all the regimes of mixed convection owing to reasons spelt out already. In the case considered here, for $Ri_w^* = 250$, θ_{max} is coming down by 3.31% as k_s increases from 0.25 to 0.5 W/m K and by a further 7.43% with k_s subsequently rising to 1 W/m K. The degree of decrement θ_{max} experiences here is looking quantitatively smaller owing to the use of lower values of k_s (0.25-1 W/m K).

4.4.5.4 Effect of aspect ratio of the channel on maximum channel temperature

A heat transfer engineer exhibits a general tendency to pack the arrays of electronic boards closely to save on space. In this context, it is appropriate to look into the effect of wall spacing on peak temperature (θ_{max}) assumed by the channel. Figure 4.14 describes the findings of such a study performed in all the three regimes of mixed convection ($Ri_w^* = 250$, 1 and 0.01) for five typical values of aspect ratio ($4 \leq AR \leq 20$) holding rest of the input fixed. The figure generally indicates a rise in θ_{max} with increasing AR in all the regimes of mixed convection. However, an unacceptedly larger rise in θ_{max} is noticed with increasing AR in the free convection dominant regime (say for $Ri_w^* = 250$), while this effect peters down as the operating environment transits to forced convection dominant regime (say for $Ri_w^* = 0.01$). Speaking quantitatively, θ_{max} is shooting up by a huge 672.86% for $Ri_w^* = 250$ as AR is increased to 20 from 4. A similar exercise, in contrast, is bringing only 103.58% and 19.98% rise in θ_{max}, respectively, for $Ri_w^* = 1$ and 0.01. These results caution the design engineer while packing the electronic boards together, for a given height, in a given application generally in any regime of convection and more specifically while working in the free convection dominant environment.

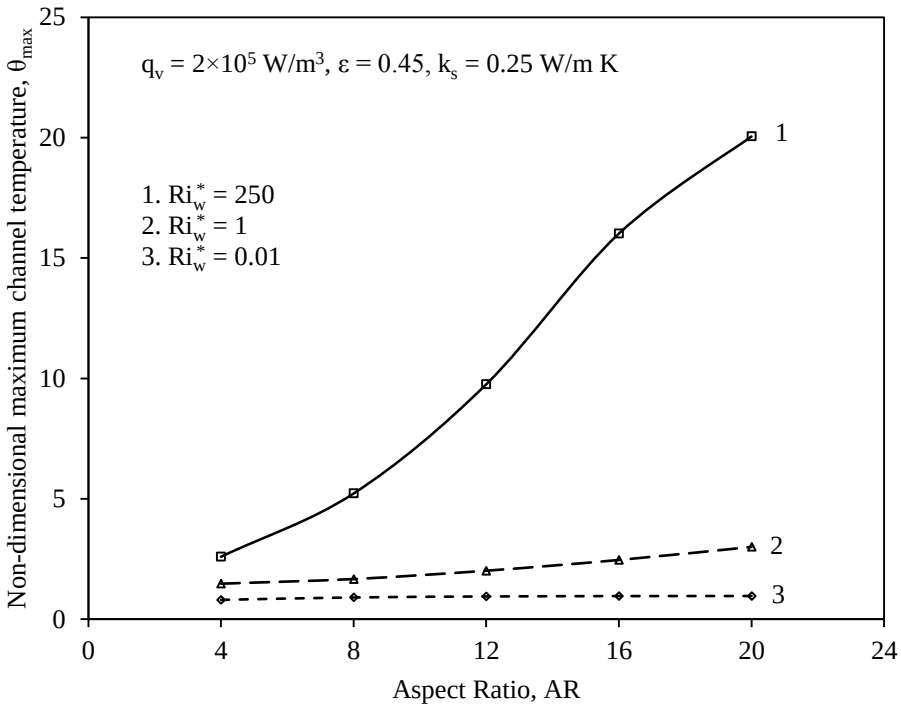

Fig. 4.14 Variation of non-dimensional maximum channel temperature with aspect ratio in different regimes of mixed convection

4.4.5.5 Exclusive effect of radiation on peak channel temperature

A study bringing out the exclusive role of ε in controlling the maximum non-dimensional channel temperature over the entire mixed convection regime has been performed and the results are depicted in Fig. 4.15. Two values of ε are considered, viz., ε = 0 (radiation absent) and ε = 0.99 (maximum possible radiation), while the rest of the input includes AR = 12, k_s = 0.25 W/m K and $q_v = 2\times10^5$ W/m^3. As many as seven values of Ri_w^* covering the entire regime of mixed convection have been chosen. The figure clearly underlines the fact that non-consideration of radiation in calculations leads to an undue overestimation of the peak channel temperature (θ_{max}) in all regimes of mixed convection, in general, and in the free convection dominant regime, in particular. This occurs to a lesser degree for $Ri_w^* = 0.01$ and is found to increase gradually with increasing Ri_w^*, with the most perceivable effect noticed at $Ri_w^* = 250$. In the present study, θ_{max} comes down by 9.44% in the asymptotic forced

convection limit ($Ri_w^* = 0.01$), upon changing the channel surface from a perfect reflector ($\varepsilon = 0$) to a perfect emitter ($\varepsilon = 0.99$). In the asymptotic free convection limit ($Ri_w^* = 250$), the above exercise of changing the surface of the channel brings a very significant drop in θ_{max} by as much as 39.29%. These observations underline the significant role exhibited by radiation in cutting down the maximum non-dimensional channel temperature in all the regimes of mixed convection.

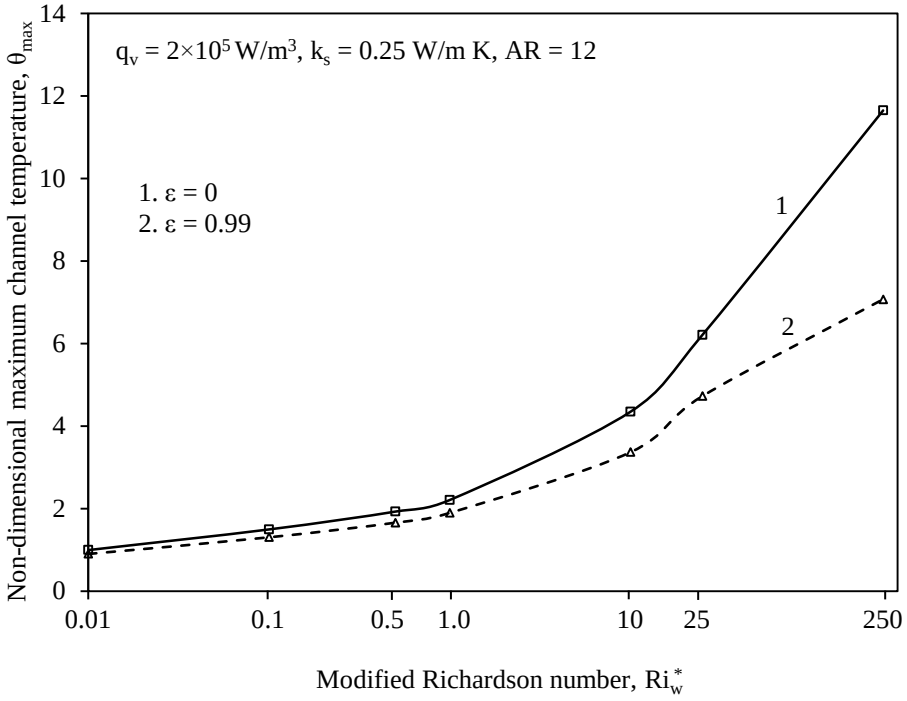

Fig. 4.15 Exclusive effect of radiation on peak channel temperature in different regimes of mixed convection

4.4.6 Relative Contributory Roles Exhibited by Mixed Convection and Radiation in Heat Dissipation from the Channel

The heat generated in the ten discrete heat sources flush-mounted in the left and right walls of the channel, after getting conducted along the walls, gets dissipated by the combined modes

of mixed convection and radiation. In this context, it has been decided to look into relative roles exhibited by mixed convection and radiation.

4.4.6.1 Variation of relative contributions with surface emissivity in different regimes of mixed convection

The heat generated in the channel due to the presence of the ten discrete heat sources in its walls is dissipated by mixed convection and surface radiation. It is appropriate to dwell into the individual contributions from mixed convection and radiation for various values of emissivity (ε) and in different regimes of mixed convection. Figure 4.16, plotted for q_v = 2×10^5 W/m^3, k_s = 0.25 W/m K and AR = 12, reveals the findings of such a study. Five typical

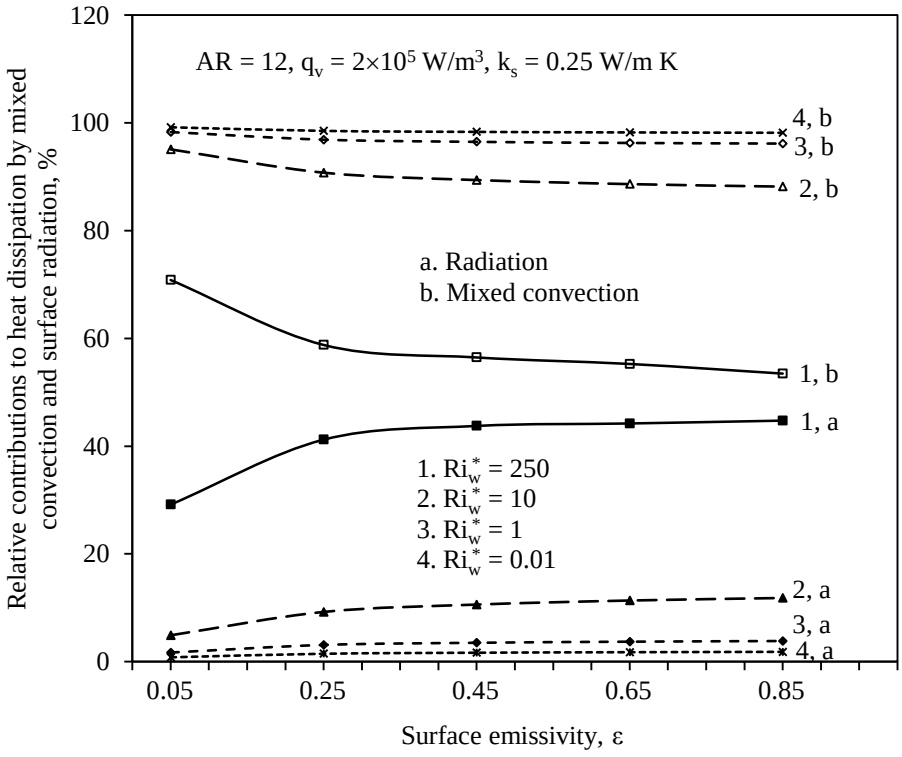

Fig. 4.16 Relative contributions of mixed convection and surface radiation in channel heat dissipation for different surface emissivities and in various regimes of mixed convection

values of surface emissivity encompassing the range ($0.05 \leq \varepsilon \leq 0.85$) and four different values of Ri_w^* catering to the entire range of mixed convection from the free convection dominant regime ($Ri_w^* = 250$) to the forced convection dominant regime ($Ri_w^* = 0.01$) are used. An increasing ε is observed to bring down the contribution from convection with a proportionate increase in that from radiation. In the present example, for $Ri_w^* = 0.01$, i.e., the asymptotic forced convection limit, the contribution from radiation rises from 0.81% to 1.83% as ε increases from 0.05 to 0.85. A similar exercise in the asymptotic free convection limit ($Ri_w^* = 250$) increases the radiative dissipation from 29.16% to 44.75%. There is a corresponding drop in the contribution from mixed convection in both the cases. It can also be noted that, for a given ε, as one moves from the forced convection dominant regime to the free convection dominant regime, the contribution of convection, expectedly, decreases with a mirror-image increase in the radiation contribution. For a good emitter (black paint with ε = 0.85), the convective heat dissipation is decreasing from 98.17% to 53.47% as Ri_w^* is changing from 0.01 to 250. It goes without saying that the role of radiation readjusts itself appropriate to the changes in the role of mixed convection owing to the above change in the flow regime (or Ri_w^*).

4.4.6.2 Variation of relative contributions with aspect ratio in different regimes of mixed convection

The role aspect ratio (AR) plays in deciding the relative contributions provided by mixed convection and radiation in channel heat dissipation in different regimes of mixed convection has been provided into, as narrated in Fig. 4.17. Five different values are chosen for AR (4, 8, 12, 16 and 20), while three typical regimes of mixed convection ($Ri_w^* = 250$, 1 and 0.01) are tried. The rest of the input that is held unaltered is also shown. The figure, in general, indicates a progressive decrease in the role of radiation with increasing AR, which gets

manifested as a corresponding rise in the contribution from mixed convection. Also, the above effect seems to be equally apparent in both the free convection dominant ($Ri_w^* = 250$) as well as forced convection dominant ($Ri_w^* = 0.01$) regimes. In the present example, for $Ri_w^* = 250$, radiation suffers 71.69% drop in its role as the channel gets progressively narrower from AR = 4 to AR = 20. The above is obviously leading to a mirror-image rise in mixed convection. Likewise, for $Ri_w^* = 0.01$ too, a similar exercise as above brings a 80.43% decrease in the role of radiation in channel heat dissipation.

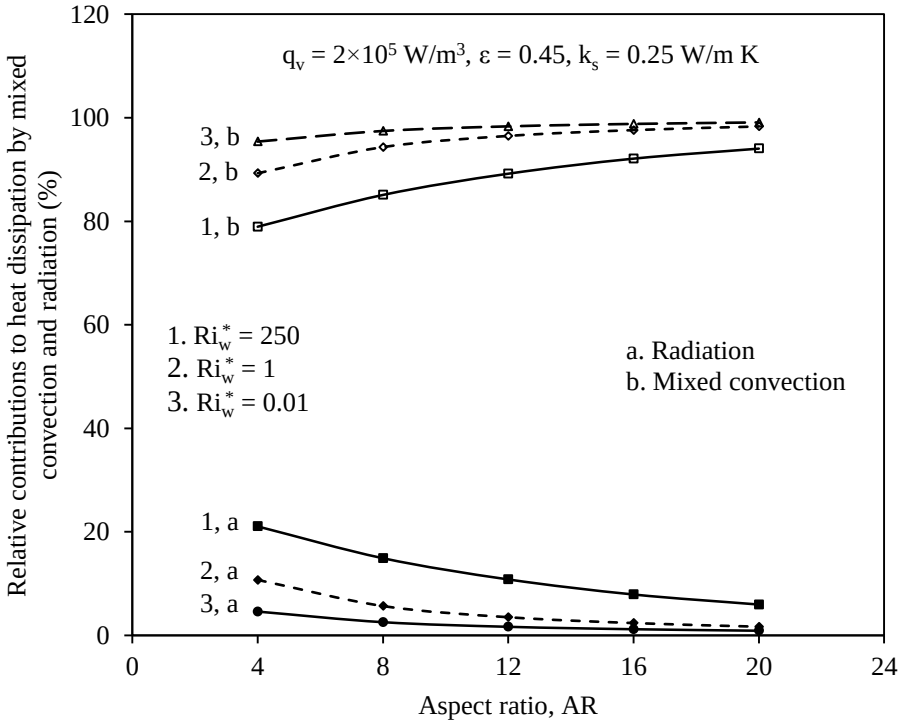

Fig. 4.17 Relative roles of mixed convection and surface radiation with aspect ratio in different regimes of mixed convection

4.4.6.3 Variation of relative contributions with thermal conductivity of the channel material in different regimes of mixed convection

The relative contributions of mixed convection and radiation in channel heat dissipation are drawn against k_s for three different values of Ri_w^*, while the remaining input parameters are

held fixed, as shown in Fig. 4.18. It is observed that, for Ri_w^* = 250 (asymptotic free convection limit), an increasing k_s brings a noticeable rise in the contribution from mixed convection with a corresponding decrease in that from radiation. In the present example, for the above value of Ri_w^*, the contribution of mixed convection is increasing from 57.19% to 65.06% with k_s increasing from 0.25 to 1 W/m K, while there is a corresponding decrease in the contribution of radiation from 42.81% to 34.94%. However, for Ri_w^* = 1 and 0.01, the

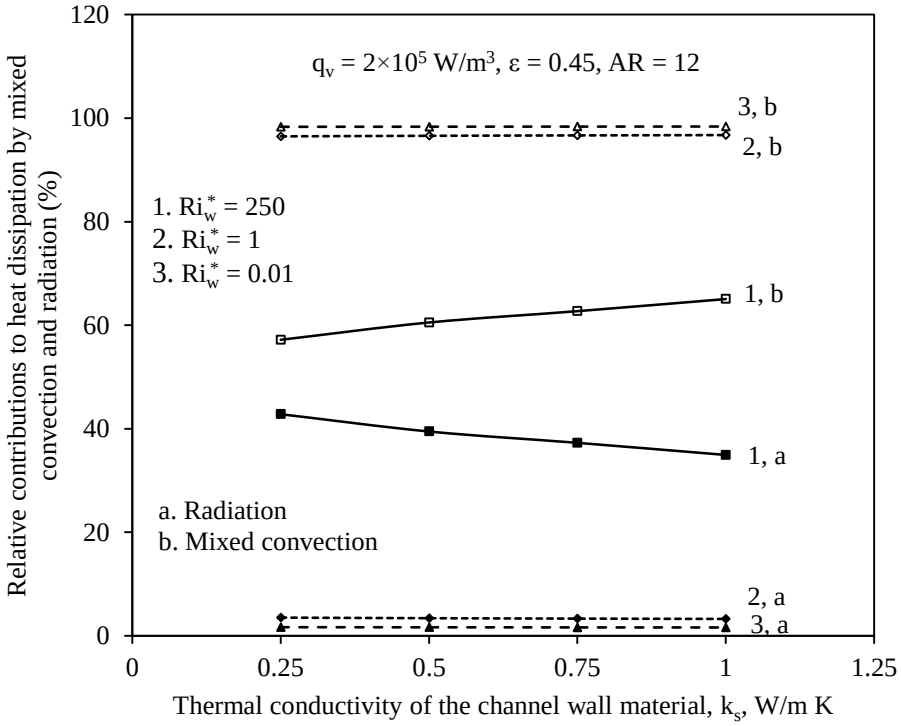

Fig. 4.18 Relative contributions of mixed convection and surface radiation with thermal conductivity of the channel wall in different regimes of mixed convection

effect of thermal conductivity on the relative contributions by mixed convection and radiation is negligible. The figure further shows an expected increase in convective heat dissipation with the flow transiting from the asymptotic free to forced convection limit with a corresponding mirror-image drop noticed in the role of radiation. For example, for k_s = 0.5 W/m K, radiation finds its role in heat dissipation enhanced from 1.6% for Ri_w^* = 0.01 to

39.47% for $Ri_w^* = 250$. By the same token, one can notice the convection contribution dipping down from 98.36% to 60.53% between the same limits of Ri_w^*.

4.4.7 Variation of Local Drag Coefficient with Other Parameters

The drag the fluid experiences as it flows through the channel assumes significance owing to its presence in the calculation of the pumping power requirement. Thus, a few studies have been performed to dwell into the nature of variation of the local drag coefficient (C_{fx}) with the remaining pertinent parameters and the current section provides an account of the same.

4.4.7.1 Variation with surface emissivity of the channel

A study is performed to understand the role surface emissivity (ε) plays in deciding the nature of variation of the local left and right wall drag coefficients ($C_{fx,L}$ and $C_{fx,R}$ respectively). Figure 4.19 provides the results thus obtained for a fixed input of q_v, Ri_w^*, AR and k_s considered as shown therein. Three representative values of ε, viz., 0.05 (replicating a good reflector like aluminum), 0.45 (signifying an average emitter) and 0.85 (concerning a good emitter like black paint), are chosen. As can be noticed from Fig. 4.19 (a), for a given ε, the local drag coefficient ($C_{fx,L}$) abruptly drops down to a local minimum at the entry of the channel due to the absence of velocity gradient there. With the wall velocity gradient gradually increasing from here, C_{fx} increases attaining a local peak near the top end of the bottommost heat source. It decreases again from hereto a local minimum in the immediately accompanying non-heat source portion. As the second heat source commences, the local drag coefficient shoots up again attaining a second local maximum a little ahead of the top end of the concerned heat source and again drops down in the immediately succeeding non-heat source portion. This continues till the channel exit thus exhibiting six local maxima and six

local minima. A similar nature of variation could be observed for all the three values of ε considered. The figure further indicates that $C_{fx,L}$ decreases with increasing emissivity owing to a decrease in wall velocity gradient due to an increased radiative heat dissipation.

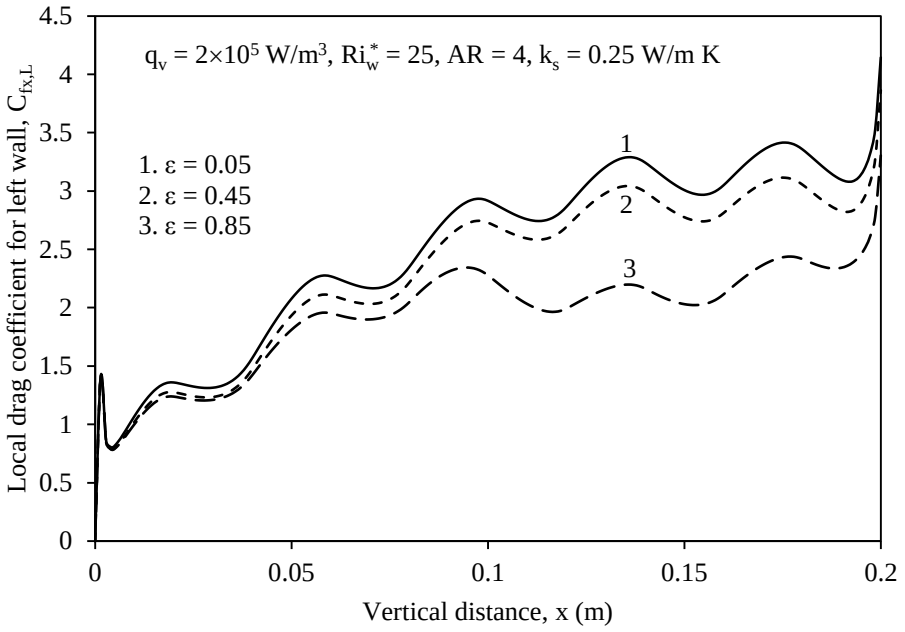

(a)

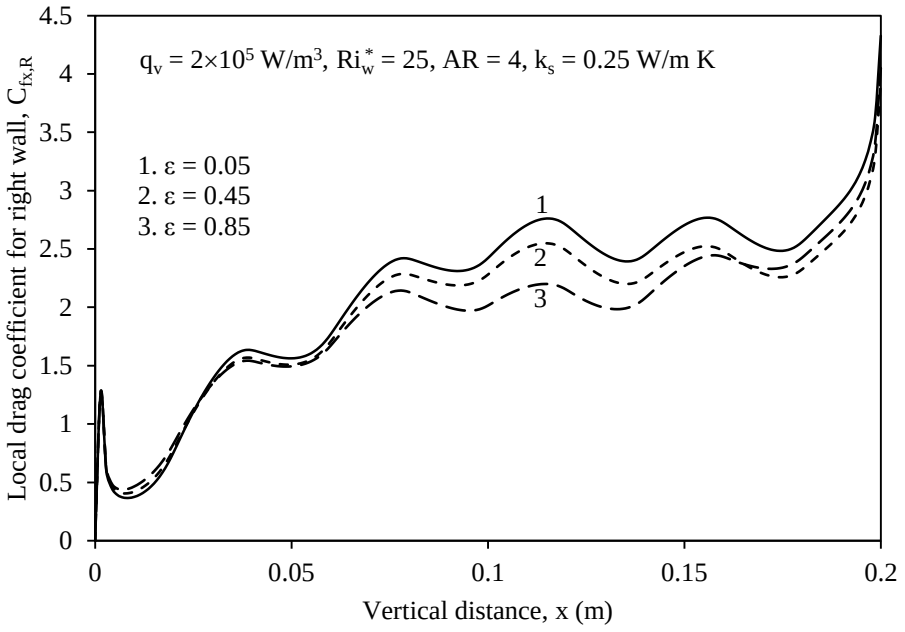

(b)

Fig. 4.19 Local drag coefficient along the (a) left and (b) right walls of the channel for different surface emissivities

In the present example, $C_{fx,L}$ at the channel exit is seen to be coming down by 20.27% with ε increasing from 0.05 to 0.85. It may further observed that the drop in $C_{fx,L}$ with increasing ε gets more eminent between ε = 0.45 and ε = 0.85 as against that between ε = 0.05 and ε = 0.45 more specifically in the top of the channel.

The asymmetricity followed in positioning the discrete heat sources in the right wall is clearly reflected in the curves pertaining to $C_{fx,R}$ shown in Fig. 4.19 (b). As can be seen, for a given ε, $C_{fx,R}$ experiences five local maxima and five local minima in contrast to six local maxima and six local minima exhibited by $C_{fx,L}$ [Fig. 4.19 (a)]. The right wall drag coefficient is seen to observe to be increasing with increasing ε near the channel entry, while it decreases with increasing ε later on. The only exception is the crossing of the curves concerning ε = 0.45 and ε = 0.85 towards the channel exit. The non-monotonic variation in the irradiation received as well as the radiation emitted by different sections of the right wall with asymmetrically and discretely positioned heat sources could be attributed to the above trends exhibited by $C_{fx,R}$.

4.4.7.2 Variation with different modified Richardson numbers

Figure 4.20 presents the nature of variation of the local left and right wall drag coefficients ($C_{fx,L}$ and $C_{fx,R}$) in various regimes of mixed convection ($0.1 \leq Ri_w^* \leq 25$) for a given constant input, as shown. As can be noticed, the trends exhibited by $C_{fx,L}$ and $C_{fx,R}$ pertaining to Ri_w^* = 25 and Ri_w^* = 10 are similar to those in Fig. 4.19. It may be noticed from the figures that both $C_{fx,L}$ and $C_{fx,R}$ decrease at any location along the walls with the flow regime shifting from free to forced convection dominance. This should be so because, in forced convection dominant regime, the flow is due to both inertia and buoyancy forces, with the effect of buoyancy and the flow arising out of it decrease towards smaller values of Ri_w^*. In the present case, at the

channel exit, $C_{fx,L}$ and $C_{fx,R}$ are getting decreased, respectively, by 99.44% and 99.42% with Ri_w^* petering down from 25 to 0.1.

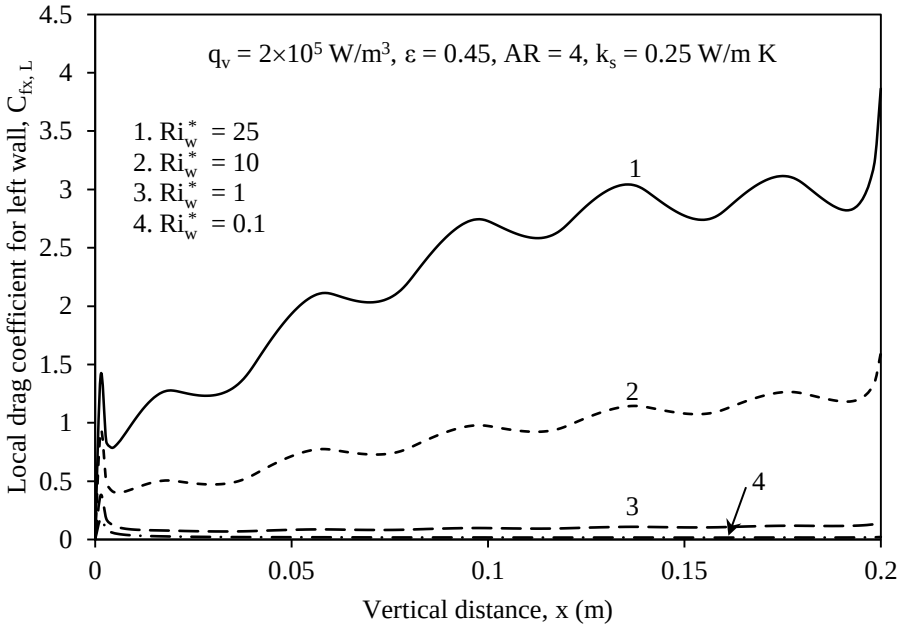

(a)

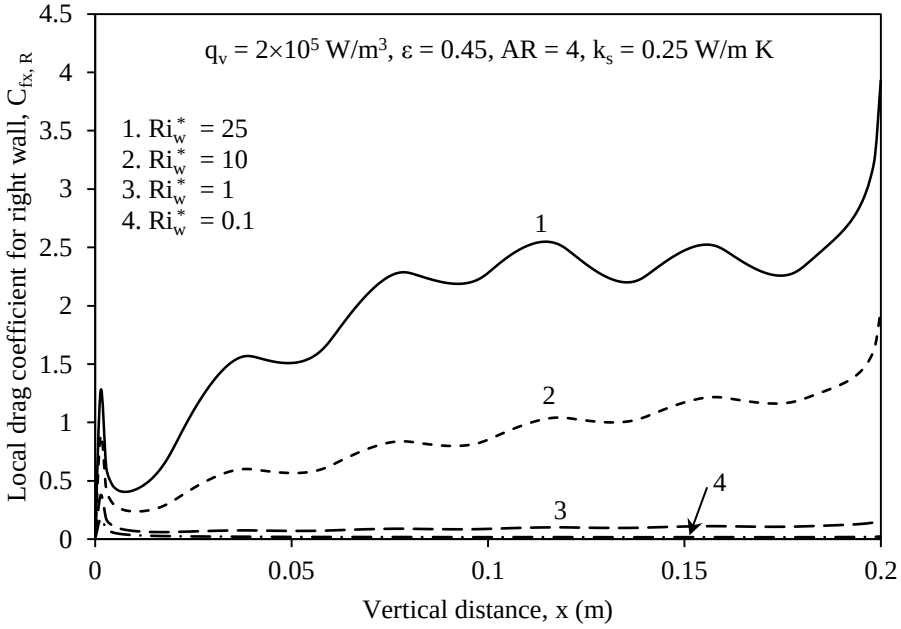

(b)

Fig. 4.20 Local drag coefficient along the (a) left and (b) right walls of the channel in different regimes of mixed convection

4.4.7.3 Variation with aspect ratio of the channel

The effect the wall spacing shows on the local drag coefficient for a given channel height (L) has been studied as shown in Fig. 4.21. Three values of AR, viz., 4, 12 and 20, are used holding the remaining input unaltered, as shown. Figures 4.21 (a) and (b) clearly indicate that, for a given AR, the local left and right wall drag coefficient profiles look to be similar to those noticed in some of the preceding studies. Further, an increasing AR brings a rise in both the left and right wall drag coefficients at any given location. This is because an increasing AR brings the walls of the channel progressively closer restricting the flow through the channel leading to increased wall drag coefficients. In the present example, at the channel exit, $C_{fx,L}$ and $C_{fx,R}$, respectively, get enhanced by 78.82% and 154.92% with AR increasing from 4 to 20.

4.4.7.4 Exclusive effect of radiation on local drag coefficient

It may be recalled that the exclusive role surface radiation plays in the local left and right wall temperature distributions has been studied in a preceding section [Section 4.4.4.5]. By the same token, the singular role exhibited by radiation in deciding the local left and right wall drag coefficients is studied as can be understood from Fig. 4.22. Two extreme values, viz., 0 and 0.99 are considered for ε with the rest of the input held unaltered as shown. One can clearly see a non-monotonic behavior in the two families of curves shown in Figs. 4.22 (a) and (b). With regard to the left wall, for example, consideration of radiation (curve 2 with $\varepsilon = 0.99$) tends to increase $C_{fx,L}$, to begin with, when compared to that in the case where radiation is ignored (curve 1 with $\varepsilon = 0$). Starting somewhere from the middle, the curves 1 and 2 cross that continues till the fag end of the channel. Here, the two curves cross again with curve 2 taking upper hand. The local right wall drag coefficient too exhibits a similar behavior in the

comparative study performed with and without radiation. The above may be attributed to the asymmetricity followed in the positioning of the discrete heat sources in the two channel walls.

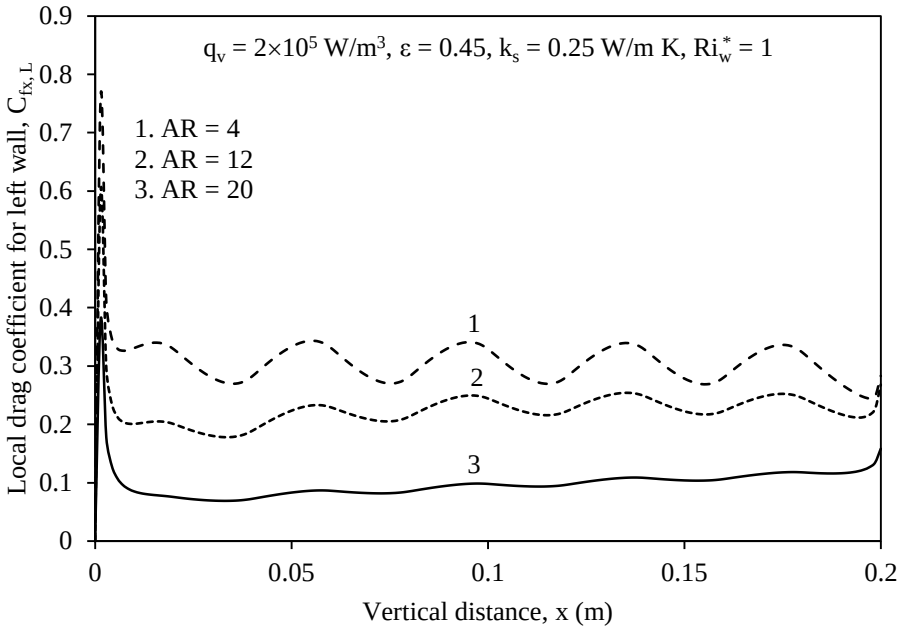

(a)

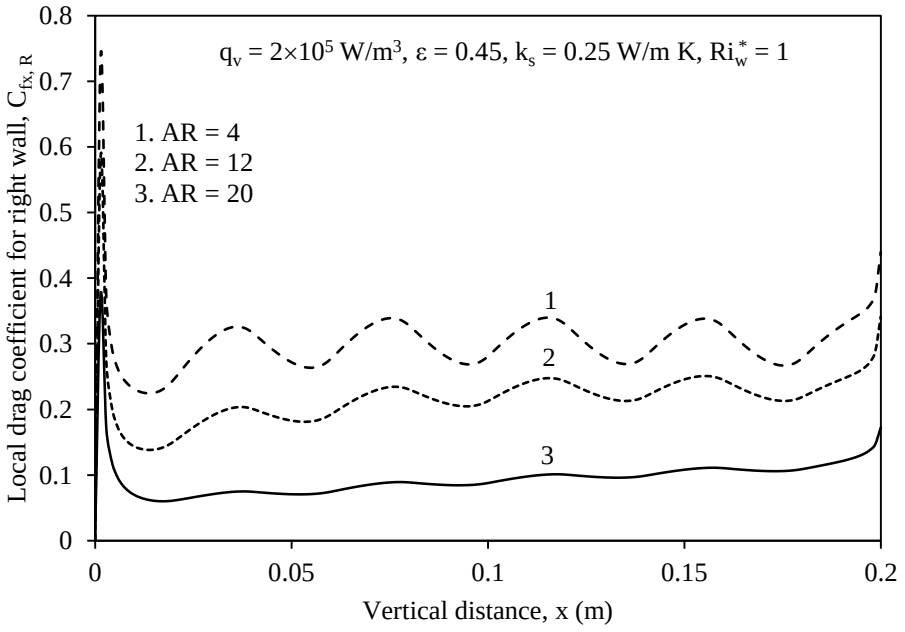

(b)

Fig. 4.21 Local drag coefficient along the (a) left and (b) right walls of the channel for different aspect ratios

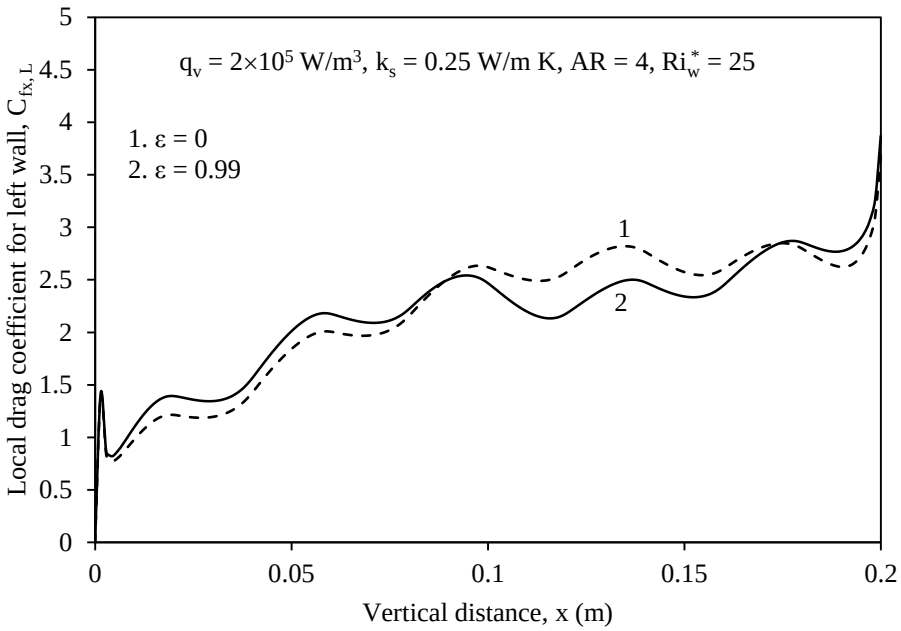

(a)

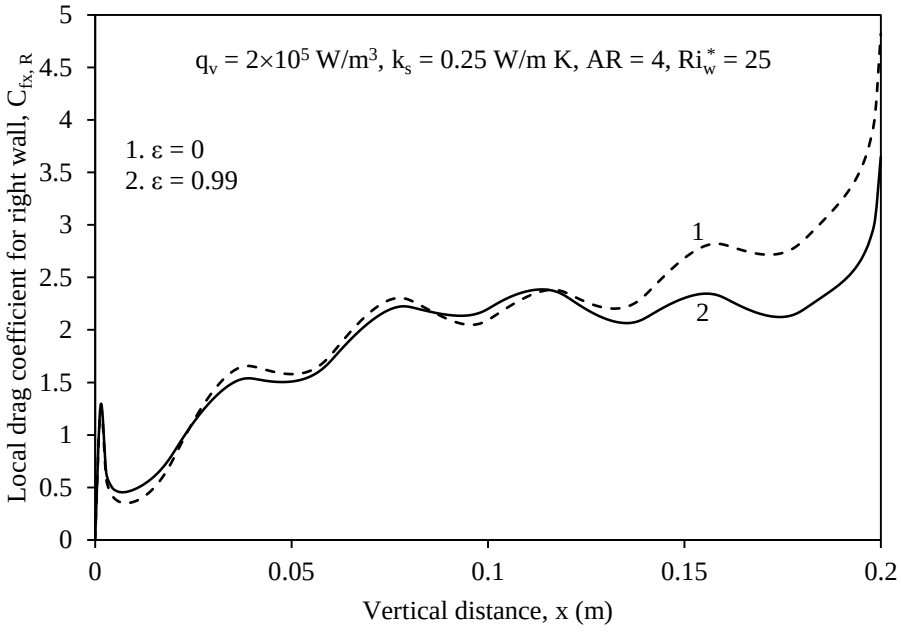

(b)

Fig. 4.22 Exclusive effect of radiation on local drag coefficient along the (a) left and (b) right walls of the channel

4.4.8 Variation of Mean Friction Coefficient with Other Parameters

Subsequent to studies on the local drag coefficient, a series of studies bringing out the dependence of the left and right wall mean friction coefficients ($\overline{C}_{f,L}$ and $\overline{C}_{f,R}$) has been performed and the current section documents some of the pertinent findings.

4.4.8.1 Variation in different regimes of mixed convection and for various surface emissivities

A probe into the dependence of the left and right wall mean friction coefficients of the channel ($\overline{C}_{f,L}$ and $\overline{C}_{f,R}$ respectively) on surface emissivity (ε) in different mixed convection regimes is made and the results are shown in Fig. 4.23. The study is performed for a fixed set of values of q_v, k_s and AR as shown. Five different values of ε signifying different kinds of channel surfaces from a near white body ($\varepsilon = 0.05$) to a near black body ($\varepsilon = 0.85$) are chosen. Four representative values are considered for Ri_w^*. Figure 4.23 (a) shows a considerable drop in $\overline{C}_{f,L}$ with increasing ε in the asymptotic free convection limit ($Ri_w^* = 25$). This may be attributed to an increasing radiative heat dissipation with increasing that tends to bring down the wall temperature gradient and thus the wall velocity gradient. This effect of ε on $\overline{C}_{f,L}$ is clearly noticed to be diminishing towards smaller values of Ri_w^*. This is so because, with decreasing Ri_w^* the flow regime transits from free to forced convection dominance, which tends to cut down the contribution of buoyancy to $\overline{C}_{f,L}$. In the specific example considered here, for $Ri_w^* = 25$, $\overline{C}_{f,L}$ is coming down by 9.79% as ε increases to 0.85 from 0.05. In contrast, for $Ri_w^* = 1$ and 0.1, respectively, $\overline{C}_{f,L}$ is seen to come down only by 1.84% and 0.69%, for the same increase in ε.

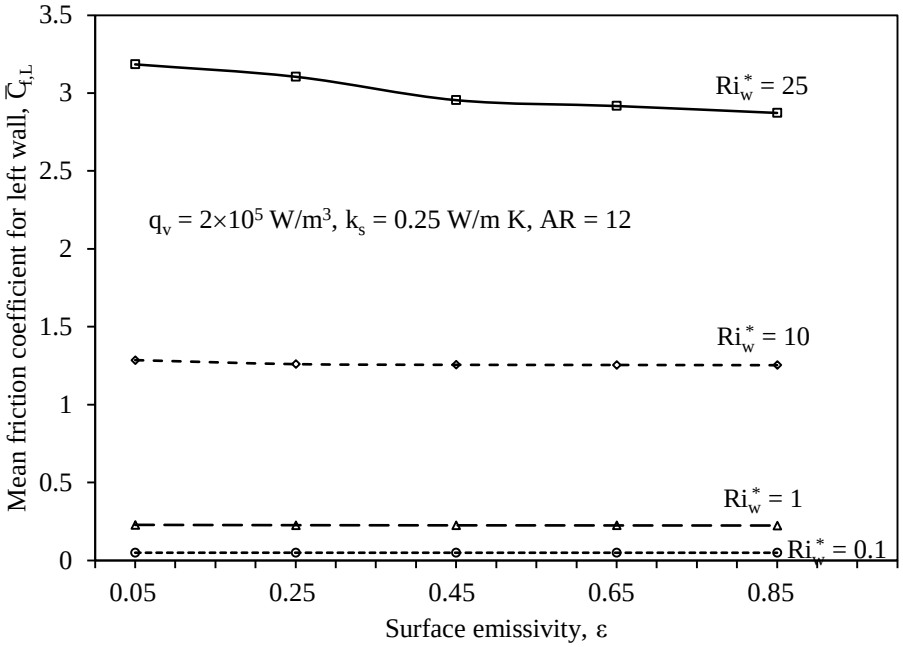

(a)

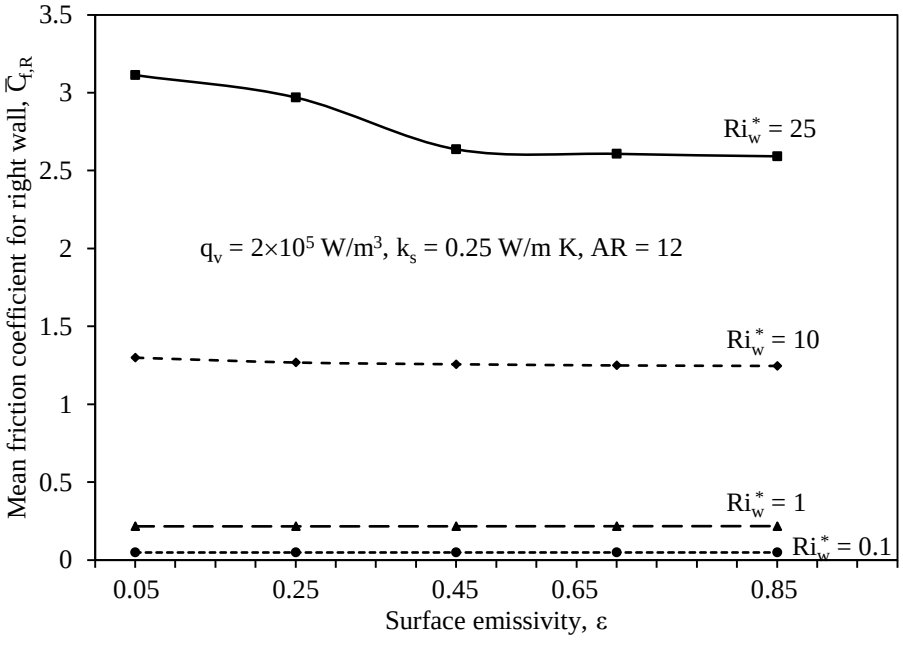

(b)

Fig. 4.23 Variation of mean friction coefficient of the (a) left and (b) right channel walls with surface emissivity in different regimes of mixed convection

Figure 4.23 (b) exhibits an almost similar trend in the variation of $\overline{C}_{f,R}$ as well. This is expected because, even here, the wall has an identical number (five) of heat sources as the left wall with the exception that there is an asymmetricity in their positioning. Quantifying the

results, for $Ri_w^* = 25$, $\overline{C}_{f,R}$ experiences a 16.75% decrease with ε increasing from 0.05 to 0.85. In contrast, for $Ri_w^* = 0.1$, the above exercise brings just a 0.37% drop in $\overline{C}_{f,R}$ on account of the reasons already explained.

4.4.8.2 Variation with different wall materials and in various regimes of mixed convection

The role wall material exhibits, in conjunction with regime of convection employed, in the left and right wall mean friction coefficients is studied for a fixed input of q_v, ε and AR, as shown in Fig. 4.24. As can be inferred, there is an almost negligible change in both $\overline{C}_{f,L}$ and $\overline{C}_{f,R}$ with increasing k_s for all values of Ri_w^*. This may be attributed to the fact that, with increasing k_s, the local wall temperature gradient and thus the wall velocity gradient increase in non-heat source portions and decrease in heat source portions. The figure further shows that the above nature of variation of $\overline{C}_f$ with k_s remains intact for all values of Ri_w^*. It can also be observed that, for a given k_s, $\overline{C}_{f,L}$ and $\overline{C}_{f,R}$ undergo a substantial decrease with the flow transforming from the dominance of free convection to that of forced convection owing to an increased impressed velocity. In the present example, for k_s = 0.25 W/m K, $\overline{C}_{f,L}$ and $\overline{C}_{f,R}$, respectively, suffer huge 74.05% and 75.73% drops as Ri_w^* changes from 250 to 25. Further, they drop down by 92.62% and 92.7% with Ri_w^* subsequently dipping down to 1.

4.4.8.3 Variation with surface emissivity for different wall thermal conductivities

Figure 4.25 reveals the interactive effect the wall material (k_s) and the surface emissivity (ε) show on the left and right wall mean friction coefficients. The study is performed in pure mixed convection regime ($Ri_w^* = 1$) considering fixed values for q_v and AR as shown. Four values of k_s and five values of ε are used to perform the study. The figure demonstrates that, for a given k_s, $\overline{C}_{f,L}$ and $\overline{C}_{f,R}$ decrease monotonically with ε. Likewise, for a given ε, $\overline{C}_{f,L}$ and

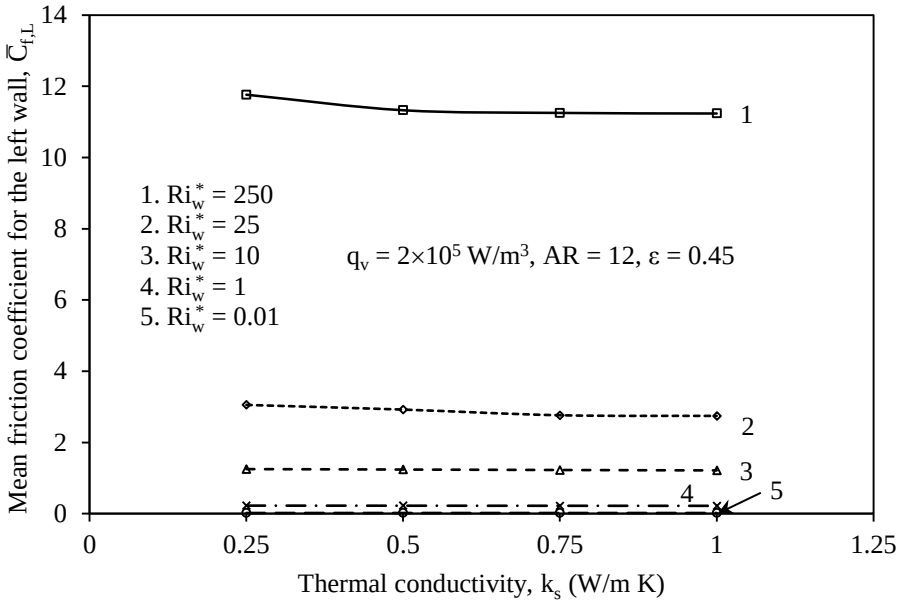

(a)

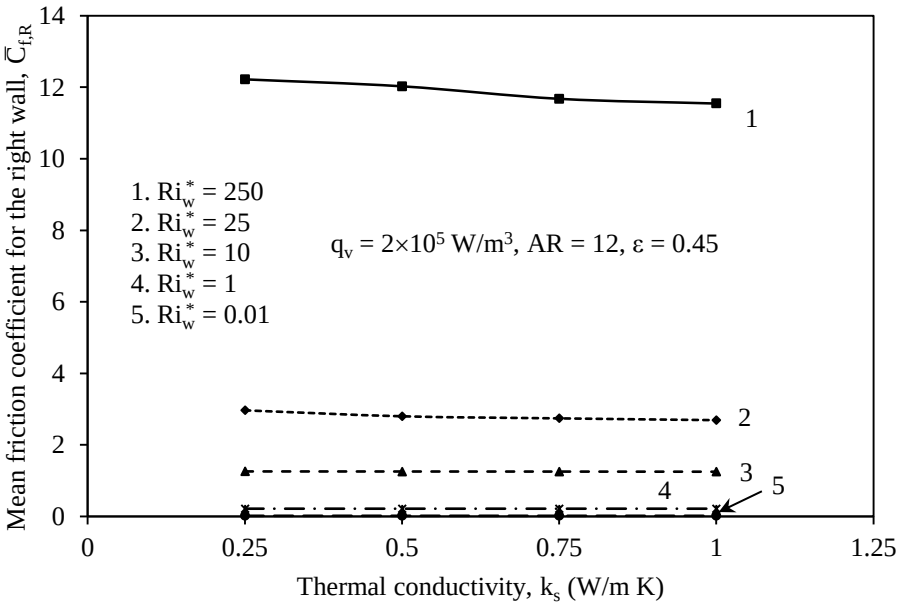

(b)

Fig. 4.24 Variation of mean friction coefficient of the (a) left and (b) right walls of the channel with thermal conductivity of the wall material in various regimes of mixed convection

$\overline{C}_{f,R}$ decrease with increasing k_s. This is because of the fact that the wall temperature gradient and thus the wall velocity gradient decrease thus decreasing $\overline{C}_{f,L}$ and $\overline{C}_{f,R}$ with increasing wall thermal conductivity.

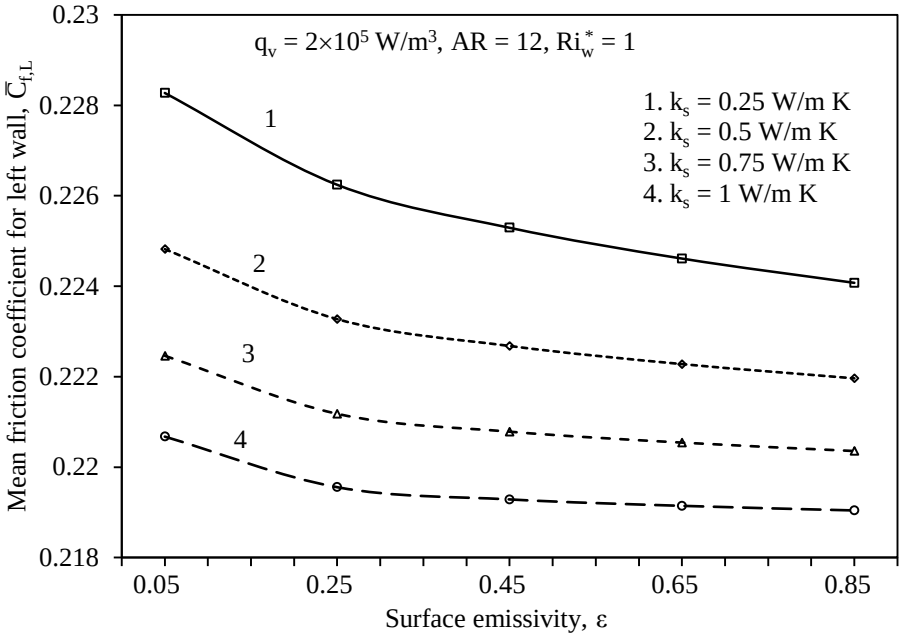

(a)

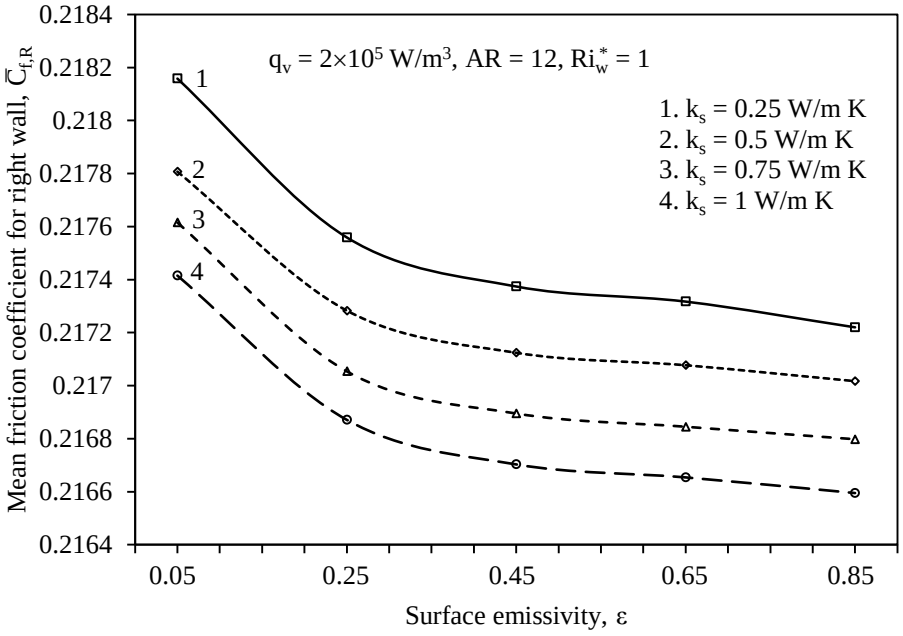

(b)

Fig. 4.25 Variation of mean friction coefficient of the (a) left and (b) right channel walls with surface emissivity for different wall thermal conductivities

4.4.8.4 Variation with aspect ratio for typical surface emissivities

Figure 4.26 depicts the results of a study made to bring out the role, if any, the aspect ratio (AR) plays, in conjunction with surface emissivity (ε), in influencing the two wall mean friction coefficients. Five typical values are considered for AR, while three different surface coatings are looked into. The remaining input that is held fixed during the study is as shown. For a given ε, an increasing AR makes the channel progressively narrower impeding the flow through it and thus leading to a sharp rise in $\overline{C}_f$ for both the walls. For the sample data considered here, for ε = 0.45, for example, $\overline{C}_{f,L}$ and $\overline{C}_{f,R}$ are found to rise quite sharply by 212.79% and 217.39%, respectively, with AR increasing to 20 from 4. Also, for a given AR, the wall mean friction coefficients decrease, rather less pronouncedly, with increasing ε. This is attributed to a decreasing wall velocity gradient due to a diminishing wall temperature gradient, which, in turn, is due to a progressively increasing radiative heat dissipation.

4.4.9 Extraction of Exclusive Effect of Buoyancy

With the present research work primarily focused on mixed convection, it would be interesting to separate out the role played by buoyancy in certain prime results of the problem.

4.4.9.1 Effect on local wall temperature distribution

Figure 4.27 shows the local non-dimensional left and right wall temperature profiles drawn with this objective. The study is made for a fixed input of $q_v = 2\times10^5$ W/m^3, k_s = 0.25 W/m K, AR = 12, $Ri_w^* = 250$ and ε = 0.05. Curve 1 pertains to the case where the effects of both free and forced convection are taken into account, while curve 2 is plotted with the result obtained by artificially suppressing the role of free convection in the present problem. As can be noticed, there is a decent influence brought in by buoyancy in a forced convection

configuration with both the left and right wall local temperatures coming down due to its presence. Quantifying the above observations, in the case considered here, the local left wall

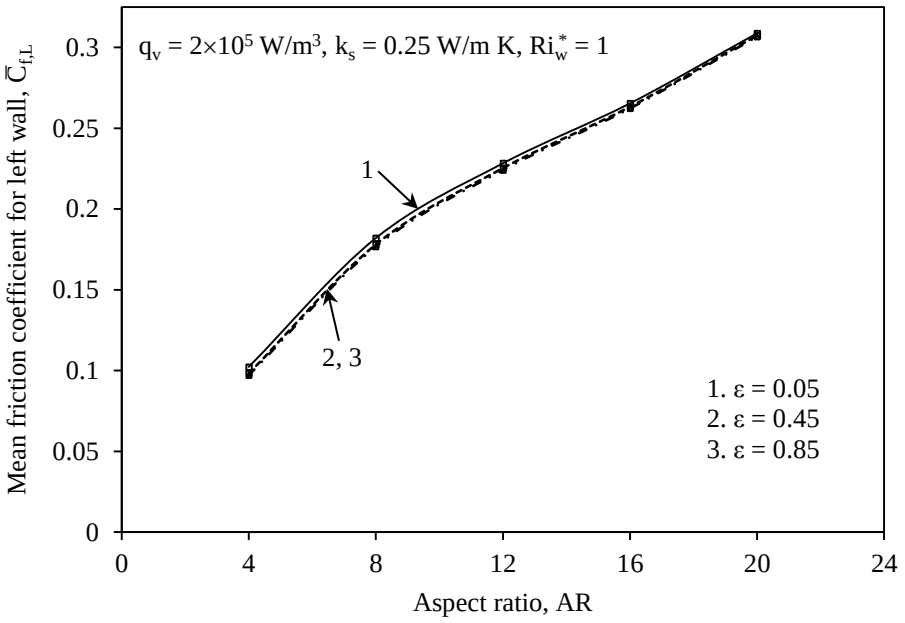

(a)

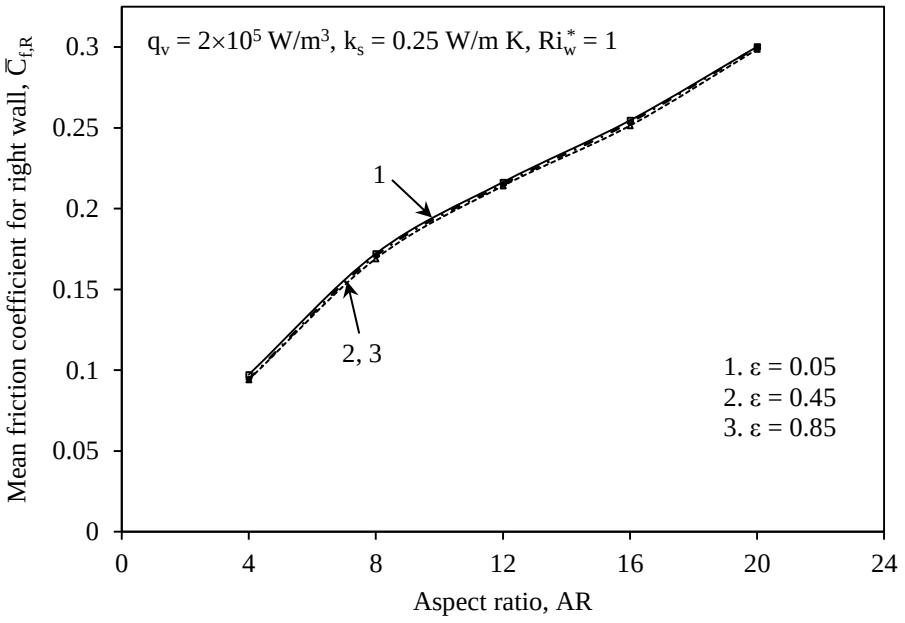

(b)

Fig. 4.26 Variation of mean friction coefficient of the (a) left and (b) right channel walls with aspect ratio for different surface emissivities

temperature at the channel exit comes down by 63.58%, while the right wall temperature at the corresponding location drops down by 61.63% upon considering buoyancy in the forced convection configuration.

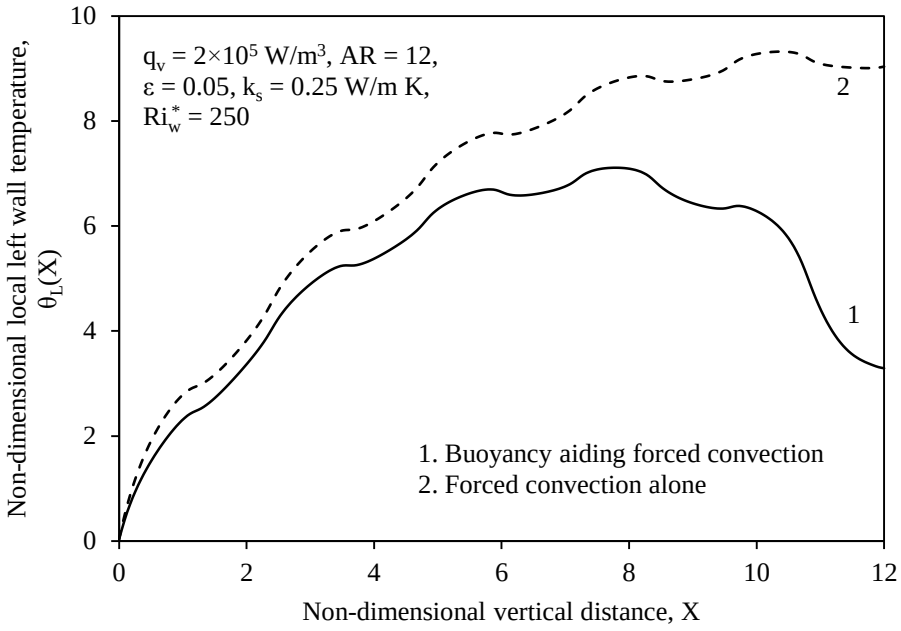

(a)

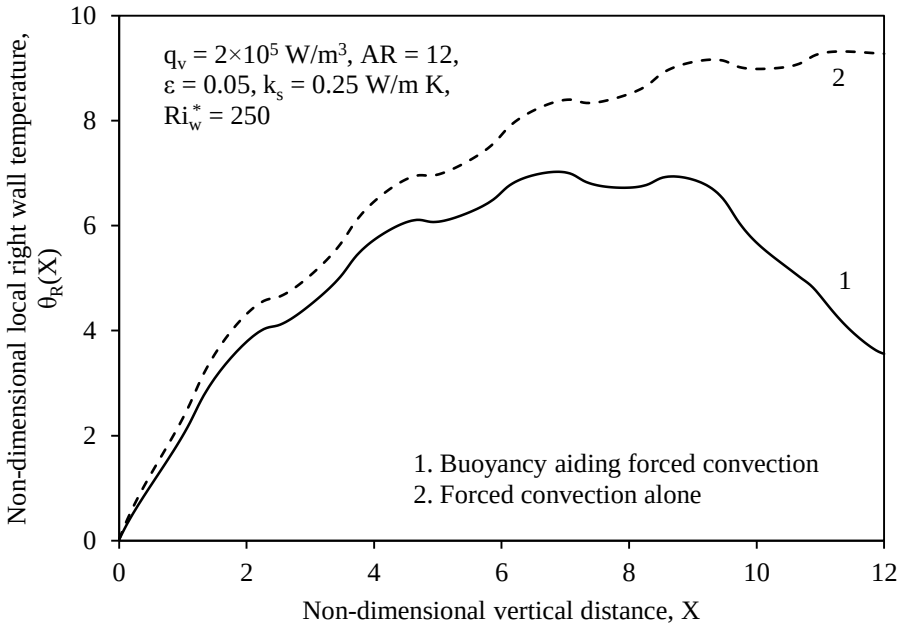

(b)

Fig. 4.27 Exclusive role played by buoyancy in non-dimensional local temperature distribution along the (a) left and (b) right walls of the channel

4.4.9.2 Effect on maximum channel temperature

Exploring the role of buoyancy in the present conjugate mixed convection problem a little further, attempts are made to separate out its effect on the peak temperature (θ_{max}) assumed by the channel in the entire mixed convection regime ($0.01 \leq Ri_w^* \leq 250$). Figure 4.28 exhibits the results of such study conducted holding the rest of the input parameters fixed as shown. The figure shows the variation of the peak channel temperature against Ri_w^* for two cases. Curve 1 belongs to the case that has both free and forced convection effects considered, while the

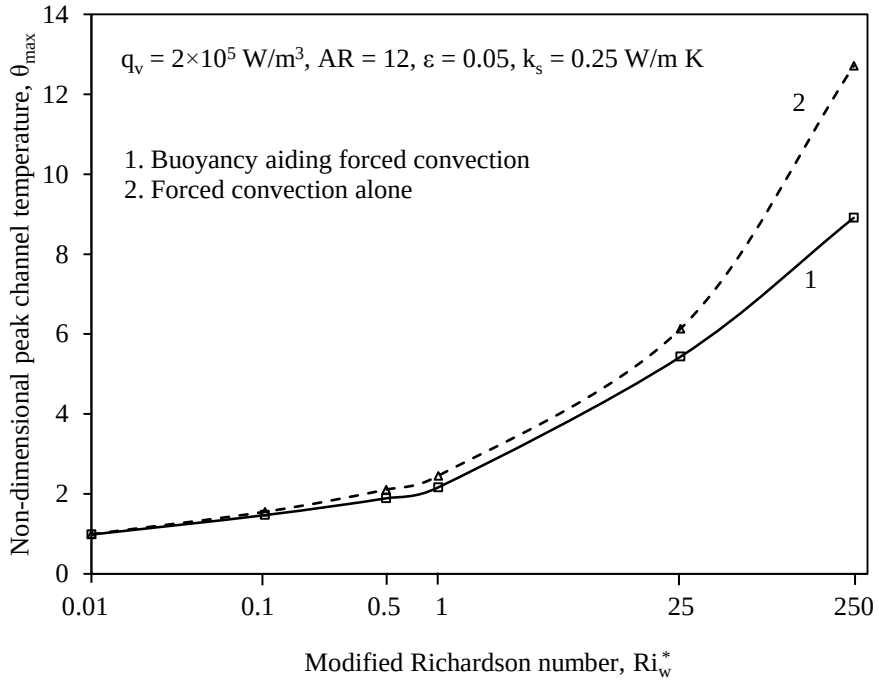

Fig. 4.28 Exclusive effect of buoyancy on non-dimensional peak channel temperature in different regimes of mixed convection

buoyancy term is artificially suppressed in curve 2. As can be clearly seen the contribution from free convection is not that pertinent up to $Ri_w^* \leq 1$. Subsequently to the above value of Ri_w^*, however, there is a well-marked divergence in the two curves. Here, buoyancy clearly starts to aid the impressed (forced convection) flow in bringing down the peak channel

temperature. In the present example, for $Ri_w^* = 250$, buoyancy is seen to cut down θ_{max} by 29.91%. This clearly highlights the importance of including buoyancy in thermal load calculations in the entire mixed convection regime, in general, and while working in a free convection dominant environment, in particular.

4.4.9.3 Effect on local left and right wall drag coefficients

Figure 4.29 elucidates the singular influence buoyancy exhibits on the local left and right wall drag coefficients. The study has been made for a set of fixed input as shown. One can clearly see a rise in the local drag that the fluid experiences during its passage through the channel upon taking buoyancy into account in a forced convection environment. This is noticed both with regard to $C_{fx,L}$ and $C_{fx,R}$. In the present example, at the channel exit, $C_{fx,L}$ and $C_{fx,R}$, respectively, go up by 67.84% and 85.28% when buoyancy aided mixed convection is considered instead of pure forced convection holding other parameters unaltered.

4.4.9.4 Effect on mean friction coefficient in different regimes of mixed convection

The contribution rendered by buoyancy in the mean friction the fluid experiences with reference to the two walls of the channel is shown in Fig. 4.30. The entire regime of mixed convection ($0.01 \leq Ri_w^* \leq 250$) is considered and the calculations are performed for seven typical values of Ri_w^* holding the rest of the input (q_v, k_s, ε and AR) unaltered. One can see a progressive increase in the contribution from buoyancy in both $\overline{C}_{f,L}$ and $\overline{C}_{f,R}$ as the flow configuration shifts to the asymptotic free convection limit ($Ri_w^* = 250$) from the asymptotic forced convection limit ($Ri_w^* = 0.01$). However, the distinction between (1) consideration and (2) non-consideration of buoyancy is quite meager from the asymptotic forced convection limit ($Ri_w^* = 0.01$) up to pure mixed convection ($Ri_w^* \approx 1$), with the role of buoyancy getting

elevated from there on. In the current study, for Ri_w^*= 1, $\overline{C}_{f,L}$ and $\overline{C}_{f,R}$ increase by 105.85% and 99.95%, respectively, when once buoyancy is reckoned with. Compared to this, for Ri_w^*= 250,

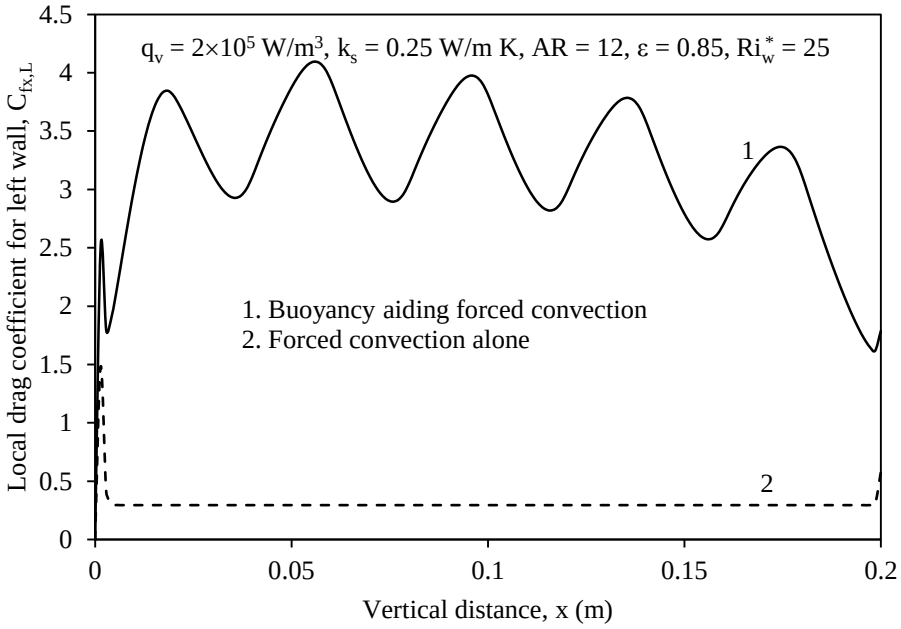

(a)

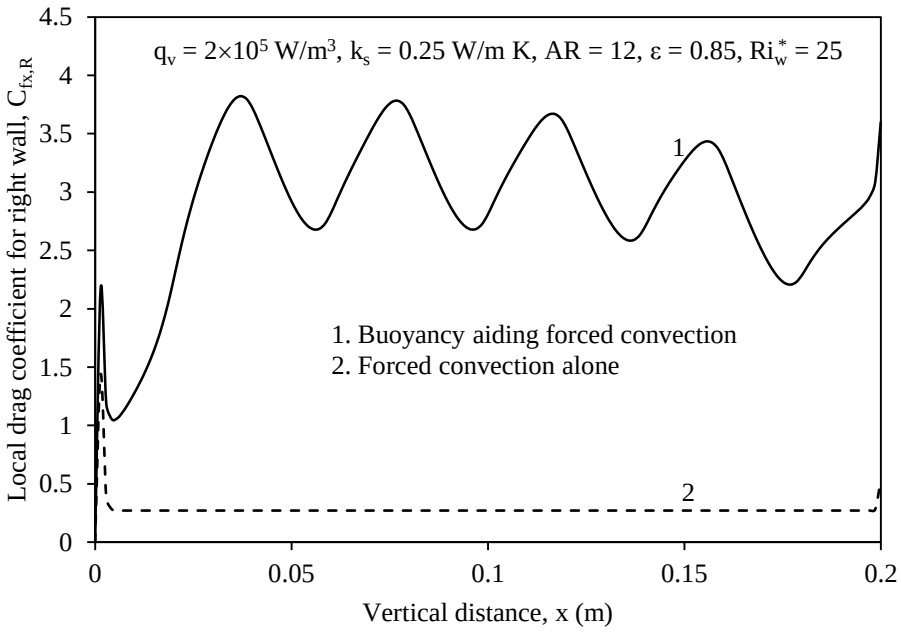

(b)

Fig. 4.29 Exclusive effect of buoyancy on local (a) left and (b) right wall drag coefficients

the same exercise increases $\overline{C}_{f,L}$ and $\overline{C}_{f,R}$ quite substantially by about 1482.87% and 2219.15%, respectively.

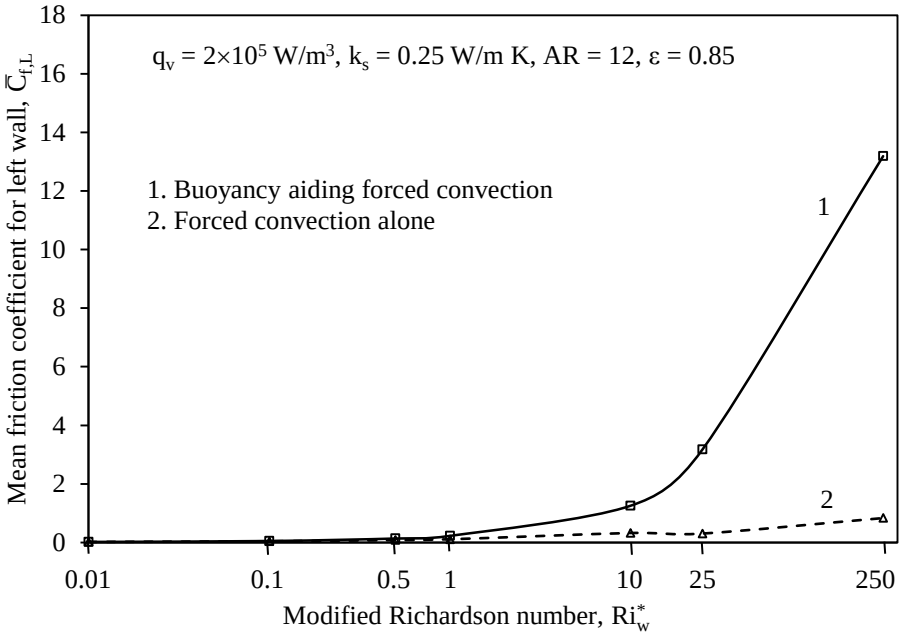

(a)

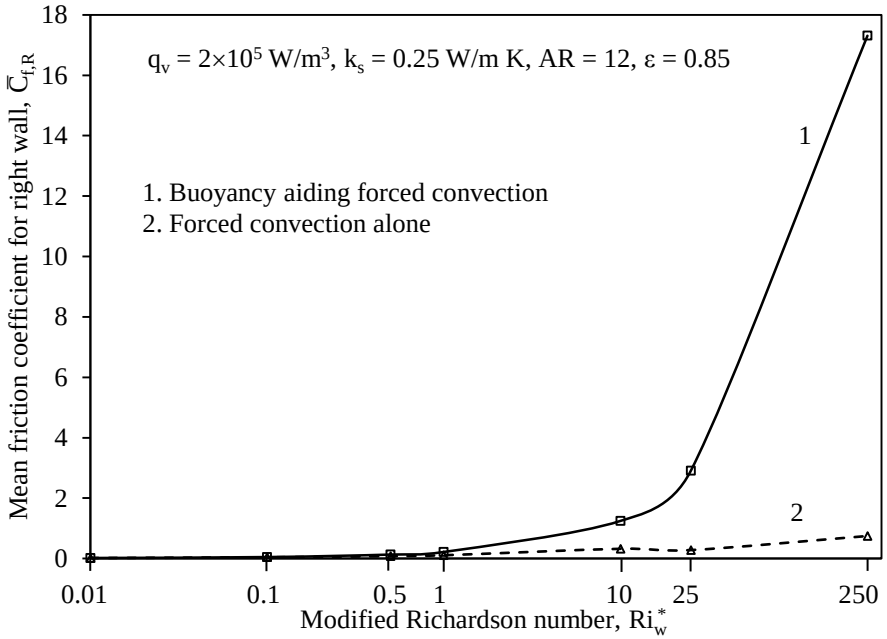

(b)

Fig. 4.30 Exclusive effect of buoyancy on (a) left and (b) right wall mean friction coefficients of the channel in different regimes of mixed convection

4.4.10 Extraction of Free and Forced Convection Components of Mean Friction Coefficient

The mean friction coefficient ($\bar{C}_f$) in the present problem has contributions provided by both free and forced convection. Attempts are made to separate out the roles of free and forced convection in both the left and right wall mean friction coefficients and to further look at their variation with surface emissivity (ε) in various regimes of mixed convection. Figure 4.31 is plotted for a fixed input of $q_v = 2\times10^5$ W/m^3, AR = 12 and $k_s = 0.25$ W/m K. It consists of six curves, with each value of Ri_w^* giving rise to two curves, one pertaining to free convection (labelled "a") and the other pertaining to forced convection (labelled "b"). The figures 4.31 (a) and (b) show that, for $Ri_w^* = 25$ (free convection dominant regime), as ε increases from 0.05 to 0.85, there is a mild drop in the contribution from free convection with a corresponding increment exhibited by that from forced convection. Further, as Ri_w^* decreases, with the flow shifting towards forced convection dominance, for a given ε, there is a drop in the contribution from free convection with a mirror-image increase exhibited by that from forced convection. Free convection, expectedly, finds its role in $\bar{C}_f$ getting diminished in the forced convection dominant regime ($Ri_w^* = 0.1$). On the whole, it can be inferred that the effect of buoyancy cannot be overlooked in the calculation of pumping power generally in any regime of convection and particularly in the free convection dominant regime.

4.4.11 Extraction of Roles of Free Convection, Forced Convection and Radiation in Channel Heat Dissipation

Since the present problem has convection heat dissipation arising out of both buoyancy and inertia forces, attempts are made to extract the exclusive effect of buoyancy in carrying the

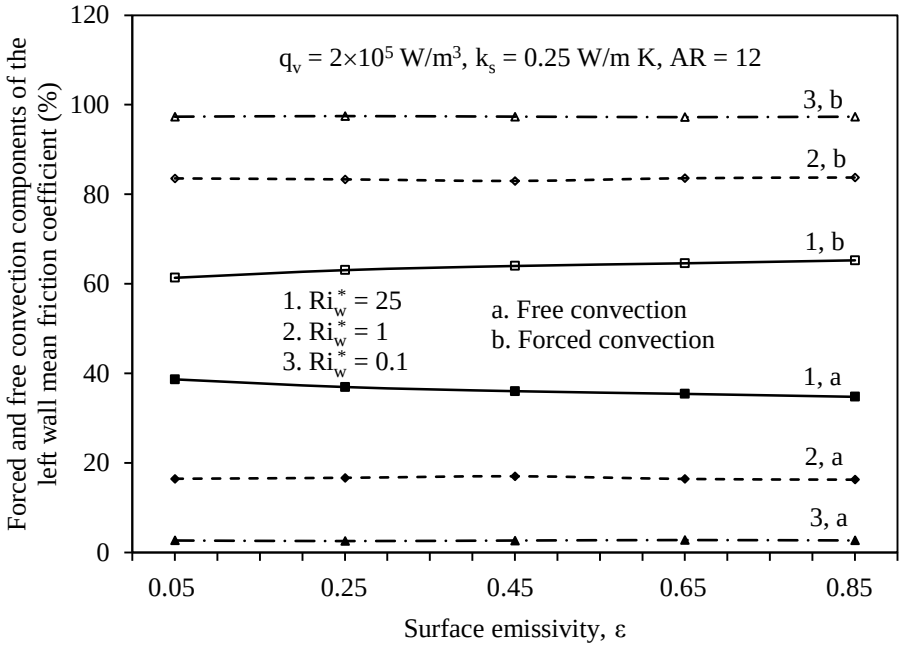

(a)

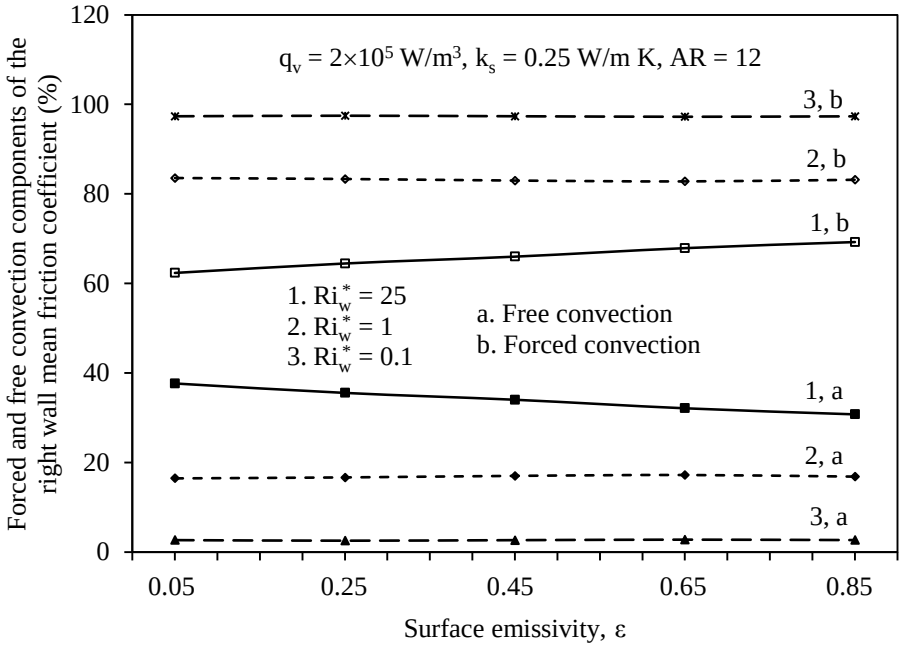

(b)

Fig. 4.31 Relative roles of forced and free convection in the (a) left and (b) right wall mean friction coefficients with surface emissivity in various regimes of mixed convection

mandated heat load. The study has been made in different regimes of mixed convection (Ri_w^* = 250, 1 and 0.01) and for various surface emissivities as can be seen in Fig. 4.32 for a fixed input of q_v = 2×10^5 W/m^3, AR = 12 and k_s = 0.25 W/m K. In all, there are nine curves, with

each value of Ri_w^* giving rise to three curves, one pertaining to free convection (labelled "a"), second corresponding to forced convection (labelled "b") and the third one denoting radiation (labelled "c"). One can notice an almost insignificant role for buoyancy (free convection) towards smaller values of Ri_w^*. This is owing to the fact that, here, the inertia forces dominate resulting in a comparatively larger role for forced convection component in heat dissipation.

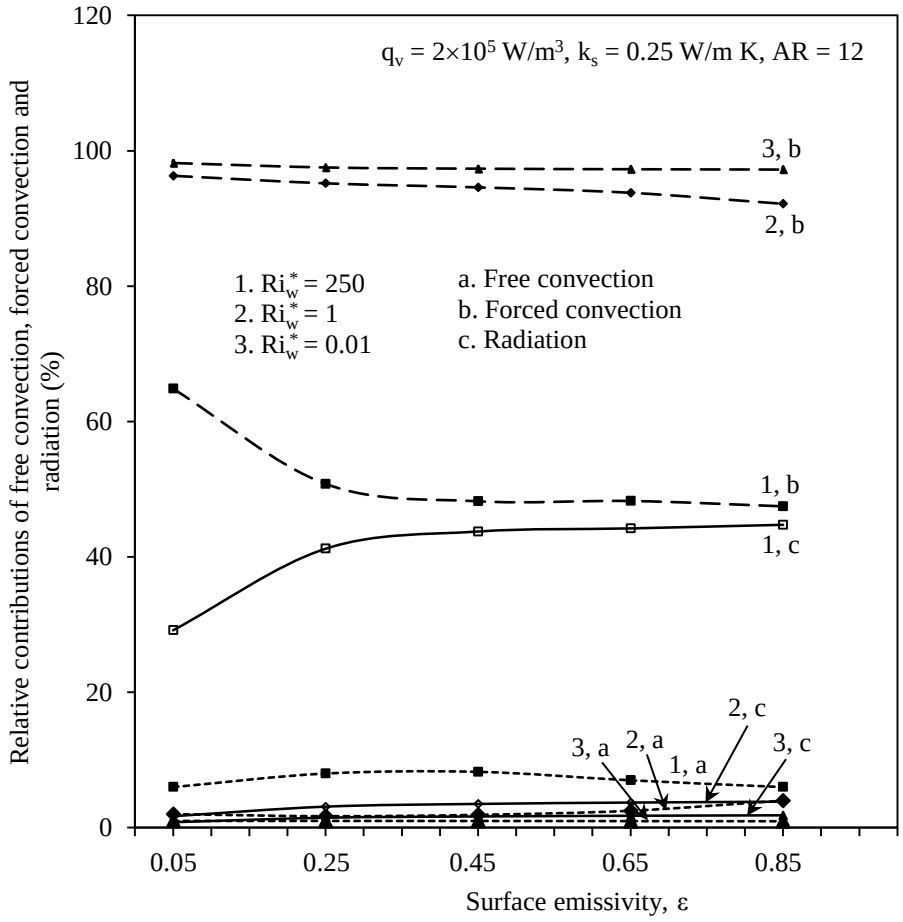

Fig. 4.32 Relative contributions of free convection, forced convection and radiation in channel heat dissipation for various surface emissivities in different regimes of mixed convection

Only for $Ri_w^* = 250$ (asymptotic free convection limit), there is an accountable change in the presence shown by free convection, which increases initially with ε, showing a maximum of 8.25% contribution for ε = 0.45, after which it is petering down. Coming to the forced convection component, there is a very large contribution in all the regimes of mixed

convection. Again here, the relative contribution of forced convection is expectedly showing an increase with decrease in Ri_w^* on account of reasons already explained. Further, for a given Ri_w^*, an increasing surface emissivity decreases the contribution from forced convection with a corresponding increase in the contribution from radiation. It can also be noticed that, for Ri_w^* = 250, in particular, when the inner surfaces of the walls of the channel are good emitter (say black paint with ε = 0.85), the role from radiation in heat dissipation is at its maximum and is equal to 44.75% with forced convection and free convection, respectively, sharing 47.47% and 7.78%.

4.5 Correlations

A large set of 550 numerical data has been generated covering the entire range of parameters taken up for study from the computer code written in the present work. This is made use of to arrive at useful correlations for (i) non-dimensional maximum temperature (θ_{max}), (ii) non-dimensional average temperature (θ_{av}) and (iii) mean friction coefficient ($\overline{C}_f$) as functions of different pertinent independent dimensionless parameters. The independent parameters that have been used are (i) surface emissivity, ε, (ii) aspect ratio, AR, (iii) modified Richardson number, Ri_w^* , (iv) Reynolds number, Re_w, (v) thermal conductance parameter, ξ and (vi) radiation-flow interaction parameter, I_{RF}.

4.5.1 Correlation for Non-Dimensional Maximum Channel Temperature

The correlation for the maximum non-dimensional channel temperature (θ_{max}), making use of the above data, turns out to be:

$$\theta_{max} = 14.13\,(1+\varepsilon)^{-0.167} AR^{-0.484} (1+Ri_w^*)^{0.241} Re_w^{-0.273} \xi^{0.036} \left(\frac{I_{RF}}{1+I_{RF}}\right)^{-6.179} \qquad (4.4)$$

The above correlation has a correlation coefficient 0.9919 and an error band of ±4.63% exhibiting an excellent parity between the data evolved and the correlation deduced as noticeable from Fig. 4.33.

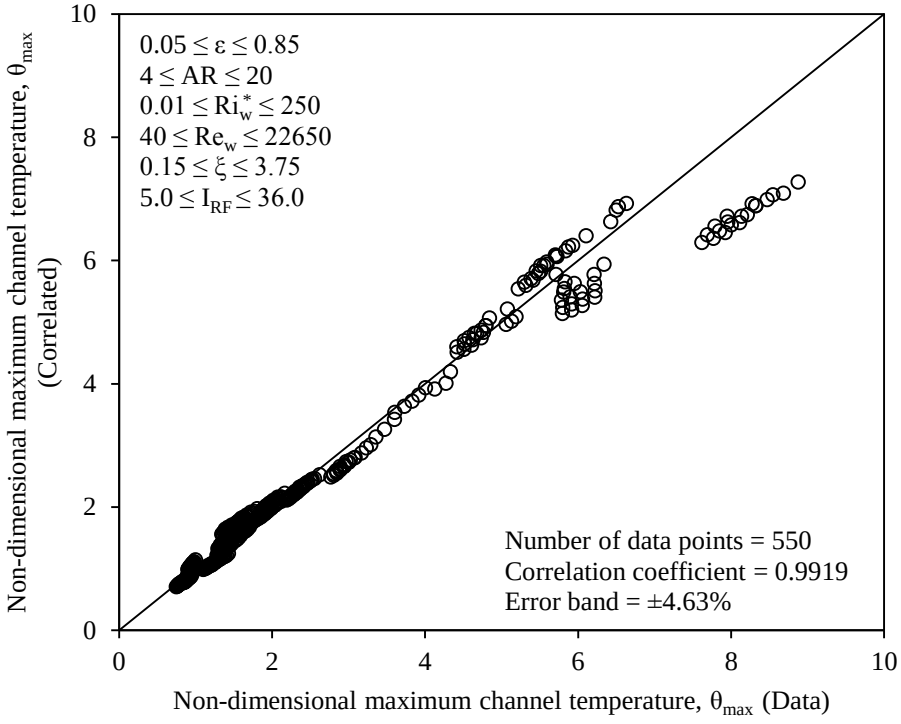

Fig. 4.33 Parity plot for non-dimensional maximum channel temperature

4.5.2 Correlation for Non-Dimensional Average Channel Temperature

Though not as relevant as the peak channel temperature (θ_{max}), it has been decided to frame a correlation even for the non-dimensional average channel temperature (θ_{av}) and the same is evolved making use of the above numerical data and it came out to be:

$$\theta_{av} = 9.404\,(1+\varepsilon)^{-0.021}\mathrm{AR}^{-0.307}(1+\mathrm{Ri}_w^*)^{0.225}\mathrm{Re}_w^{-0.321}\xi^{0.023}\left(\frac{I_{RF}}{1+I_{RF}}\right)^{-1.246} \qquad (4.5)$$

A very good agreement has again been noticed between the data and the correlation with the correlation coefficient and the error band, respectively, 0.991 and ±4.97%. This may be noticed pictorially from the parity plot (Fig. 4.34).

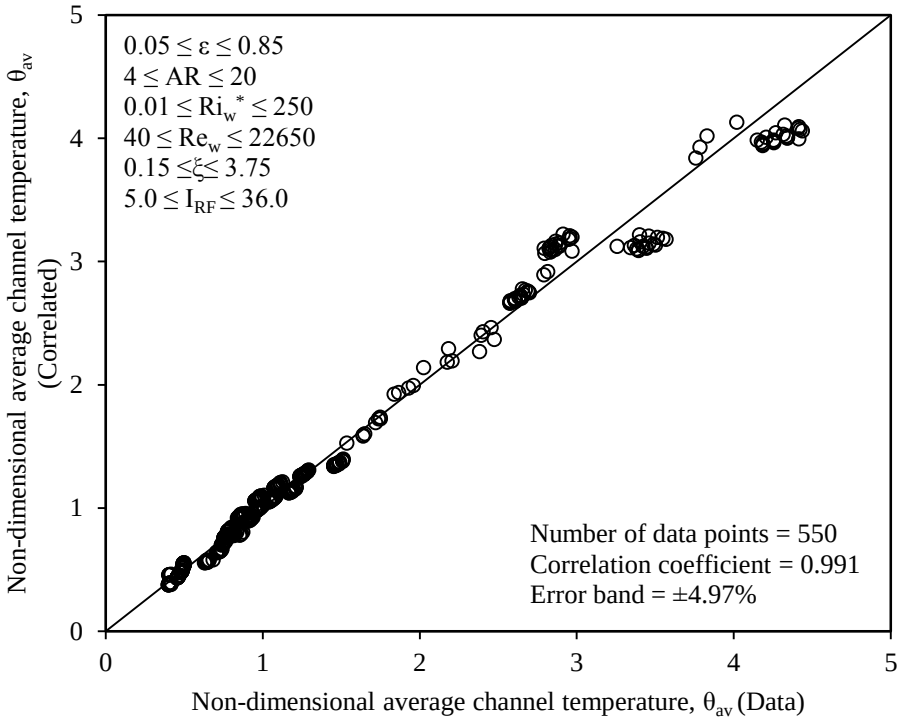

Fig. 4.35 Parity plot for non-dimensional average channel temperature

4.5.3 Correlation for Mean Friction Coefficient

It has been decided to cast a correlation for mean friction coefficient ($\overline{C}_f$) covering the whole range of mixed convection regime ($0.01 \leq Ri_w^* \leq 250$). Using the above data, the pertinent correlation for $\overline{C}_f$ comes out to be:

$$\overline{C_f} = 204.181\,(1+\varepsilon)^{-0.025} AR^{-0.74} (1+Ri_w^*)^{0.322} Re_w^{-0.96} \xi^{0.018} \left(\frac{I_{RF}}{1+I_{RF}}\right)^{-0.53} \qquad (4.6)$$

Adequate parity has been observed between the data and the correlation with the corresponding correlation coefficient and error band turning out to be, respectively, 0.9974 and ±4.81%. Figure 4.35 shows the goodness of the above fit.

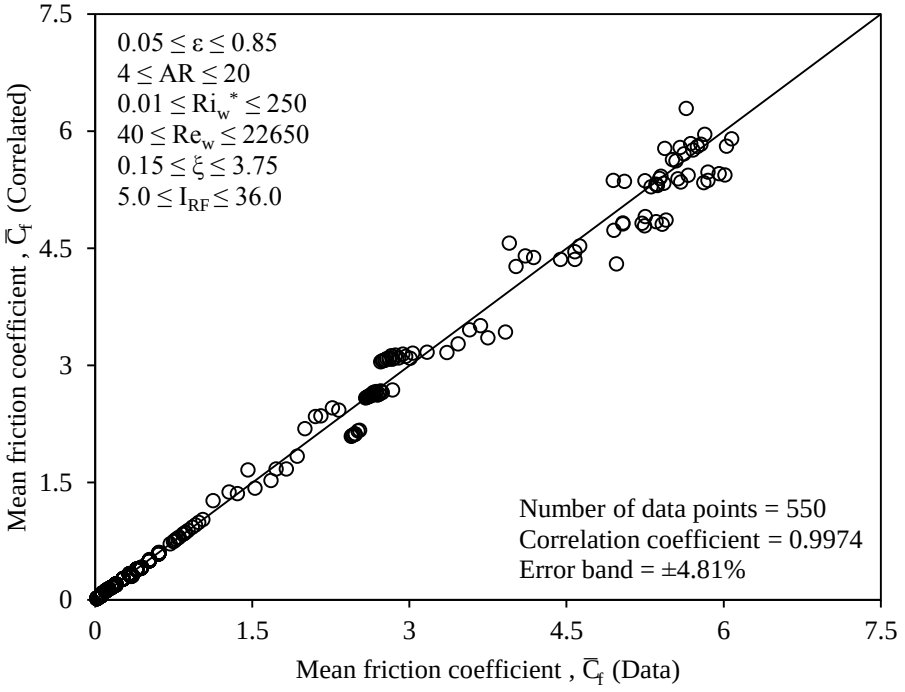

Fig. 4.36 Parity plot exhibiting the goodness of correlation for mean friction coefficient

4.6 Conclusions

The prominent conclusions derived from the studies performed on the problem in the present research work are:

(1) It would be unwise to pack the walls of the channel closer together for want of space or any other reason since an increasing aspect ratio has been observed to bring an unwanted rise in both the left and right wall temperatures leading to an increase in the cooling load on the system.

(2) A significant drop both in the left and right wall temperatures of the channel is noticed with the flow regime transiting from free convection dominance to forced convection dominance owing to an increased convective heat dissipation with its radiation counterpart remaining unaltered.

(3) Surface emissivity (ε) renders a significant role in the nature of variation of the local temperatures of both the left and right channel walls. Due to asymmetricity employed in positioning the discrete heat sources along the two walls, though the wall temperature rises with increasing ε at the channel entry, it, expectedly, decreases as one progresses along the channel. On an average, the local left or right wall temperature has been observed to be coming down by about 25% owing to an increasing surface emissivity from 0.05 to 0.85.

(4) The peak temperature the channel assumes decreases with increasing surface emissivity in all the regimes of mixed convection with the degree of decrease noticed to be more apparent in the free convection dominant regime when compared to that in the forced convection dominant regime. This is attributed to an augmented convection activity in the forced convection dominant regime that overrides the role of radiation.

(5) The singular role surface radiation exhibits in both the local and peak temperatures of the channel has been extracted in detail. The fact that radiation assumes significance in thermal control of the channel in the entire mixed convection regime has been adequately established with the peak channel temperature dropping down, respectively, by about 10% and 40% in the forced convection and free convection dominant regimes when once radiation is taken into reckoning with the channel walls coated with, say, lamp black with $\varepsilon = 0.99$.

(6) The wall material chosen also influences the peak temperature attained by the channel with an increasing thermal conductivity bringing it down with other parameters held unaltered.

(7) The relative contributions of mixed convection and radiation in channel heat dissipation have been probed into. It is seen that even in electronic cooling applications involving moderate temperatures too, radiation makes its presence felt by contributing to the channel heat dissipation. Though its share is a feeble 2% in the asymptotic forced convection limit ($Ri_w^* = 0.01$), it becomes as much as 45% in the asymptotic free convection limit ($Ri_w^* = 250$) provided one coats the channel walls with black paint ($\varepsilon = 0.85$).

(8) The role of radiation, in general, has been found to be decreasing with increasing aspect ratio, which gets manifested as an appropriate rise in the role of mixed convection. The above effect is found to be quite substantial in the free convection dominant regime, while it becomes progressively non-apparent as the flow transits to forced convection dominance.

(9) Buoyancy has been seen to play a fairly significant role in deciding both the local and peak channel temperatures in the entire mixed convection regime. In particular, consideration of buoyancy in a forced convection configuration turns more productive while operating in free convection dominant regime (towards larger values of Ri_w^*). This observation suggests the heat transfer engineer to locate the fan at the channel entry paving way for buoyancy-aided mixed convection.

(10) The local left and right wall drag coefficients ($C_{fx,L}$ and $C_{fx,R}$) have been observed to be varying fairly pronouncedly with surface emissivity (ε) of the channel in any given regime of convection. Both of them typically decrease with increasing ε.

(11) The local left and right wall drag coefficients ($C_{fx,L}$ and $C_{fx,R}$) shoot up quite significantly with the flow regime transiting from forced convection dominance to free convection dominance.

(12) Both the left and right wall mean friction coefficients ($\bar{C}_{f,L}$ and $\bar{C}_{f,R}$) strongly depend on surface emissivity in the entire mixed convection regime and get decreased with increasing ε. The above effect of ε on $\bar{C}_f$ is rather mild in the forced convection dominant regime and gets more apparent towards the free convection dominant regime.

(13) The aspect ratio (AR) of the channel strongly influences $\bar{C}_f$ with its value shooting up quite substantially with increasing AR for any given ε. Too closer packing of the channel walls is thus unadvisable as it tends to unfavorably increase the drag coefficient.

(14) The thermal conductivity of the wall material shows a non-significant effect on the left and right wall mean friction coefficients in all the regimes of mixed convection.

(15) The interplay between the material property (wall thermal conductivity) and the surface property (emissivity) is observed to be influencing the left and right wall mean friction coefficients. An increasing ε, for a given k_s, leads to decreased $\bar{C}_{f,L}$ and $\bar{C}_{f,R}$. Likewise, an increasing k_s, for a given ε, tends to bring down both the mean friction coefficients.

(16) The singular role exhibited by buoyancy in both local and mean friction coefficients has been extracted in all the regimes of mixed convection. When compared to the case that considers forced convection flow alone, the buoyancy aided forced convection tends to increase the values of both the local and mean friction coefficients. These observations gain significance in the free convection dominant regime as against the forced convection dominant regime.

(17) Studies aiming at the separation of the components of free convection, forced convection and radiation in channel heat dissipation have been performed. The necessity of preferring buoyancy aided mixed convection to achieve optimum heat dissipation has been amply demonstrated through quantitative outputs obtained. The above becomes specifically significant while working in free convection dominant environment.

(18) Pertinent correlations that help in calculating maximum and average non-dimensional channel temperatures and mean friction coefficient are evolved with the help of a fairly large set of 550 numerical data generated from the computer code written in the current work.

4.7 Closure

The present chapter provided a detailed account on the numerical investigation performed on an asymmetrically and discretely heated vertical parallel-plate channel taking part in conjugate mixed convection with surface radiation. As many as ten heat sources of identical dimensions and volumetric heat generation have been considered with each wall comprising five of them. As clearly mentioned in the preceding chapter, the governing fluid flow and heat

transfer equations have been considered in their full-strength without the simplifying boundary layer approximations. After initially transforming the governing equations, considered in primitive variables, into stream function-vorticity formulation, appropriate normalization is made defining pertinent non-dimensional parameters. The resulting equations, together with appropriate boundary conditions, have been solved using finite volume method. One important contribution has been the preparation of a full-fledged computer code to solve the problem.

Comprehensive parametric studies have been performed highlighting the roles played by different independent parameters in influencing all the relevant fluid flow and heat transfer results. The singular roles exhibited by surface radiation as well as buoyancy are thoroughly elucidated. Making use of a huge set of numerical data generated from the computer code correlations that help in calculation of the maximum and the average channel temperatures and the mean friction coefficient have been deduced. The ensuing chapter (**Chapter 5**) takes up certain interesting comparative studies between the discretely heated channel of the current chapter and a uniformly heated channel.

Chapter 5

Comparative Studies on Discretely and Uniformly Heated Channels

5.1 Introduction

A detailed numerical investigation into the problem of interaction of surface radiation with conjugate mixed convection from an asymmetrically and discretely heated vertical channel has been taken up in the preceding chapter. As may be recollected, the two walls of the channel were equipped with a total of ten identical discrete heat sources with each of the walls possessing five of them. An asymmetricity was followed to position the heat sources along the walls. A question arises as to how the different fluid flow and heat transfer results behave upon replacing the discretely heated walls with uniformly heated walls. The current chapter does the same and considers the channel with its two walls having uniform internal heat

generation holding the net rate of uniform heat generation the same as that in the discretely heated channel handled in the previous chapter. It is pertinent to note that, in what follows, the discretely and asymmetrically heated channel is called configuration 1, while the uniformly heated channel is referred to as configuration 2.

An identical net rate of heat generation is ensure in both the configurations by fixing the volumetric heat generation q_{v1} in each of the five heat sources of a given wall to be 2×10^5 W/m^3. This amounts to a net rate of heat generation of $5\times q_{v1}\times L_h\times t$ (W) in each channel wall. This is later equated to the net rate of heat generation in each of the walls in configuration 2, which is equal to $q_{v2}\times L\times t$ (W). This leads to a value of q_{v2} equal to 1×10^5 W/m^3 as volumetric heat generation in each wall of configuration 2. The above is done in all the studies performed in the present chapter.

The mathematical formulation and solution methodology employed to tackle configuration 2 are the same as those employed with configuration 1 barring certain changes to address the temperature boundary conditions along the two channel walls. The computer code prepared to solve the original research problem dealing with configuration 1 has been appropriately modified to meet the requirements of configuration 2. The different parameters taken up for performing comparison between the two configurations include the local temperature distribution, the maximum channel temperature, the mean friction coefficient and the contributions of mixed convection and surface radiation to channel heat dissipation.

5.2 Description of Uniformly Heated Channel Problem with Solution Methodology

Figure 5.1 shows the schematic of the configuration 2 considered for study in the present chapter along with the system of coordinates employed. It constitutes a vertical parallel-plate

channel of dimensions (L, t and W) that are similar to those of the geometry used in the preceding chapter as configuration 1 (Fig. 4.1).

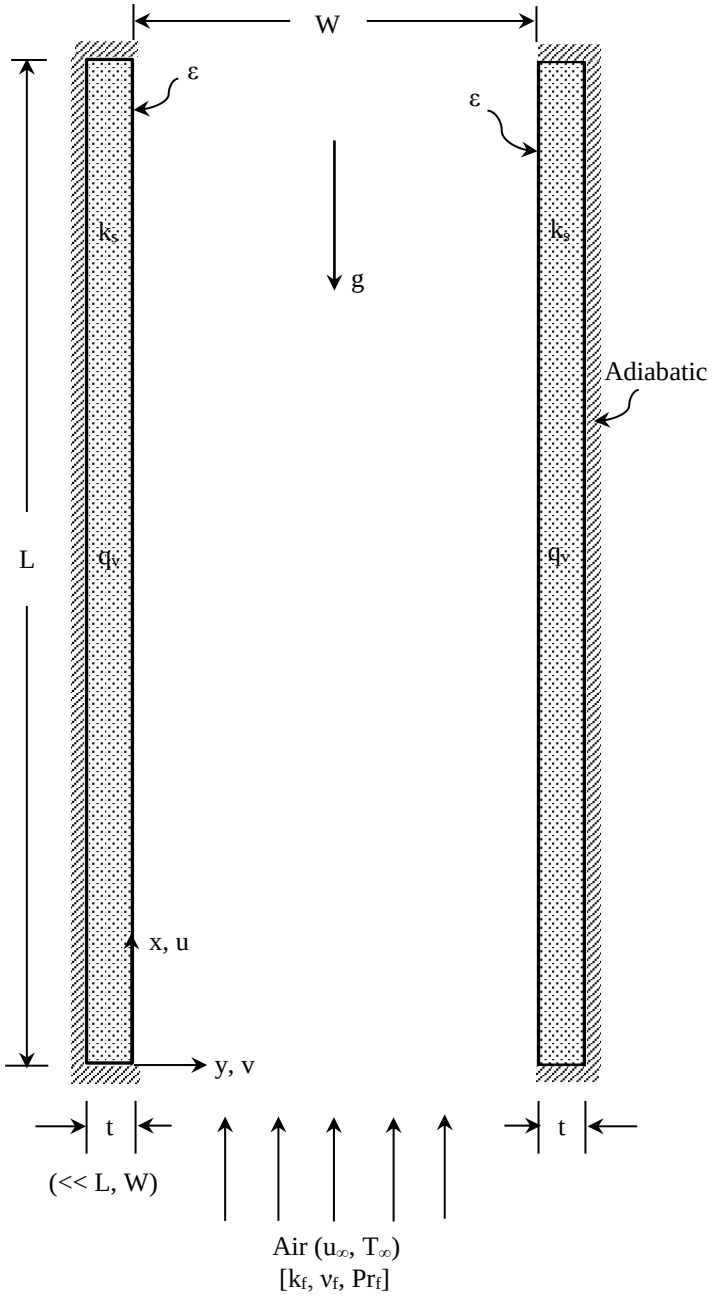

Fig. 5.1 Vertical channel with uniform internal heat generation in its walls considered for study as configuration 2 along with system of coordinates

The essential difference is that, while the walls of the channel in configuration 1 possessed ten identical flush-mounted discrete heat sources arranged asymmetrically, the configuration 2 has the channel walls with uniform volumetric heat generation. Here too, k_s and ε, respectively, indicate thermal conductivity and surface emissivity of the walls, while q_v is the rate of volumetric heat generation in each of them. Buoyancy-aided mixed convection is considered again with air (cooling agent) getting admitted from the bottom of the channel at a characteristic velocity u_∞ and characteristic temperature T_∞. It follows that, even for the present problem, the final set of governing equations for fluid flow and heat transfer remain unaltered as compared to configuration 1 and these are Eqs. (4.1) to (4.3) [see Chapter 4].

Once again, after a fairly thorough numerical experimentation, an extended computational domain of height 2L and width W is employed as shown in Fig. 5.2. It has been noticed that the same grid system as used with regard to configuration 1 would suffice for discretizing the computational domain while handling the configuration 2 as well. The major contrast, however, comes vis-à-vis the temperature boundary condition along the left and right walls. Making an energy balance on a typical interior element of the left wall (excluding the bottom and top adiabatic ends) and following the mathematical treatment as employed in Chapter 3, one gets the pertinent governing equation as:

$$\frac{\partial^2\theta}{\partial X^2} + \xi\left(\frac{\partial\theta}{\partial Y}\right)_{Y=0} + A_{r1}\,A_{r2} - \frac{\varepsilon}{1-\varepsilon}\,\xi\,I_{RF}\left[\left(\frac{T_i}{T_\infty}\right)^4 - J_i'\right] = 0 \qquad (5.1)$$

Further, the governing equations for the bottom and top adiabatic end temperatures of the left wall, respectively, come out to be:

$$\frac{2}{\Delta X_{hs}}\,\frac{\partial\theta}{\partial X} + \xi\left(\frac{\partial\theta}{\partial Y}\right)_{Y=0} + A_{r1}\,A_{r2} - \frac{\varepsilon}{1-\varepsilon}\,\xi\,I_{RF}\left[\left(\frac{T_i}{T_\infty}\right)^4 - J_i'\right] = 0 \qquad (5.2)$$

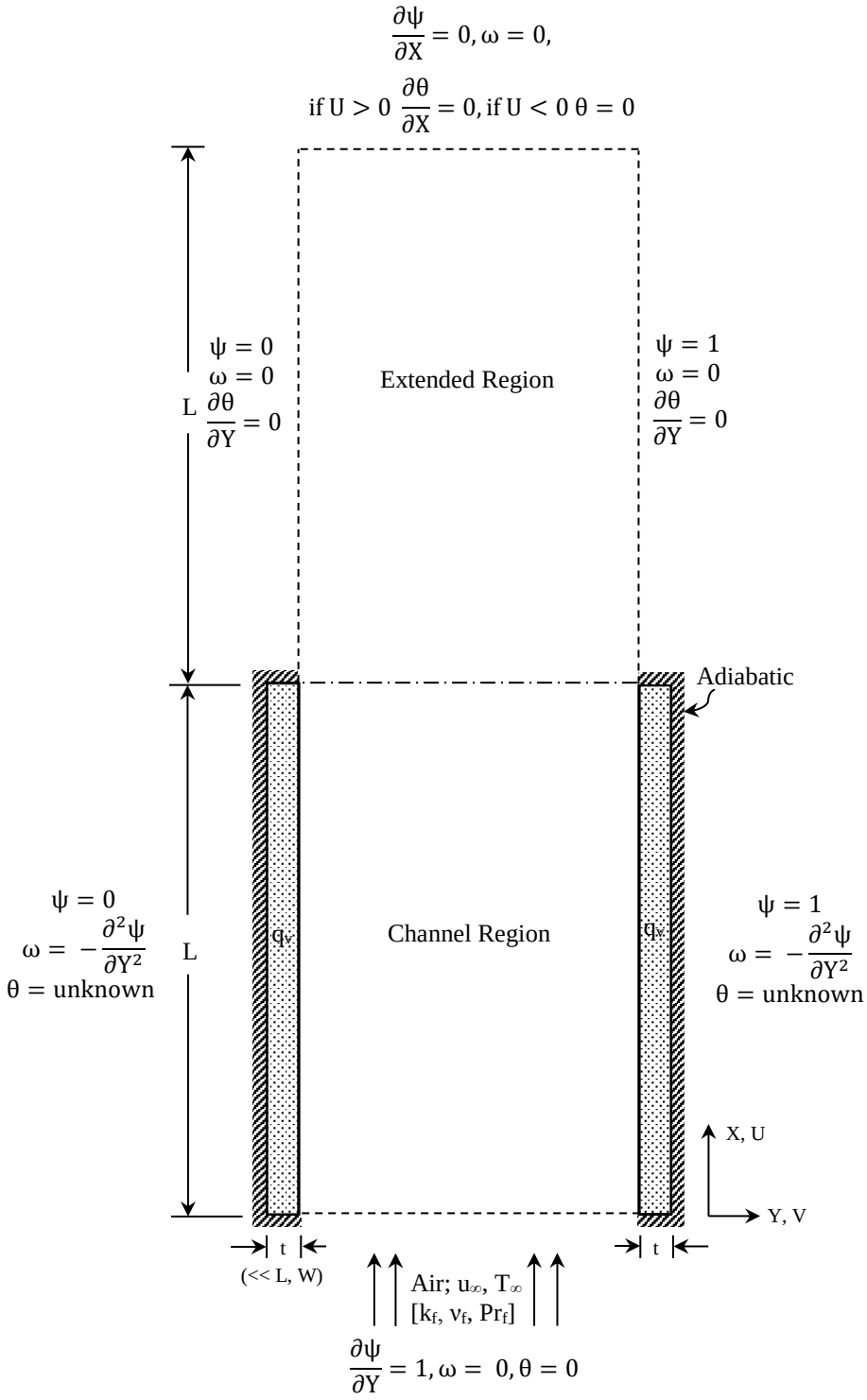

Fig. 5.2 Extended computational domain used for configuration 2 together with different boundary conditions

$$\frac{2}{\Delta X_{hs}}\frac{\partial\theta}{\partial X} - \xi\left(\frac{\partial\theta}{\partial Y}\right)_{Y=0} + A_{r1}\,A_{r2} + \frac{\varepsilon}{1-\varepsilon}\,\xi\,I_{RF}\left[\left(\frac{T_i}{T_\infty}\right)^4 - J_i'\right] = 0 \tag{5.3}$$

Similarly, separate governing equations are required to be deduced for the temperature of the interior elements, the bottom adiabatic end and the top adiabatic end of the right wall, and these, respectively, get evolved as:

$$\frac{\partial^2\theta}{\partial X^2} - \xi\left(\frac{\partial\theta}{\partial Y}\right)_{Y=1} + A_{r1}\,A_{r2} - \frac{\varepsilon}{1-\varepsilon}\,\xi\,I_{RF}\left[\left(\frac{T_i}{T_\infty}\right)^4 - J_i'\right] = 0 \tag{5.4}$$

$$\frac{2}{\Delta X_{hs}}\frac{\partial\theta}{\partial X} - \xi\left(\frac{\partial\theta}{\partial Y}\right)_{Y=1} + A_{r1}\,A_{r2} - \frac{\varepsilon}{1-\varepsilon}\,\xi\,I_{RF}\left[\left(\frac{T_i}{T_\infty}\right)^4 - J_i'\right] = 0 \tag{5.5}$$

$$\frac{2}{\Delta X_{hs}}\frac{\partial\theta}{\partial X} + \xi\left(\frac{\partial\theta}{\partial Y}\right)_{Y=1} - A_{r1}\,A_{r2} + \frac{\varepsilon}{1-\varepsilon}\,\xi\,I_{RF}\left[\left(\frac{T_i}{T_\infty}\right)^4 - J_i'\right] = 0 \tag{5.6}$$

The conditions pertaining to ψ and ω along all the boundaries and those pertaining to θ on the boundaries other than the channel walls remain the same as those employed for configuration 1 in the preceding chapters and are as depicted in Fig. 5.2. The broad method of solution, the relaxation parameters and the convergence criteria are all similar to those used there. A computer code in C++ is written here too to solve the problem. The ranges of different independent parameters too are identical to those considered for studies on configuration 1.

5.3 Results and Discussion

5.3.1 Check for Mass and Energy Balance

As is customary, the mass and energy balance checks are performed on the results of configuration 2 as well in the entire mixed convection regime. The results are obtained for a typical input comprising $q_v = 1\times10^5$ W/m^3, $k_s = 0.25$ W/m K, $\varepsilon = 0.45$ and AR = 12 with five different values of Ri_w^* chosen between 0.01 and 250. The net rate of mass in-flow is compared with the net rate of mass out-flow to check mass conservation and it is found that the mass balance is satisfactory within ±0.15%. Further, energy conservation is checked by comparing the net rate of heat generation in both the channel walls ($2\times q_v\times L\times t$) with the total rate of heat dissipation by mixed convection and radiation. It is seen that the energy balance is satisfactory within ±0.75%. Similar trends have been noticed with regard to both mass and energy balance checks even while operating with various other sets of independent parameters.

5.3.2 Validation

A fairly thorough validation for fluid flow and heat transfer results performed already in **Chapter 4** remains appropriate even for proving the correctness of the results of the modified version of the computer code written to solve configuration 2 tackled in the current chapter.

5.4 Comparison of Local Wall Temperature Profiles Concerning the Two Channel Configurations

A comparative study on non-dimensional local temperature distribution along the two walls of the channel concerning the two configurations is performed in three typical regimes of mixed convection keeping the remaining input parameters unchanged. In order to maintain the net rate of heat generation identical, the volumetric heat generation in discretely and uniformly heated channels is taken to be, respectively, $q_{v1} = 2\times10^5$ W/m^3 and $q_{v2} = 1\times10^5$ W/m^3, while the common input employed for both the channels is $k_s = 0.25$ W/m K, AR = 12 and $\varepsilon = 0.45$. Figures 5.3-5.5 depict the results thus obtained, respectively, for $Ri_w^* = 0.01$, 1 and 250, thus encompassing the entire regime of mixed convection. In each of these figures, curve 1 represents the profile for the case where the vertical channel has discrete heating in both of its walls, while curve 2 indicates the profile concerning the case that has the vertical channel with uniform heating. With regard to the left wall, in all the regimes of mixed convection, the local temperature profile exhibits waviness owing to asymmetricity employed in positioning the heat sources in the case of discretely heated channel (configuration 1), while the temperature is seen to be monotonically increasing in the case of uniformly heated channel (configuration 2). A similar behavior is exhibited by the right wall temperature distribution too in the case of configuration 1, while monotonous increase is observed in the case of configuration 2. The local wall temperatures are seen to be larger in configuration 2 as compared to those noticed with configuration 1.

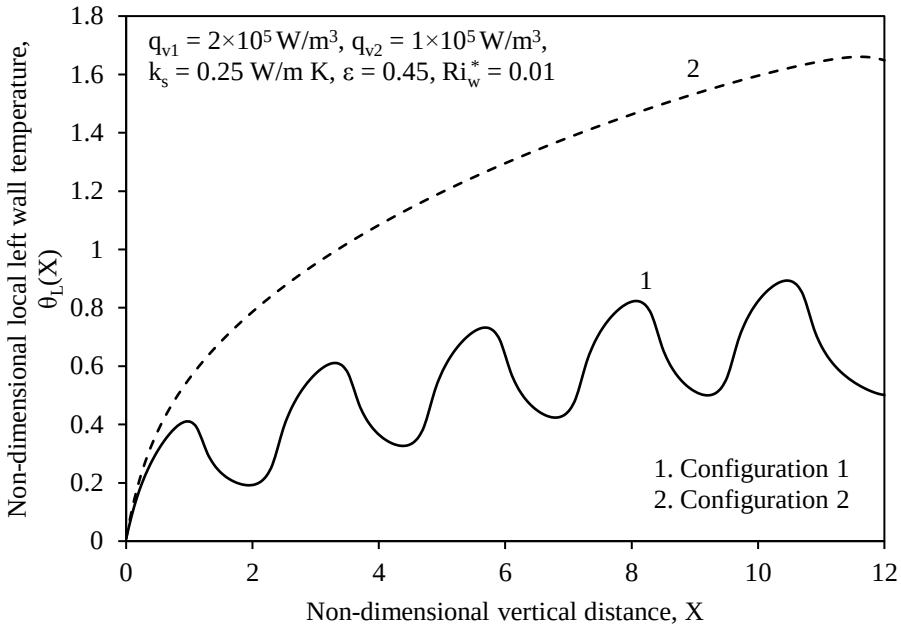

(a)

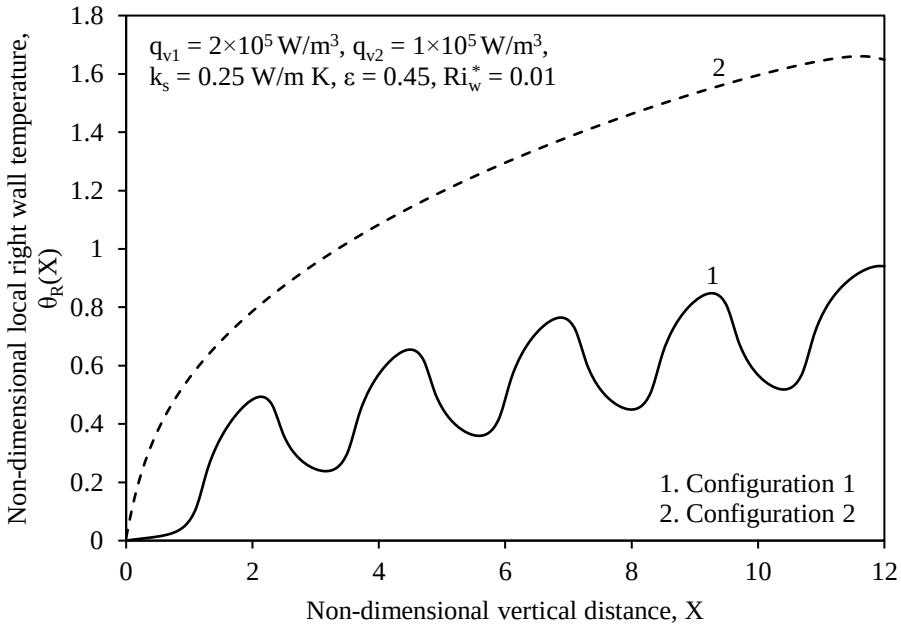

(b)

Fig. 5.3 Comparative study on local non-dimensional temperature profiles for (a) left and (b) right walls of the two channel configurations for $Ri_w^* = 0.01$

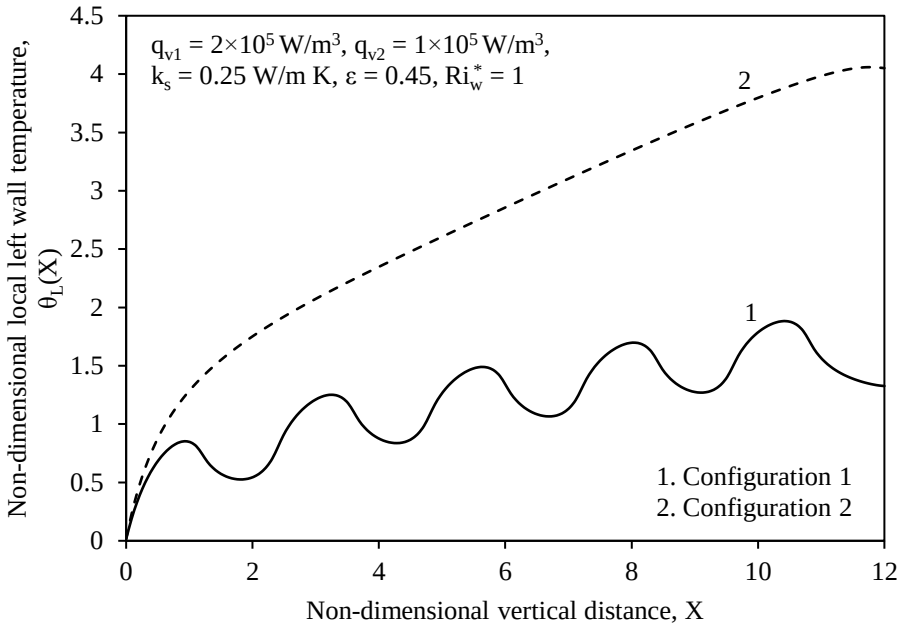

(a)

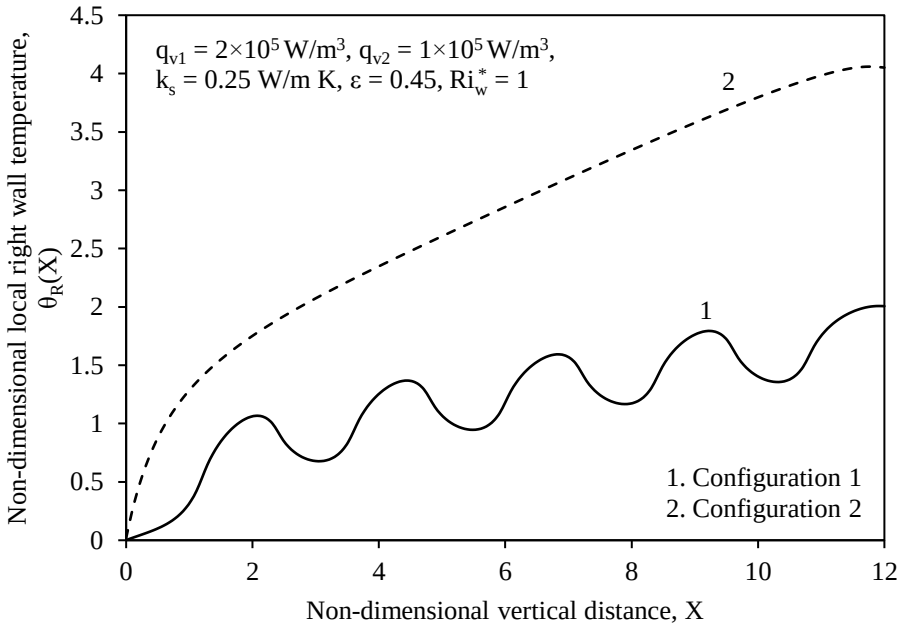

(b)

Fig. 5.4 Comparative study on local non-dimensional temperature profiles for (a) left and (b) right walls of the two channel configurations for $Ri_w^* = 1$

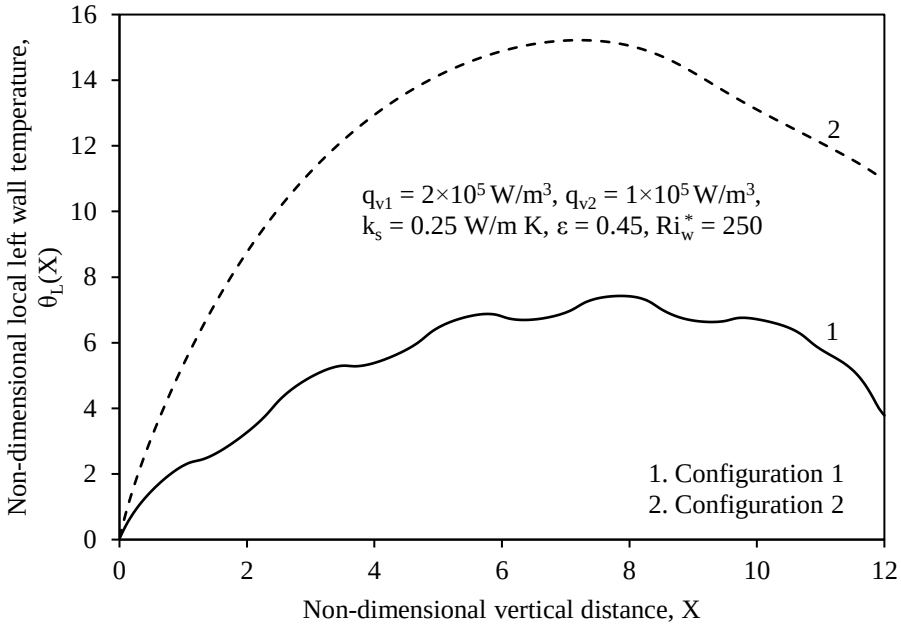

(a)

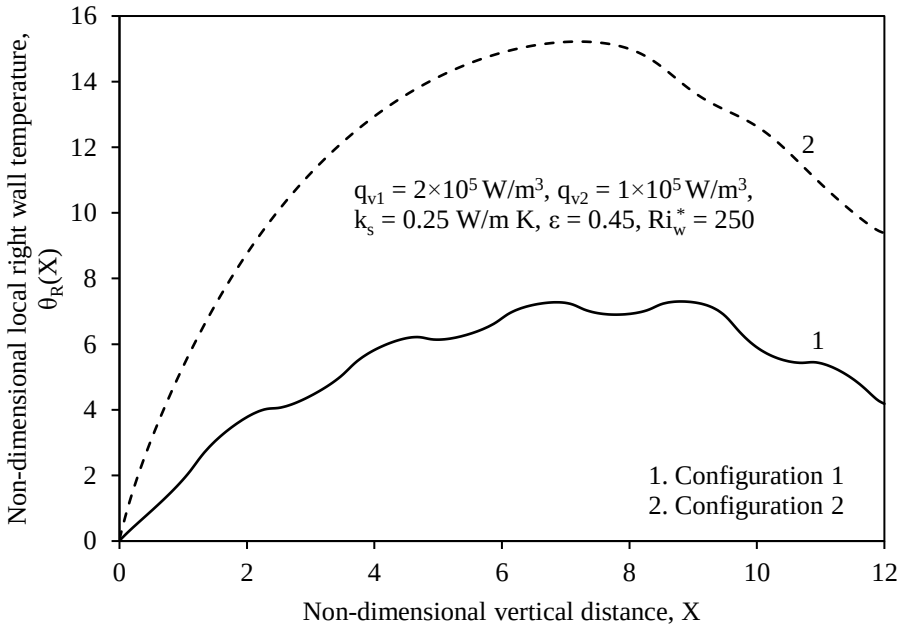

(b)

Fig. 5.5 Comparative study on local non-dimensional temperature profiles for (a) left and (b) right walls of the two channel configurations for $Ri_w^* = 250$

5.5 Comparison of Peak Wall Temperature Profiles Concerning the Two Channel Configurations

5.5.1 Variation with Surface Emissivity in Different Mixed Convection Regimes

A comparative study on non-dimensional peak channel temperature (θ_{max}) is performed with respect to surface emissivity (ε) in different mixed convection regimes. As spelt out already, the focus has been on the discretely heated and the uniformly heated channels subject to the condition that both of them bear an identical net cooling load. The results are summarized in Fig. 5.6 for $q_{v1} = 2\times10^5$ W/m^3, $q_{v2} = 1\times10^5$ W/m^3, $k_s = 0.25$ W/m K and AR = 12. Five values are considered for emissivity (ε = 0.05, 0.25, 0.45, 0.65 and 0.85) with four values tried for Ri_w^*(0.01, 1, 25 and 250) addressing the entire mixed convection regime. For a given Ri_w^*, the peak temperature assumed by the channel turns out to be larger when it has uniformly heated walls (configuration 2) compared to the case that has discrete heating employed in its walls (configuration 1). This is attributed to the fact that the irradiation received by the walls is more in a uniformly heated channel as against that in a discretely heated channel. This, in turn, is owing to the fact that heat generation is uniform in both the channel walls in a uniformly heated channel while it is confined to five locations per each of the walls in a discretely heated channel. A similar trend is noticed in all the regimes of convection considered. In the present example, for $Ri_w^* = 250$ and 0.01, for $\varepsilon = 0.05$, the peak channel temperature in configuration 1 as compared to that in configuration 2 decreases, respectively, by 89.28% and 91.29%. The figure also reveals that θ_{max}, for a given Ri_w^*, drops down with increasing ε due to increased radiative heat dissipation. In configuration 1, for $Ri_w^* = 25$ and 1, θ_{max} is decreasing, respectively, by 9.73% and 11.49% as ε increases to 0.85 from 0.05. A

similar exercise with configuration 2 reports a decrease in θ_{max}, respectively, by 8.74% and 5.15%. Further, for a given surface coating employed (i.e., for a given ε), the peak channel temperature expectedly decreases with the flow regime transiting from free to forced convection. In the current example, for ε = 0.45, θ_{max} in the first and second configurations is decreasing, respectively, by 87.32% and 89.52% with Ri_w^* coming down from 250 to 0.01.

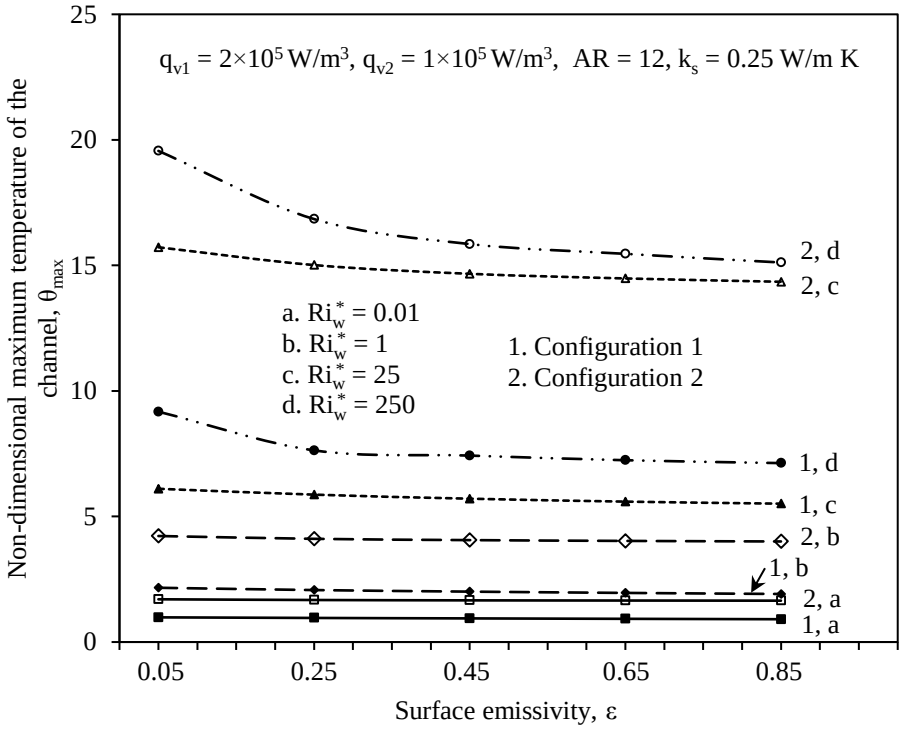

Fig. 5.6 Comparison of variation of non-dimensional peak wall temperature for the two channel configurations with surface emissivity in different regimes of mixed convection

5.5.2 Variation with Aspect Ratio in Different Mixed Convection Regimes

The effect of aspect ratio (AR) on the maximum channel temperature in the two configurations is compared in different mixed convection regimes as shown in Fig. 5.7. The results are obtained for five values of AR and in four mixed convection regimes. Rest of the input that is held fixed during the study is as mentioned. Owing to reasons spelt out in the

preceding chapter, the peak channel temperature rises quite substantively in both the configurations with the wall spacing getting narrower (i.e., with increasing AR). This is more

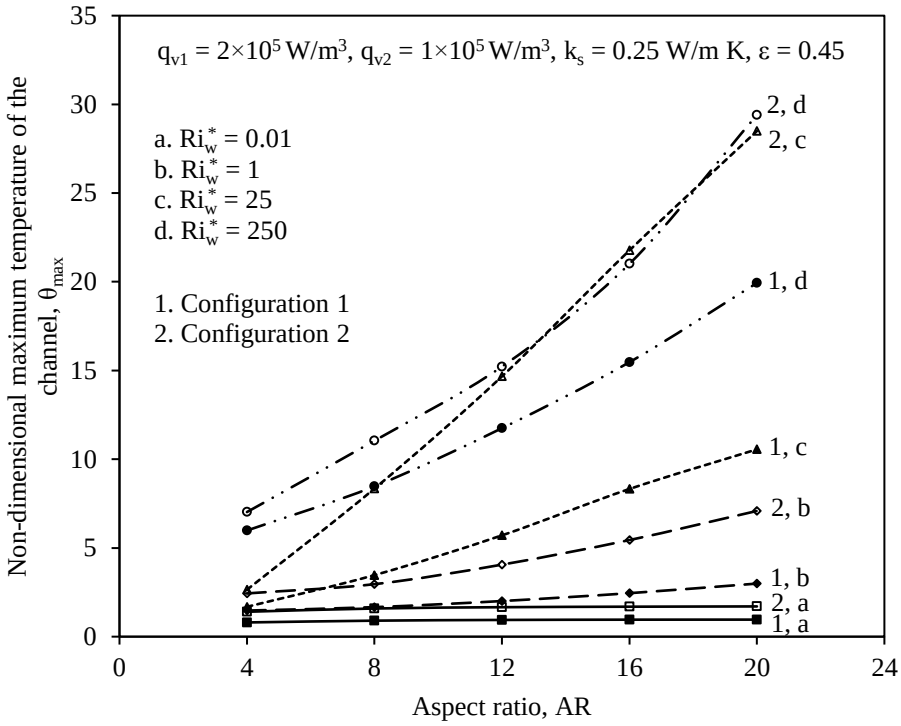

Fig. 5.7 Comparison of variation of non-dimensional peak wall temperature for the two channel configurations with aspect ratio in different regimes of mixed convection

so while operating in free convection dominant regime (Ri_w^* = 250) as compared to the situation that has forced convection dominance (Ri_w^* = 0.01). Though this is the general trend exhibited by both the configurations, in particular, θ_{max} turns out to be larger in the case that employs a uniformly heated channel. Looking at the above observations quantitatively, for AR = 12, θ_{max} decreases by 22.81% and 43.31%, respectively, in the free (Ri_w^* = 250) and forced (Ri_w^* = 0.01) convection limits, when a discretely heated channel is preferred over a uniformly heated channel. If one is constrained to increase AR to 20 from 4, for want of space, θ_{max} is observed to be shooting up by 233.12%, 103.3% and 19.92%, respectively, for Ri_w^* = 250, 1 and 0.01, in a discretely heated channel. A uniformly heated channel, when faced

with the same constraint as above vis-à-vis AR finds θ_{max} increasing, respectively, by 318.56%, 190.77% and 21.46% for the same values of Ri_w^* as above.

5.6 Comparison of Mean Friction Coefficients Concerning the Two Channel Configurations

5.6.1 Variation with Surface Emissivity in Different Mixed Convection Regimes

Figure 5.8 brings out comparison of the nature of variation of both the left and right wall mean friction coefficients ($\overline{C}_{f,L}$ and $\overline{C}_{f,R}$) of the channel with surface emissivity (ε) for the two configurations. The study is performed for four values of Ri_w^*, as shown, with the remaining parameters (q_{v1}, q_{v2}, k_s and AR) held fixed. In general, for both the configurations, it is observed from Fig. 5.8 (a) and Fig. 5.8 (b) that the left and right wall mean friction coefficients drop down, for a given Ri_w^*, with increasing wall emissivity (ε). The reasons for the above have been spelt out already in the preceding chapter. For a given regime of mixed convection, both $\overline{C}_{f,L}$ and $\overline{C}_{f,R}$ are noticed to be larger with configuration 2 compared to those with configuration 1. This is due to an enhancement in the respective wall temperature gradients and thus the respective wall velocity gradients. However, the above observations with respect to both $\overline{C}_{f,L}$ and $\overline{C}_{f,R}$ get less apparent as one moves towards the forced convection dominant regime. Reporting quantitatively, in the free convection dominant regime ($Ri_w^* = 25$), for $\varepsilon = 0.45$, $\overline{C}_{f,L}$ and $\overline{C}_{f,R}$ are increasing, respectively, by 83.07% and 67.69% in configuration 2 (i.e., uniformly heated channel) compared to configuration 1 (i.e., discretely heated channel).

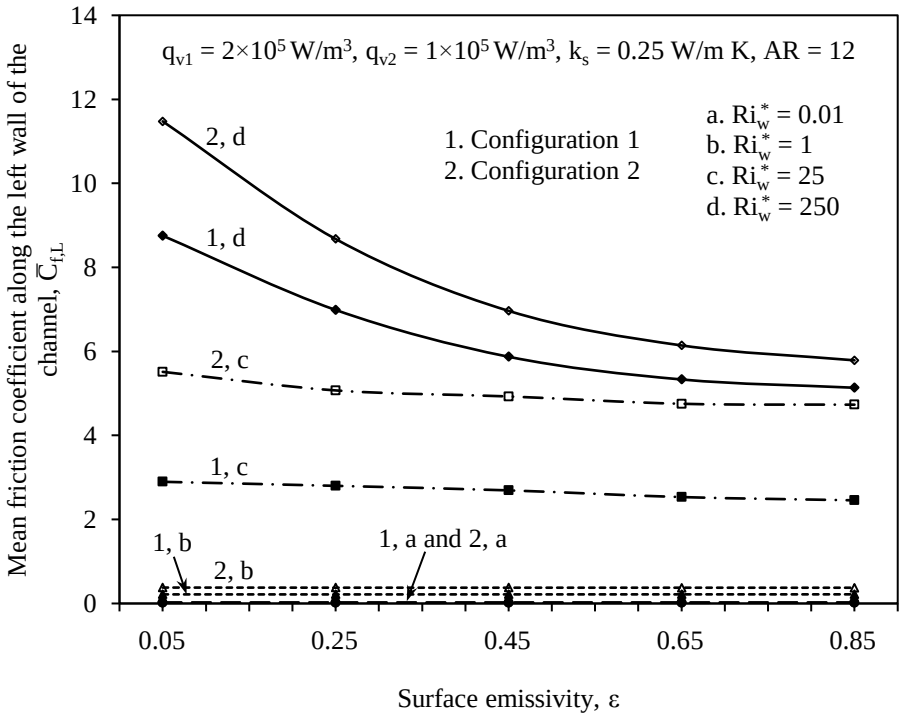

(a)

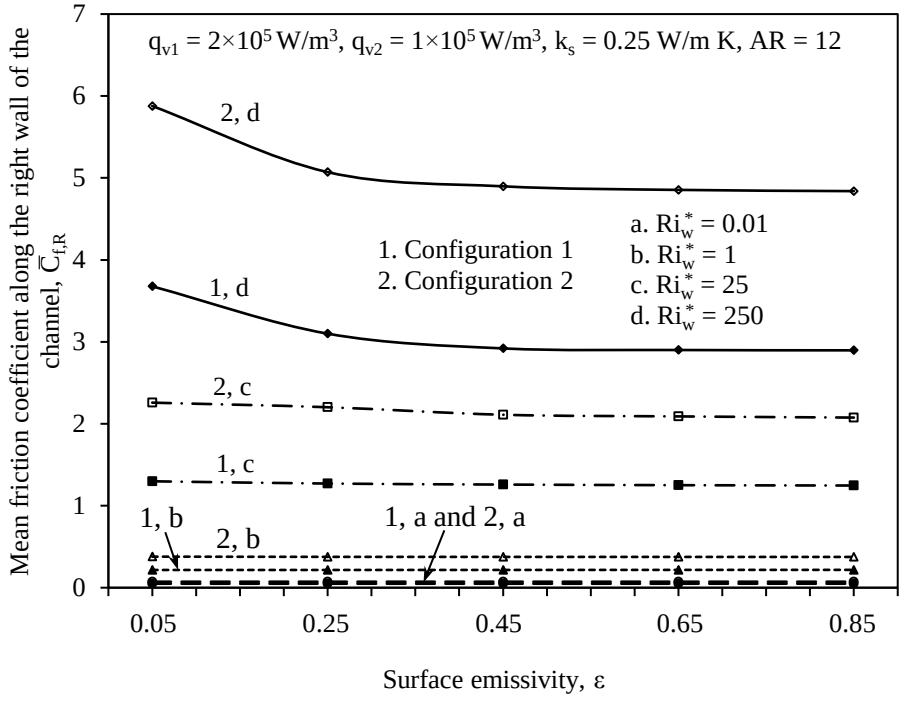

(b)

Fig. 5.8 Comparison of variation of (a) left and (b) right wall mean friction coefficients of the two channel configurations with surface emissivity in different mixed convection regimes

5.6.2 Variation with Aspect Ratio for Different Surface Emissivities

A comparative study on the role enacted by aspect ratio (AR), in conjunction with surface emissivity (ε), in influencing $\bar{C}_f$ for both the walls is performed as shown in Fig. 5.9. Five typical values are considered for AR (4, 8, 12, 16 and 20) with three surface coatings (ε = 0.05, 0.45 and 0.85) employed. The general nature of variation of both the left and right wall mean friction coefficients with aspect ratio remains the same as what has been discussed in the preceding chapter with reference to configuration 1. Focusing on comparison between the two channel configurations chosen, the figure reveals that, for a given ε, the mean friction coefficient, irrespective of the wall chosen, is increasing upon opting a uniformly heated channel in the place of a discretely heated one. Further, though a similar observation holds for all values of AR chosen, a slightly increased contrast is noticed between the two configurations with the walls getting closer (AR tending to 20).

5.7 Comparison of Relative Contributions of Mixed Convection and Radiation Concerning the Two Channel Configurations

An attempt is made to compare and contrast between the relative contributions of mixed convection and radiation from the two channel configurations. The study is performed for two limiting values of Ri_w^* (0.01 and 250) and with five representative values of ε (0.05, 0.25. 0.45, 0.65 and 0.85). Figure 5.10 shows the above results that are obtained for a fixed input of q_{v1}, q_{v2}, k_s and AR. As can be noticed, the general trend followed by the curves pertaining to both convection and radiation is similar for both the configurations 1 and 2 in the asymptotic free and forced convection limits. In any given regime of mixed convection, the contribution from radiation to heat dissipation increases substantially as ε is increased to 0.85 from 0.05.

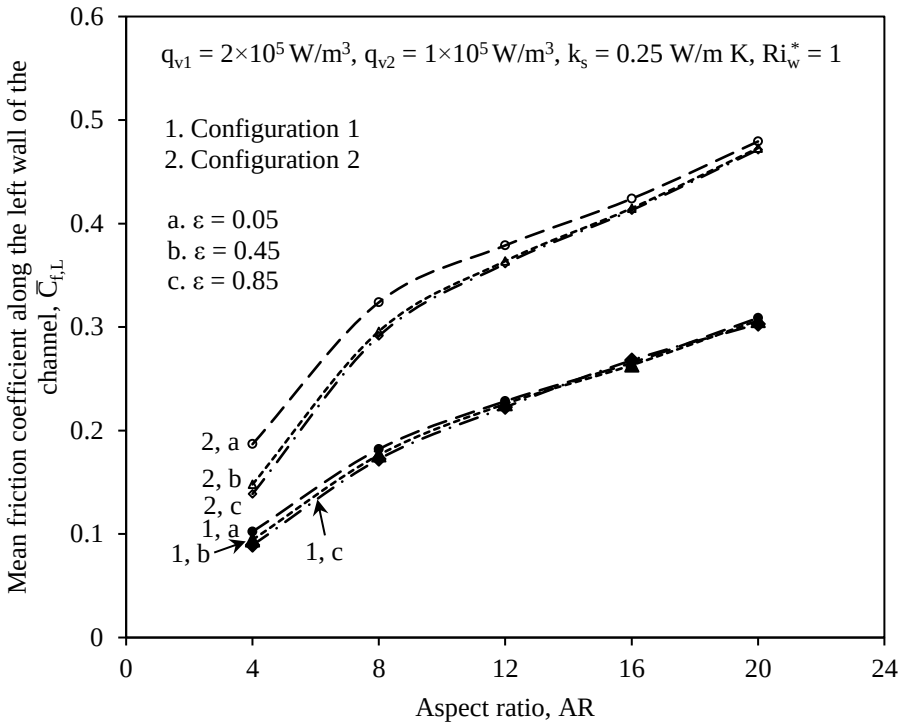

(a)

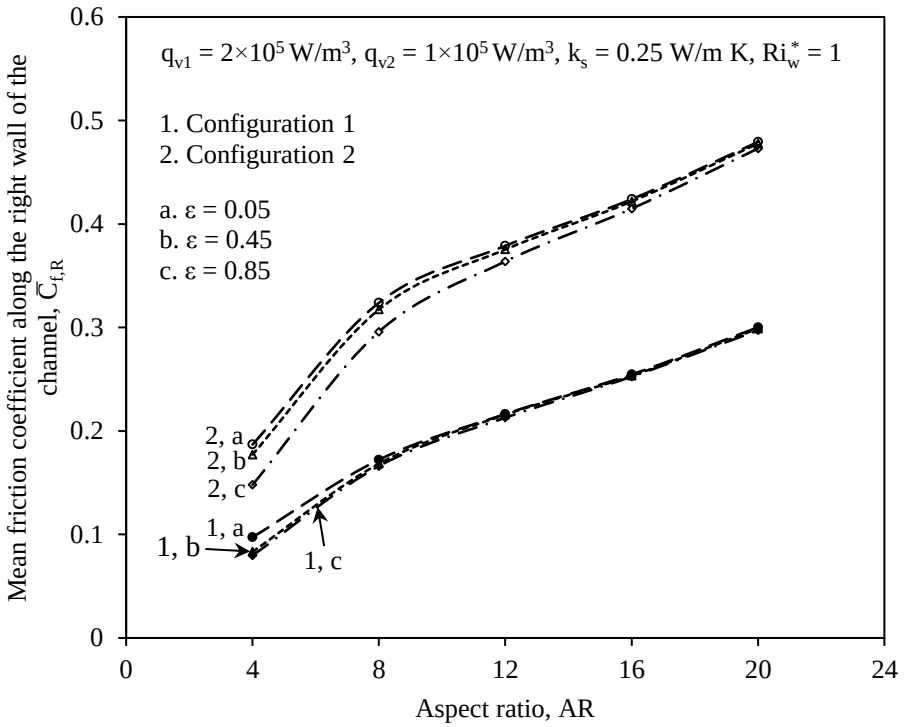

(b)

Fig. 5.9 Comparison of variation of (a) left and (b) right wall mean friction coefficients of the two channel configurations with aspect ratio for different wall surface emissivities

Further, for all values of ε, contribution by radiation in the asymptotic free convection limit ($Ri_w^* = 250$) is observed to be larger in a uniformly heated channel (configuration 2) compared to that in a discretely heated channel (configuration 1). Upon switching to the asymptotic forced convection limit ($Ri_w^* = 0.01$), in contrast to the above, there is hardly anything to choose between the two configurations with regard to radiative (and thus convective) dissipation. Quantifying some of the above observations, for ε = 0.45, in the free convection dominant regime ($Ri_w^* = 250$), radiative dissipation from a uniformly heated channel is 48.42% as against 43.75% possible from a discretely heated channel. Holding all the parameters fixed, with the flow transiting to forced convection dominant regime ($Ri_w^* = 0.01$), the radiative dissipation from discretely and uniformly heated channels, respectively, is 1.66% and 1.94%.

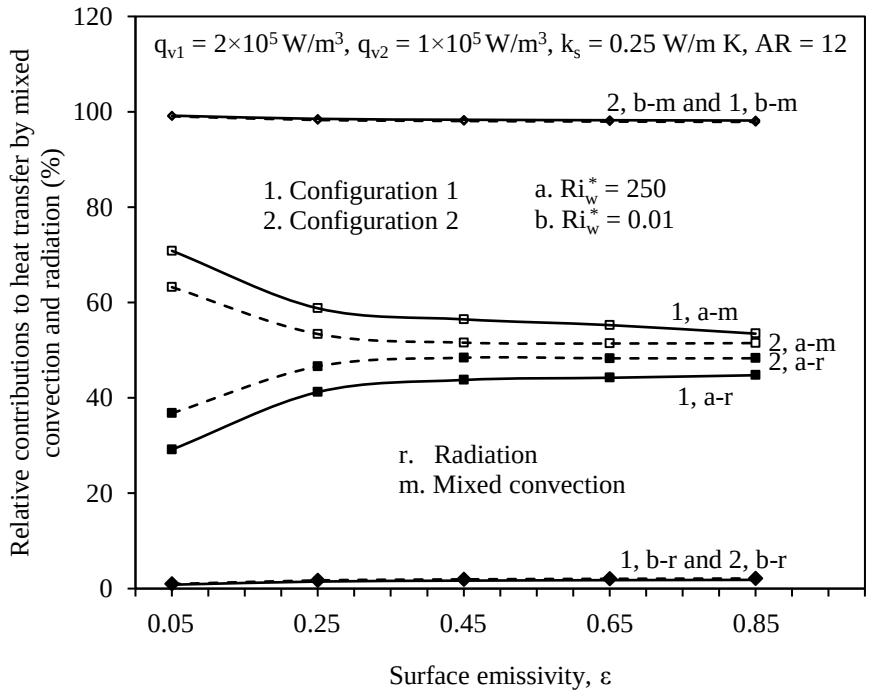

Fig. 5.10 Comparison of relative contributions of mixed convection and radiation in heat dissipation from the two channel configurations with surface emissivity in the two limiting regimes of mixed convection

5.8 Conclusions

A qualitative as well as quantitative comparison between the two problem configurations taken up in the present thesis, viz., vertical channel with multiple identical discrete asymmetrically spaced heat sources and vertical channel with uniform wall heat generation, has been made in this chapter holding the net rate of heat generation identical in both the cases. Some of the prominent observations include:

(1) The local left and right wall non-dimensional temperatures of the configuration 2 are larger as compared to those of the configuration 1 in all the regimes of mixed convection.

(2) A comparison between the two problem geometries with regard to peak channel temperature (θ_{max}) revealed that a better thermal control is feasible when one uses a discretely heated channel than a uniformly heated channel, in general, for any given value of ε and in any given regime of mixed convection.

(3) As has been noticed in the preceding chapter that addressed discretely heated channel, even with a uniformly heated channel, the peak temperature shoots up with increasing aspect ratio with the degree of increase getting substantive while operating in free convection dominant regime. Switching attention to comparison, the peak temperature, once again, turns out to be larger in the case that employs uniform heating as against the case that has discrete heating, no matter what the aspect ratio chosen is.

(4) As a general observation, the left and right wall mean friction coefficients decrease with increasing ε in both discretely and uniformly heated channels. A comparison

between the two configurations considered reveals that the left and right wall mean friction coefficients increase when once uniform heating replaces discrete heating. This observation gains more significance for smaller values of ε.

(5) In tune with the observations already made in the previous chapter, both the left and right wall mean friction coefficients rise quite sharply with aspect ratio for both the configurations employed. On a comparative basis, for a given surface emissivity, $\overline{C}_f$ is found to come down, quite substantially, when a uniformly heated channel is replaced with a discretely heated one.

(6) The general observation that the radiative contribution to heat dissipation increases with ε for a discretely heated channel is noticed to be so with an uniformly heated channel as well. In particular, the radiation contribution would be larger upon employing a uniformly heated channel in the place of a discretely heated channel specifically while working in a free convection dominant environment. This observation, however, gets insignificant while working in the forced convection environment.

5.9 Closure

Qualitative as well as quantitative comparative studies between discretely and uniformly heated channels have been taken up in the present chapter maintaining identical net rate of heat generation in both the cases. The local channel temperature distribution, the peak channel temperature, the mean friction coefficient and the contributions of mixed convection and radiation have been the prominent dependent parameters looked into. The channel with discrete heat generation turned out to be the better proposition when compared to that with

uniform heat generation for a given set of rest of the operating parameters. The ensuing chapter (**Chapter 6**), which is also the concluding chapter of the thesis, will be listing the various findings of the present research work. It will also be hinting at some of the possible challenges that could be taken up for furthering research in areas of this kind.

Chapter 6

Salient Conclusions from Present Work and Scope for Further Work

6.1 Introduction

The prime objective of the present thesis has been a fundamental numerical investigation into the interplay between the various modes of heat transfer [conduction, mixed convection and radiation] concerning the geometry of a vertical parallel-plate channel that has multiple discrete heat sources flush-mounted along its walls asymmetrically. The cooling of electronic equipment and devices has been the closest engineering application for the studies performed in the thesis. Comprehensive parametric studies have been conducted on the problem taken up with the help of an explicitly prepared computer code and the various results have been provided in **Chapter 4** of the thesis. Further, a qualitative as well as quantitative comparison between the geometries of (i) asymmetrically and discretely heated channel and (ii) uniformly heated channel has been made and the pertinent results are elucidated in **Chapter 5**.

Over and above the parametric studies of different kinds performed as mentioned above, useful correlations that aid in calculating (i) maximum non-dimensional channel temperature, (ii) average non-dimensional channel temperature and (iii) mean friction coefficient too have been evolved employing a very huge set of data generated from the computer code prepared as part of the thesis. The prominent conclusions concerning the parametric studies on the research problem have been listed in Chapter 4, while those arising out of comparative studies between discretely and uniformly heated channels have been documented in Chapter 5. Notwithstanding the above, with the objective of providing completeness to the thesis, the various broad conclusions of the complete research work are provided in the present (final) chapter of the thesis.

As is known, no research work on any given problem will be complete in itself. There will always be a number of avenues opening up while tackling a particular research problem. Keeping this in mind, a good number of suggestions that help in furthering research on problems of this kind have been provided in conclusion to the current chapter.

6.2 Broad Conclusions from Various Parametric Studies Performed in the Present Thesis

(1) It is not advisable to pack the walls of the channel closer together since an increasing aspect ratio leads to an unwanted rise in both the left and right wall temperatures resulting in an increased in the cooling load on the system.

(2) Transit of the regime of flow from free convection dominance to forced convection dominance brings a significant drop both in the left and right wall temperatures of the

channel owing to an increased in convective heat dissipation with its radiation counterpart remaining unaltered.

(3) Surface emissivity (ε) is found to be rendering a prominent role in deciding the variation of the local left and right wall temperatures of the channel. Due to asymmetricity employed in positioning the discrete heat sources along the two walls, though the wall temperature rises with increasing ε at the channel entry, it, expectedly, decreases as one progresses along the channel. Globally, the local left (or right) wall temperature has been observed to be dropping down by about 25% due to an increasing surface emissivity from 0.05 to 0.85.

(4) The peak temperature the channel attains decreases with increasing surface emissivity in all the regimes of mixed convection with the degree of decrease being more apparent in the free convection dominant regime as against that in the forced convection dominant regime. This is attributed to an enhanced convection activity in the forced convection dominant regime overriding the role of radiation.

(5) The explicit role enacted by surface radiation in both the local and peak channel temperatures has been elucidated at length. The fact that radiation gains importance in the thermal control of the channel in the entire mixed convection regime has been exhaustively demonstrated with the peak channel temperature dropping down, respectively, by about 10% and 40% in the forced convection and free convection dominant regimes when once radiation is accounted for with the channel walls coated with, say, lamp black with $\varepsilon = 0.99$.

(6) The wall material selected too influences the peak temperature the channel attains with an increasing thermal conductivity tending to bring it down with other parameters held fixed.

(7) A probe into the relative contributions of mixed convection and radiation in channel heat dissipation has been made. It is seen that even in moderate temperature applications like cooling of electronic equipment and devices, radiation makes its presence felt by contributing to the channel heat dissipation. Though it amounts to only 2% in the asymptotic forced convection limit ($Ri_w^* = 0.01$), its share is augmented to as much as 45% in the asymptotic free convection limit ($Ri_w^* = 250$) provided one coats the channel walls with black paint ($\varepsilon = 0.85$).

(8) An increasing aspect ratio generally brings down the role of radiation that gets manifested as an appropriate rise in the role of mixed convection. The above effect is found to be quite eminent in the free convection dominant regime and it gets progressively insignificant with the flow transiting to forced convection dominance.

(9) Buoyancy exhibits a fairly significant role in deciding both the local and peak channel temperatures in the entire mixed convection regime. In particular, considering buoyancy in a forced convection configuration would be more beneficial while operating in free convection dominant regime (towards larger values of Ri_w^*). This observation advises the heat transfer engineer to provide the fan at the channel entry that amounts to buoyancy-aided mixed convection.

(10) The local left and right wall drag coefficients ($C_{fx,L}$ and $C_{fx,R}$) have been observed to be varying fairly largely with surface emissivity (ε) of the channel in any given regime of mixed convection. Both of them tend to decrease with increasing ε.

(11) The local left and right wall drag coefficients ($C_{fx,L}$ and $C_{fx,R}$) increase quite largely with the flow regime transforming from forced convection dominance to free convection dominance.

(12) The left as well as the right wall mean friction coefficients ($\bar{C}_{f,L}$ and $\bar{C}_{f,R}$) are observed to be strongly depending on the surface emissivity in the entire mixed convection regime. They get decreased with increasing ε. The above effect of ε on $\bar{C}_f$ is fairly mild in the forced convection dominant regime, while it becomes more apparent towards the free convection dominant regime.

(13) The aspect ratio (AR) of the channel strongly influences $\bar{C}_f$ with an increasing AR increasing its value quite substantially for a given ε. Too closer packing of the channel walls is to be discouraged as it tends to an unwanted increase in the drag coefficient.

(14) The thermal conductivity of the wall material shows a non-significant effect on the left and right wall mean friction coefficients in all the regimes of mixed convection.

(15) The interplay between the material property (wall thermal conductivity) and the surface property (emissivity) is observed to be influencing the left and right wall mean friction coefficients. An increasing ε, for a given k_s, decreases both $\bar{C}_{f,L}$ and $\bar{C}_{f,R}$. By the same token, an increasing k_s, for a given ε, tends to bring down both the mean friction coefficients.

(16) The explicit influence of buoyancy on both local and mean friction coefficients has been extracted in all the regimes of mixed convection. When compared to the case that considers forced convection flow alone, the buoyancy aided forced convection increases the values of both the local and mean friction coefficients. These

observations assume more importance in the free convection dominant regime when compared to the forced convection dominant regime.

(17) Studies that help in delineating the components of free convection, forced convection and radiation in channel heat dissipation have also been performed. The necessity of preferring buoyancy aided mixed convection to derive optimum heat dissipation has been amply demonstrated through quantitative outputs obtained. The above becomes increasingly important while working in free convection dominant environment.

(18) Pertinent correlations that help in calculating maximum and average non-dimensional channel temperatures and mean friction coefficient are evolved with the help of a fairly large set of 550 numerical data generated from the computer code written in the current work.

(19) Attempts are made to compare the performance of asymmetrically and discretely heated channel (configuration 1) with a uniformly heated channel (configuration 2) holding the net rate of generation identical for both. The local left and right wall non-dimensional temperatures of the configuration 2 are observed to be larger as compared to those of the configuration 1 in all the regimes of mixed convection.

(20) A comparison between the two problem geometries with regard to peak channel temperature (θ_{max}) revealed that a better thermal control is feasible when one uses a discretely heated channel than a uniformly heated channel, in general, for any given value of ε and in any given regime of mixed convection.

(21) The peak channel temperature shoots up with increasing aspect ratio with the degree of increase getting substantive while operating in free convection dominant regime. Moving on to comparison, the peak temperature, once again, turns out to be larger in

the case that employs uniform heating as against the case that has discrete heating, no matter what the aspect ratio chosen is.

(22) The left and right wall mean friction coefficients generally decrease with increasing ε in both discretely and uniformly heated channels. A comparison between the two configurations considered reveals that the left and right wall mean friction coefficients increase upon replacing discrete wall heating with uniform wall heating. This observation gains more significance for smaller values of ε.

(23) Both the left and right wall mean friction coefficients rise quite sharply with aspect ratio for both the configurations employed. On a comparative basis, for a given surface emissivity, $\overline{C}_f$ is found to be coming down largely upon replacing a uniformly heated channel with a discretely heated one.

(24) The general observation that the radiative contribution to heat dissipation increases with ε for a discretely heated channel turns out to be true even with an uniformly heated channel. In particular, the radiation contribution would be larger upon employing a uniformly heated channel in the place of a discretely heated channel specifically while working in free convection dominant regime. This observation, however, loses significance while working in the forced convection environment.

6.3 Scope for Subsequent Research

The fundamental objective of the present thesis has been to perform exhaustive parametric studies on the problem of conjugate mixed convection with surface radiation from the classical geometry of a vertical parallel-plate channel. The channel has discrete heating through multiple identical heat sources that are flush-mounted asymmetrically in its two

walls. For comparison purposes, another configuration that has channel with uniform heat generation in its walls has been taken up. One of the important applications of the above studies could be found in the cooling of electronic equipment and devices. The present work had heat sources flush-mounted in the channel walls, while the real life applications have the electronic boards with protruding heat sources. In view of this, studies on a channel that has protruding heat sources on its walls would be a pertinent extension to the current work.

Further, the prime concentration in the present thesis has been on the channel that has identical discrete heat sources mounted asymmetrically along its walls. It would be interesting, therefore, to look into problems of multi-mode heat transfer involving channels that have non-identical heat sources embedded in both of its walls.

The present studies involved one-dimensional (axial) conduction in the channel walls with a fairly acceptable assumption that the wall thickness is quite small. Thus, consideration of two-dimensional conduction in the channel walls with accompanying mixed convection and radiation would be another welcome addition to the present thesis work.

The problem considered in the present thesis has two-dimensional laminar mixed convection coupled with conduction and radiation. An increased challenge would, therefore, lie if one attempts the problem of three-dimensional mixed convection in conjunction with conduction and radiation.

References

1. **Agrawal, H. C.** (1962) A variational method for combined free and forced convection in channels, *International Journal of Heat and Mass Transfer*, **5**, 439-444.

2. **Al-Amri, F. G.**, and **El-Shaarawi, M. A. I.** (2012) Mixed convection with surface radiation between two asymmetrically heated vertical parallel plates, *International Journal of Thermal Sciences*, **58**, 70-78.

3. **Alves, T. A.**, and **Altemani, C. A. C.** (2012) An invariant descriptor for heaters temperature prediction in conjugate cooling, *International Journal of Thermal Sciences*, **58**, 92-101.

4. **Aminossadati, S. M.**, and **Ghasemi, B.** (2009) A numerical study of mixed convection in a horizontal channel with a discrete heat source in an open cavity, *European Journal of Mechanics- B/Fluids*, **28**, 590-598.

5. **Amirouche, Y.**, and **Bessaih, R.** (2012) Three-dimensional numerical simulation of air cooling of electronic components in a vertical channel, *Fluid Dynamics and Materials Processing*, **8**, 295-309.

6. **Anand, N. K.**, **Kim, S. H.**, and **Aung, W.** (1990) Effect of wall conduction on free convection between asymmetrically heated vertical plates: uniform wall temperature, *International Journal of Heat and Mass Transfer*, **33**, 1025-1028.

7. **Andreozzi, A.**, **Bianco, N.**, **Manca, O.**, and **Naso, V.** (2013) Turbulent mixed convection in a uniformly heated vertical channel with an assisting moving surface, *International Journal of Thermal Sciences*, **71**, 20-31.

8. **Aung, W.**, and **Worku, G.** (1986a) Developing flow and flow reversal in a vertical channel with asymmetric wall temperatures, *ASME Journal of Heat Transfer*, **108**, 299-304.

9. **Aung, W.**, and **Worku, G.** (1986b) Theory of fully developed combined convection including flow reversal, *ASME Journal of Heat Transfer*, **108**, 485-488.

10. **Aung, W.**, and **Worku, G.** (1987) Mixed convection in ducts with asymmetric wall heat fluxes, *ASME Journal of Heat Transfer*, **109**, 947-951.

11. **Avelar, A. C.**, and **Ganzarolli, M. M.** (2004) Natural convection in an array of vertical channels with two-dimensional heat sources: uniform and non-uniform plate heating, *Heat Transfer Engineering*, **25**, 947-951.

12. **Bahlaoui, A.**, **Raji, A.**, and **Hasnaoui, M.** (2005) Multiple steady state solutions resulting from coupling between mixed convection and radiation in an inclined channel, *Heat and Mass Transfer*, **41**, 899-908.

13. **Bar-Cohen, A.**, and **Rohsenow, W. M.** (1984) Thermally optimum spacing of vertical natural convection cooled parallel plates, *ASME Journal of Heat Transfer*, **106**, 116-123.

14. **Barletta, A.** (1998) Laminar mixed convection with viscous dissipation in a vertical channel, *International Journal of Heat and Mass Transfer*, **41**, 3501-3513.

15. **Barletta, A.,** and **Zanchini**, **E.** (2001) Mixed convection with variable viscosity in an inclined channel with prescribed wall temperatures, *International Communications in Heat and Mass Transfer*, **28**, 1043-1052.

16. **Barletta, A.**, **Rossi di Schio, E.**, **Comini, G.**, and **D'Agaro, P.** (2008) Conjugate forced convection heat transfer in a plane channel: longitudinally periodic regime, *International Journal of Thermal Sciences*, **47**, 43-51.

17. **Barletta, A.**, **Rossi di Schio, E.**, **Comini, G.**, and **D'Agaro, P.** (2009) Wall coupling effect in channel forced convection with streamwise periodic boundary heat flux variation, *International Journal of Thermal Sciences*, **48**, 699-707.

18. **Barhaghi, D. G.**, and **Davidson, L.** (2009) Large-eddy simulation of mixed convection-radiation heat transfer in a vertical channel, *International Journal of Heat and Mass Transfer*, **52**, 3918-3928.

19. **Baskaya, S.**, **Erturhan, U.**, and **Sivrioglu, M.** (2005) An experimental study on convection heat transfer from an array of discrete heat sources, *International Communications in Heat and Mass Transfer*, **32**, 248-257.

20. **Bazdidi-Tehrani, F.** and **Shahini**, **M.** (2009) Combined mixed convection-radiation heat transfer within a vertical channel: investigation of flow reversal, *Numerical Heat Transfer- Part A: Applications*, **55**, 289-307.

21. **Bejan, A.** Convection Heat Transfer, *Wiley-Interscience, New York*, 1984.

22. **Bhowmik, H.**, **Tso, C. P.**, **Tou, K. W.** and **Tan, F. L.** (2005) Convection heat transfer from discrete heat sources in a liquid cooled rectangular channel, *Applied Thermal Engineering*, **25**, 2532-2542.

23. **Blasius, H.** (1908) Grenzschichten in Flussigkeiten mit kleiner Reibung, *Z. Math. Phys.*, 56, 1.

24. **Bouttout, A.**, **Benissaad**, **A.** and **Bessaı¨h**, **R.** (2014), Numerical study of forced convection in a horizontal channel with heated blocks due to oscillation of incoming flow, *Numerical Heat Transfer, Part A: Applications*, **65**, 584-600.

25. **Cadafalch, J.**, **Oliva, A.**, **van der Graaf**, **G.** and **Albets, X.** (2003) Natural convection in a large, inclined channel with asymmetric heating and surface radiation, *ASME Journal of Heat Transfer*, **125**, 812-820.

26. **Campo, A.**, **Manca, O.**, and **Morrone, B.** (2006) Numerical investigation of the natural convection flows for low-Prandtl fluids in vertical parallel-plates channel, *ASME Journal of Applied Mechanics*, **73**, 96-107.

27. **Carpenter, J. R.**, **Briggs, D. G.**, and **Sernas, V.** (1976) Combined radiation and developing laminar free convection between vertical flat plates with asymmetric heating, *ASME Journal of Heat Transfer*, **98**, 95-100.

28. **Chang, T.** (2007) Effects of a finite section with linearly varying wall temperature on mixed convection in a vertical channel, *International Journal of Heat and Mass Transfer*, **50**, 2346-2354.

29. **Cherif, Y.**, **Joulin, A.**, **Zalewski, L.**, and **Lassue, S.** (2009) Superficial heat transfer by forced convection and radiation in a horizontal channel, *International Journal of Thermal Sciences*, **48**, 1696-1706.

30. **da Silva, A. K.**, **Lorenzini, G.**, and **Bejan, A.** (2005) Distribution of heat sources in vertical open channels with natural convection, *International Journal of Heat and Mass Transfer*, **48**, 1462-1469.

31. **Desrayaud, G.**, and **Fichera, A.** (2003) On natural convective heat transfer in vertical channels with a single surface mounted heat-flux module, *ASME Journal of Heat Transfer*, **125**, 734-739.

32. **Dogan, A.**, **Sivrioglu, M.**, and **Baskaya, S.** (2006) Investigation of mixed convection heat transfer in a horizontal channel with discrete heat sources at the top and at the bottom, *International Journal of Heat and Mass Transfer*, **49**, 2652-2662.

33. **Dritselis, C. D.**, **Iatridis, A. J.**, **Sarris, I. E.**, and **Vlachos, N. S.** (2013) Buoyancy-assisted mixed convection in a vertical channel with spatially periodic wall temperature, *International Journal of Thermal Sciences*, **65**, 28-38.

34. **Dutta, S.**, **Zhang, X.**, **Khan, J. A.** and **Bell, D.** (1999) Adverse and favourable mixed convection heat transfer in a two-side heated square channel, *Experimental Thermal and Fluid Science*, **18**, 314-322.

35. **Elenbass, W.** (1942) Heat dissipation of parallel plates by free convection, *Physica*, **9**, 1–28.

36. **El-Morshedy, S. E.**, **Alyan, A.**, and **Shouman, L.** (2012) Experimental investigation of natural convection heat transfer in narrow vertical rectangular channel heated from both sides, *Experimental Thermal and Fluid Science*, **36**, 72-77.

37. **Ermolaev, I. A.**, and **Zhbanov, A. I.** (2009) Mixed convection in a vertical channel with discrete heat sources at the wall, *Fluid Dynamics*, **44**, 511-516.

38. **Gosman, A. D.**, **Pun, W. M.**, **Runchal, A. K.**, **Spalding, D. B.**, and **Wolfshtein, M.** Heat and mass transfer in recirculating flows, *Academic Press, London and New York*, 1969.

39. **Guimaraes, P. M.**, and **Menon, G. J.** (2008) Combined free and forced convection in an inclined channel with discrete heat sources, *International Communications in Heat and Mass Transfer*, **35**, 1267-1274.

40. **Gunes, H.**, and **Liakopoulos, A.** (2003) Three-dimensional convective cooling in a vertical channel with flush-mounted heat sources, *International Journal of Heat and Mass Transfer*, **46**, 791-808.

41. **Gururaja Rao, C., Balaji, C.,** and **Venkateshan, S. P.** (2000) Numerical study of laminar mixed convection from a vertical plate, *International Journal of Transport Phenomena,* **2,** 143-157.

42. **Gururaja Rao, C., Balaji. C.,** and **Venkateshan, S. P.** (2001) Conjugate mixed convection with surface radiation from a vertical plate with a discrete heat source, *ASME Journal of Heat Transfer,* **123**, 698-702.

43. **Gururaja Rao, C.**, **Balaji, C.**, and **Venkateshan, S. P.** (2002) Effect of surface radiation on conjugate mixed convection in a vertical channel with a discrete heat source in each wall, *International Journal of Heat and Mass Transfer*, **45**, 3331-3347.

44. **Gururaja Rao, C.** (2004) Buoyancy-aided mixed convection with conduction and surface radiation from a vertical electronic board with a traversable discrete heat source, *Numerical Heat Transfer, Part A: Applications*, **45**, 935-956.

45. **Hacohen, J.**, **Chiu, T. W.**, and **Wragg, A. A.** (1995) Forced and free convective heat transfer coefficients for a model printed circuit board channel geometry, *Experimental Thermal and Fluid Science*, **10**, 327-334.

46. **Hamadah, T. T.**, and **Wirtz, R. A.** (1991) Analysis of laminar fully developed mixed convection in a vertical channel with opposing buoyancy, *ASME Journal of Heat Transfer,* **113**, 507-510.

47. **Hernandez, J.**, and **Zamora, B.** (2005) Effects of variable properties and non-uniform heating on natural convection flows in vertical channels, *International Journal of Heat and Mass Transfer*, **48**, 793-807.

48. **Higuera, F. J.**, and **Ryazantsev, Yu. S.** (2002) Natural convection flow due to a heat source in a vertical channel, *International Journal of Heat and Mass Transfer*, **45**, 2207-2212.

49. **Ichimiya, K.**, and **Matsushima, Y.** (2009) Performance evaluation of mixed convection in an inclined square channel with uniform temperature walls, *International Journal of Heat and Mass Transfer*, **52**, 1802-1810.

50. **Incropera, F. P.** (1998) Convection heat transfer in electronic equipment cooling, *ASME Journal of Heat Transfer,* **110**, 1097-1111.

51. **Kim, S. H.**, **Anand, N. K.**, and **Aung, W.** (1990) Effect of wall conduction on free convection between asymmetrically heated vertical plates: uniform wall heat flux, *International Journal of Heat and Mass Transfer*, **33**, 1013-1023.

52. **Kim, S. H.**, **Anand, N. K.** and **Fletcher, L. S.** (1991) Free confection between series of vertical parallel plates with embedded line heat sources, *ASME Journal of Heat Transfer*, **113**, 108-115.

53. **Kim, S. H.**, and **Anand, N. K.** (1994) Laminar developing flow and heat transfer between a series of parallel plates with surface-mounted discrete heat sources, *International Journal of Heat and Mass Transfer*, **37**, 2231-2244.

54. **Kim, S. H.**, and **Anand, N. K.** (1995) Laminar heat transfer between a series of parallel plates with surface-mounted discrete heat sources, *ASME Journal of Electronic Packaging*, **117**, 52-62.

55. **Ko, M.**, and **Anand, N. K.** (2007) Numerical simulation of three-dimensional combined convective radiative heat transfer- a finite volume method, *International Journal for Computational Methods in Engineering Science and Mechanics*, **8**, 429-437.

56. **Li, R.**, **Bousetta, M.**, **Chénier, E.**, and **Lauriat, G.** (2013) Effect of surface radiation on natural convective flows and onset of flow reversal in asymmetrically heated vertical channels, *International Journal of Thermal Sciences*, **65**, 9-27.

57. **Madhusudhana Rao, G.**, and **Narasimham, G. S. V. L.** (2007) Laminar conjugate mixed convection in a vertical channel with heat generating components, *International Journal of Heat and Mass Transfer*, **50**, 3561-3574.

58. **Madhusudhana, G.** (2012) Natural convection in a vertical channel with arrays of flush-mounted heaters on opposite conductive walls, *Numerical Heat Transfer, Part A: Applications*, **62**, 111-135.

59. **Olsson, C.** (2004) Prediction of Nusselt number and flow rate of buoyancy driven flow between vertical parallel plates, *ASME Journal of Heat Transfer*, **126**, 97-104.

60. **Peterson, G. P.**, and **Ortega, A.** (1990) Thermal control of electronic equipment and devices, In: **Hartnett, J. P.**, and **Irvine, T. F. Jr.** (Eds.) Advances in Heat Transfer, *Academic Press Inc., San Diego, California*.

61. **Poskas, P.**, **Poskas, R.**, **Sirvydas, A.**, and **Smaizys, A.** (2011) Experimental investigation of opposing mixed convection heat transfer in the vertical flat channel in a laminar-turbulent transition region, *International Journal of Heat and Mass Transfer*, **54**, 662-668.

62. **Premachandran, B.**, and **Balaji, C.** (2011) Conjugate mixed convection with surface radiation from a vertical channel with protruding heat sources, *Numerical Heat Transfer, Part A: Applications*, **60**, 171-196.

63. **Puangsombut, W.**, **Hirunlabh, J.**, **Khedari, J.**, and **Zeghmati, B.** (2007) An experimental study of free convection in an inclined rectangular channel using radiant barrier, *Experimental Heat Transfer*, **20**, 171-184.

64. **Quintiere, J.**, and **Mueller, W. K**. (1973) An analysis of laminar free and forced convection between finite vertical parallel plates, *ASME Journal of Heat Transfer*, **95**, 53-59.

65. **Ramjee, R.**, and **Satyamurty, V. V.** (2010) Local and average heat transfer in the thermally developing region of an asymmetrically heated channel, *International Journal of Heat and Mass Transfer*, **53**, 1654-1665.

66. **Roache, P. J.** Computational fluid dynamics, *Hermosa, Albuquerque, New Mexico, USA*, 1972.

67. **Roeleveld, D.**, **Naylor, D.**, and **Oosthuizen, P. H.** (2009) Empirical correlations for free convection in an isothermal asymmetrically heated vertical channel, *Heat Transfer Engineering*, **30**, 189-196.

68. **Roeleveld, D.**, **Naylor, D.**, and **Leong, W. H.** (2014) Free convection in antisymmetrically heated vertical channels, *ASME Journal of Heat Transfer*, **136**, 12502-1−12502-7.

69. **Sakurai, A.**, **Matsubara, K.**, **Takakuwa, K.**, and **Kanbayashi, R.** (2012) Radiation effects on mixed turbulent natural and forced convection in a horizontal channel using direct numerical simulation, *International Journal of Heat and Mass Transfer*, **55**, 2539-2548.

70. **Siegel, R.,** and **Howell, J. R.** Thermal radiation heat transfer, 3rd ed., *Taylor and Francis, Washington and London*, 1992.

71. **Sparrow, E. M.**, **Shah, S.**, and **Prakash, C.** (1980) Natural convection in a vertical channel: I. Interacting convection and radiation. II. The vertical plate with and without shrouding, *Numerical Heat Transfer*, **3**, 297-314.

72. **Sun, H.**, **Li, R.**, **Chénier, E.**, **Lauriat, G.**, and **Padet, J.** (2012) Optimal plate spacing for mixed convection from an array of vertical isothermal plates, *International Journal of Thermal Sciences*, **55**, 16-30.

73. **Tao, L. N.** (1960) On combined free and forced convection in channels, *ASME Journal of Heat Transfer*, **82**, 233-238.

74. **Terekhov, V. I.**, and **Ekaid, A. L.** (2011) Laminar natural convection between vertical isothermal heated plates with different temperatures, *Journal of Engineering Thermophysics*, **20**, 416-433.

75. **Watson, J. C.**, **Anand, N. K.**, and **Fletcher, L. S.** (1996) Mixed convective heat transfer between a series of vertical parallel plates with planar heat sources, *ASME Journal of Heat Transfer*, **118**, 984-990.

76. **Yadav, V.**, and **Kant, K.** (2007a) Air cooling of variable array of heated modules in a vertical channel, *ASME Journal of Electronic Packaging*, **129**, 205-215.

77. **Yadav, V.**, and **Kant, K.** (2007b) Convective cooling of a PCB like surface with mixed heating conditions in a vertical channel, *ASME Journal of Electronic Packaging*, **129**, 129-143.

78. **Yao, L. S.** (1983) Free and forced convection in the entry region of a heated vertical channel, *International Journal of Heat and Mass Transfer*, **26**, 65-72.

79. **Yucel, N.**, and **Guven, R. T.** (2007) Forced-convection cooling enhancement of heated elements in a parallel-plate channels using Porous Inserts, *Numerical Heat Transfer, Part A: Applications*, **51**, 293-312.

List of Publications Based on the Present Research Work

International Journals:

1. **Sudhakar Babu, S., Gururaja Rao, C.,** and **Narasimha Rao, A. V.,** (2014), Parametric studies on combined conduction-convection-radiation from a discretely and non-identically heated rectangular electronic board, *International Journal of Advanced Mechanical Engineering*, ISSN 2250-3234, Vol. 4, No. 5, pp. 527-534, 2014

2. **Sudhakar Babu, S., Gururaja Rao, C.,** and **Narasimha Rao, A. V.,** (2016), Simulation studies on an asymmetrically heated vertical channel involved in multi-mode heat transfer, *Journal of Material Science and Mechanical Engineering*, Vol. 3, No. 3, pp. 213-218, 2016

3. **Sudhakar Babu, S., Gururaja Rao, C.,** and **Narasimha Rao, A. V.,** (2014), Effect of surface radiation on conjugate convection from a non-identically and discretely heated electronic board, *Journal of the Institution of Engineers (India)-Mechanical Engineering*, Springer Publication (Awaiting Final Editorial Decision)

4. **Sudhakar Babu, S., Gururaja Rao, C.,** and **Narasimha Rao, A. V.,** (2016), Interaction of radiation with conjugate mixed convection from an asymmetrically heated vertical channel embedded with multiple discrete heat sources, *Heat Transfer Engineering*, Taylor & Francis Publication (Under Review)

International Conferences:

5. **Sudhakar Babu, S., Gururaja Rao, C.,** and **Narasimha Rao, A. V.,** Parametric studies on combined conduction-convection-radiation from a discretely and non-identically heated rectangular electronic board, *Advances in Mechanical, Material, Manufacturing, Automobile, Aeronautical Engineering and Applied Physics* (AMAEAP-2014), Jawaharlal Nehru University, New Delhi, June 07-08, 2014

6. **Sudhakar Babu, S., Gururaja Rao, C.,** and **Narasimha Rao, A. V.,** Conjugate mixed convection with radiation from a vertical channel with multiple asymmetrically mounted

discrete heat sources, "*ISME Conference on Advances in Mechanical Engineering*", IIT Delhi, October 3-4, 2015

7. **Sudhakar Babu, S., Gururaja Rao, C.,** and **Narasimha Rao, A. V.,** Buoyancy-aided conjugate mixed convection with radiation from a discretely and asymmetrically heated vertical channel, *Proceedings of the 2nd International Conference on advances in Steel, Power and Construction Technology* (ICASPCT-2016),OP Jindal University, Raigarh, March 17-19, 2016

8. **Sudhakar Babu, S., Gururaja Rao, C.,** and **Narasimha Rao, A. V.,** Simulation studies on an asymmetrically heated vertical channel involved in multi-mode heat transfer, *Recent Trends in Mechanical, Material Science, Manufacturing, Automobile, Aerospace Engineering and Applied Physics* (AMAEAP-2016), Jawaharlal Nehru University, New Delhi, April 30, 2016